MECHANORESPONSIVE POLYMERS BASED ON SPIROPYRAN MECHANOPHORE

MECHANORESPONSIVE POLYMERS BASED ON SPIROPYRAN MECHANOPHORE

By MENG LI, B. ENG.

A Thesis Submitted to the School of Graduate Studies

in Partial Fulfilment of the Requirements for

the Degree of Doctor of Philosophy

DOCTOR OF PHILOSOPHY (2017) McMaster University

(Chemical Engineering) Hamilton, Ontario

TITILE: Mechanoresponsive Polymers based on Spiropyran Mechanophore

AUTHOR: Meng Li

B. ENG. (Zhejiang University, China)

SUPERVISOR: Dr. Shiping Zhu

NUMBER OF PAGES: xxx, 201

Lay Abstract

Smart polymer has been a research focus for recent decades. One of the most critical responses is to monitor mechanical failures of structural materials, such as stress fraction, fatigue and hysteresis within the polymer by giving off early warnings to prevent the catastrophic failure from occurring. The most prevalent approaches to design a mechanoresponsive polymer is to incorporate a "mechanophore", containing mechanically labile bonds that are subjective to change under exogenous forces. Spiropyrans (SP) are great candidates for stress/strain sensing in terms of mechanochromism. When mechanical force is applied onto C_{spiro}-O bond, SP undergoes reversible 6-π ring opening reaction to yield merocyanine (MC). The ring-closed form SP is colorless or yellow and nonfluorescent, whereas the ring-open form MC is purple or blue or red and fluorescent. In this project we first designed and synthesized divinyl spiropyran cross-linker, fitting for chain growth polymerization, which accounts for more than 80% of polymer products. Then the divinyl spiropyran cross-linker was covalently incorporated into polymethylacrylate, polyolefins, acrylic latex coating and CO_2-breathing microgels, aiming to broaden the potential applications of mechanophore into various polymers. We also summarized the recent development and studies of spiropyran mechanophore into a comprehensive review from an engineering prospective to provide insights into polymer mechanochemistry and study approaches for other mechanophores.

Abstract

Spiropyran (SP) is an effective mechanophore because it is easy to be covalently incorporated into polymers and capable of changing color upon mechanical loading. SP motif is a model mechanophore in fundamental studies of mechanochemistry. Therefore, it is of great significance to gain a deep and comprehensive knowledge of SP mechanochemistry for the exploration of mechanochemistry in general. In the beginning of this thesis, a review of SP mechanophore was presented from an engineering perspective. A workflow for SP mechanochemistry, applications in various polymeric systems, impacting factors and characterization techniques as well as conclusions were thoroughly presented. The review aimed to offer deep insight into polymer mechanochemistry and provide approaches to study other mechanophores using the example of SP mechanochemistry in polymers.

So far there have been three types of SP mechanophores (SP1, SP2 and SP3) reported in the literature. SP1 and SP2 are sensitive to both UV light and mechanical force, whereas SP3 is sensitive to mechanical force but not to UV, which is an excellent candidate for outdoor applications. Due to the unique feature of SP3, this project is mainly focused on applying SP3 mechanophore into functional and structural polymeric materials.

- We designed and synthesized divinyl SP3 mechanophore cross-linker, which can be employed in chain growth polymerization, accounting for more than 80% of total polymer products. As a demonstration, SP3 was incorporated as a cross-linker in the free radical polymerization of

methyl acrylate (MA). The mechanoactivation and UV activation of SP3-cross-linked PMA were investigated in details.

- SP3 mechanophore cross-linker was covalently incorporated into two widely used polyolefins through facile cross-linking. It represents the first example of smart polyolefins that feel the force by color changing, opening the possibilities of applying SP mechanophore into widely used polyolefin materials, accounting for more than half of the total polymer materials.
- We prepared force sensitive acrylic latex coating via covalent incorporation of SP3 mechanophore cross-linker. It is the first example of mechanochromic acrylic latexes, and it provides insight into the design of force-sensitive and self-reporting polymer coatings.
- We reported the CO_2-breathing induced reversible activation of SP3 mechanophore within microgels. This work provides an effective approach to study the forces inside swollen microgels. It also demonstrates the biomimetic processes with shape deformation and concomitant color/fluorescence change.

Acknowledgement

Back in the fall of 2012, I started to apply for graduate studies in North America and Hong Kong. In the dilemma of choices, Song Guo, the teacher of our class, recommended me to come to Prof. Shiping Zhu's group. Coming to Canada to study for PhD under Dr. Zhu's supervision was a wise life decision. Thank you Song Guo for introducing me to Prof. Shiping Zhu.

Thank you Dr. Zhu for always believing in me and being patient with me all the way during my PhD studies. In the beginning of the research path, I had a difficult time in the transition to become a good researcher. Never have I felt so frustrated towards countless experimental failures. Dr. Zhu told me that studying undergrad is like studying in the light, whereas studying for PhD is like exploring in the dark. Through the "darkness" of research, I finally found a bit of light to find the door and finally knock it open. Thank you Dr. Zhu for your constant support and tremendous encouragement. He always told me success needs both "thinking smart" and "working hard". His advice on jumping out of the area and looking at the big picture motivated me greatly in my PhD study.

Thank you Dr. Qi Zhang for guiding me into the smart polymer world and also teaching me how to become a good researcher. I remember he stressed the importance to keep up with latest literature, balance the time of experiments and research, and organize experiments and write papers in a logical way. Without his advice, I would not grow up so quickly and achieve so much. I believe

the most important thing I learned from Dr. Zhang was being strict with yourself and working efficiently. Additionally, I would like to thank Dr. Weifeng Liu and Dr. Yinning Zhou for providing expertise help and novel ideas.

I would also like to thank my committee members, Dr. Harald Stover and Dr. Todd Hoare for providing research guidance and valuable input. Your support and advice helped me consider different angles. I would like to thank Michelle Whalen, Linda Ellis, Kristina Trollip, Paul Gatt, Tim Stephens, Doug Keller, Mike Clarke, and Liu Lina, who have always been ready to help. I would like to sincerely thank the Department of Chemical Engineering in McMaster University for allowing me to perform my research in a technically accommodating and safe laboratory environment. Moreover, it is my great honor to be granted with Ontario Trillium Scholarship. I am very thankful for the generous financial support.

I would like to thank all my friends in McMaster and especially the PolyMac Zhu group. I truly enjoyed four years that I spent with you guys, who would always encourage me, help me and support me. Though I cannot list all of their names here, their support has been a great importance to me through the entire PhD study. I would especially thank Erlita Mastan, Darko Ljubic and Liya Niu, who gave me unconditional support in guiding me through the stressful times in my research and daily life. It is them who made me understand the meaning of “a friend in need is a friend indeed”. Though thousands of miles away from home, I don't feel lonely here because I have you, my friends.

To my mother, Yashuang Han, I owe my deepest gratitude for your endless love and kind support throughout the years. My mother is a woman like no other. Without a father around, she nurtured me, put me through school, and taught me to be a better person. She gave me both mother's love and father's discipline. She made me who I am today. I am very sorry for not being around all these years and leaving her worried and anxious about me all the time. Thank you for giving me unconditional love and care, giving me freedom, and supporting me pursuing my dream so far from home. You give me strength that leads me through difficult times and makes me continue marching on even when I believe I could not go any further. My appreciation for my mother is beyond words that can describe.

Last but not least, I must thank Jeff Rudd, who has been with me through the last two years of my PhD. I remembered you were so interested in my research project in our first conversation over the phone. Even though you are in Akron, USA, which is 500 km away from me, you have always been there for me. Your love and support have been a great motivation for me to work hard. You are also such a great example of being professional, hard-working and multi-tasking that I have been learning from. With your love and support, I have been very productive and published four papers with one more under submission within two years. I also enjoy seeing the world with you. We have traveled to Florida, Arizona, North Carolina and China, been on so many adventures. Our future is ahead of us, and I look forward to many more years of laughers and holding each other's hands.

Table of Contents

List of Figures

Figures in Supporting Information

List of Tables

List of Schemes

List of Abbreviations and Symbols

Abbreviations

3D	three dimensional
ATR	attenuated total reflectance
ATRP	atom transfer radical-polymerization
BPO	benzoyl peroxide
CAD	computer aided design
DCP	dicumyl peroxide
DLS	dynamic light scattering
DMA	*N*, *N*-dimethylaniline
DSC	differential scanning calorimetry
DTGS	deuteriotriglycine sulfate
EGDMA	ethylene glycol dimethacrylate
EOC	poly(ethylene octene)
EVA	poly(ethylene-vinyl acetate)
FRL	fluorescent room light

FRP	free radical polymerization
FTIR	fourier transform infrared spectroscopy
KPS	potassium persulfate
MC	merocyanine
MS	mass spectrometry
$NaHCO_3$	sodium bicarbonate
NIPAM	isopropylacrylamide
NMR	nuclear magnetic resonance
PAM	polyacrylamide
PCL	polycaprolactone
PDEA	poly(2-(diethylamino)ethyl-methacrylate)
PDMS	poly(dimethylsiloxane)
PEA	poly(ethyl acrylate)
PEO	poly(ethylene glycol) dimethacrylate
PiBA	poly(*iso*-butyl acrylate)
PLA	poly(lactic acid)
PMA	poly(methacrylate)

PMMA	poly(methyl methacrylate)
PnBA	poly(*n*-butylacrylate)
PS	polystyrene
PTA	phosphotungstic acid
PtBA	poly(*tert*-butyl acrylate)
PTFE	polytetrafluoroethylene
PTT	pentaerythritol
PU	polyurethane
rBC	ratio of blue component of RGB
RGB	red, green and blue channel
rGC	ratio of green component of RGB
ROP	ring opening polymerization
rRC	ratio of red component of RGB
SDS	Sodium dodecyl sulfate
SFEP	soap free emulsion polymerization
SHM	structural health monitoring
SP	spiropyran

TEM	transmission electron microscope
THF	tetrahydrofuran
UPy	2-ureido-4-pyrimidone
VOC	volatile organic compounds
VTES	vinyltriethoxysilane

Symbols

A_t	absorbance at time t
$\dot{r}$	shearing rate
ΔH_c	enthalpy of crystallization
a	swelling ratio of microgels after breathing
D_h	hydrodynamic diameter of microgels
F	loading on the grips
k	rate constant
L	distance between grips after stretching
L_0	distance between grips before stretching
M_W	molecular weight

S_0	cross section area before stretching
T_c	crystallization temperature
T_g	glass transition temperature
T_m	melting temperature
ε	strain
ε_{sp}	strain threshold of mechanoactivation of spiropyran
σ	stress
τ	time constant for first order exponential decay

Declaration of Academic Achievement

This dissertation is organized in a "sandwich" style, consisting of five journal articles and used to fulfill the requirements of the Ph.D. degree. Four research papers (Chapter 3-6) are published, and the review paper (Chapter 2) is under submission. Appendix A-C are unpublished work, providing valuable data for future studies. The contributions of the authors of the articles are as follows:

- Meng Li is the primary author of all the five journal articles, reproduced in this thesis (Chapter 2-6).
- Meng Li generated the original idea of the four research papers jointly with Prof. Shiping Zhu, Dr. Qi Zhang and Dr. Weifeng Liu (Chapter 3-6).
- Prof. Shiping Zhu is the supervisor of all the journal articles, brainstorming sessions, giving constructive guidance, and revisions of the manuscripts.
- Dr. Qi Zhang is the co-author of the review article (Chapter 2) and the three research papers (Chapter 3, 5, 6), giving necessary revisions to the manuscript drafts.
- Dr. Weifeng Liu is the co-author of two research papers (Chapter 4, 5), giving necessary revisions to the manuscript drafts.
- Dr. Yinning Zhou is the co-author of the review article (Chapter 2), providing inputs to the manuscript drafts.
- Lei Lei is the co-author of the research paper (Chapter 6), providing assistance in the experiments.

Chapter 1 Introduction

This chapter gives a brief research background, research objectives and thesis organization as follows.

1.1 Research Background

Recent decades have witnessed a growing interest in smart materials that are responsive to external stimuli, such as pH,[1] temperature,[2] light,[3] ultrasound,[4] redox agent,[5] and voltage.[6] Among all fascinating responsiveness, mechanoresponsive polymers are of particular interest and importance due to their potential applications in stress/strain sensing and damage reporting. The most prevalent approach to design a mechanoresponsive polymer is to incorporate "mechanophore", which contains mechanically labile bonds that are subjective to change under the influence of exogenous forces.[7] Based on different mechanoresponsiveness, mechanophores fall into several categories, such as mechanoluminescence,[8] mechanochromism (optical changes under mechanical loadings),[9] mechanocatalysis,[10] damage-healing,[11] polymer remodeling,[11] small molecule release.[12]

In this project, we mainly focus on spiropyran (SP) mechanochemistry, the most established and intensively studied among all mechanophores. When force is transmitted to the labile spiro C-O

bond, the colorless SP form is mechanically activated to a colorful merocyanine (MC) form. SP motif is a model mechanophore in fundamental studies of the mechanoactivation behaviors in polymers. Because it is not only easy to be incorporated into polymer backbones or networks, but also capable of changing color and fluorescence upon mechanical loading, which are easy and direct to be detected. Therefore, investigating SP mechanochemistry and its application into polymers is of great significance in the study of mechanochemistry in general.

When the C-O bond is cleaved by mechanical force, SP is activated to MC. The closed SP is colorless/yellow and nonfluorescent, whereas the open MC form is blue/red/purple and fluorescent, as shown in Figure 1-1a. Since the spiro C-O is the determining point for SP mechanoactivation, the attachment points on SP molecule should be on the opposing sides of the spiro junction so that the force can be effectively transmitted across the labile bond to rupture it. Based on this designing principle of active SP mechanophores, three types of SP mechanophores, as shown in Figure 1-1b, have been reported and intensively studied in literature so far. Being "super smart", SP1 and SP2 are sensitive to both UV light and mechanical force. However, it is not always advantageous to be super smart, since either UV irradiation or mechanical activation can result in the ring-opening of SP for outdoor materials. Compared to SP1 and SP2, SP3 shows advantages in damage sensing in outdoor materials since it is sensitive to mechanical force but not to UV irradiation due to the absence of electron withdrawing nitro group.[13,14] In this project, SP3 is chosen as the mechanophore to be incorporated into various polymer systems, due to its unique properties.

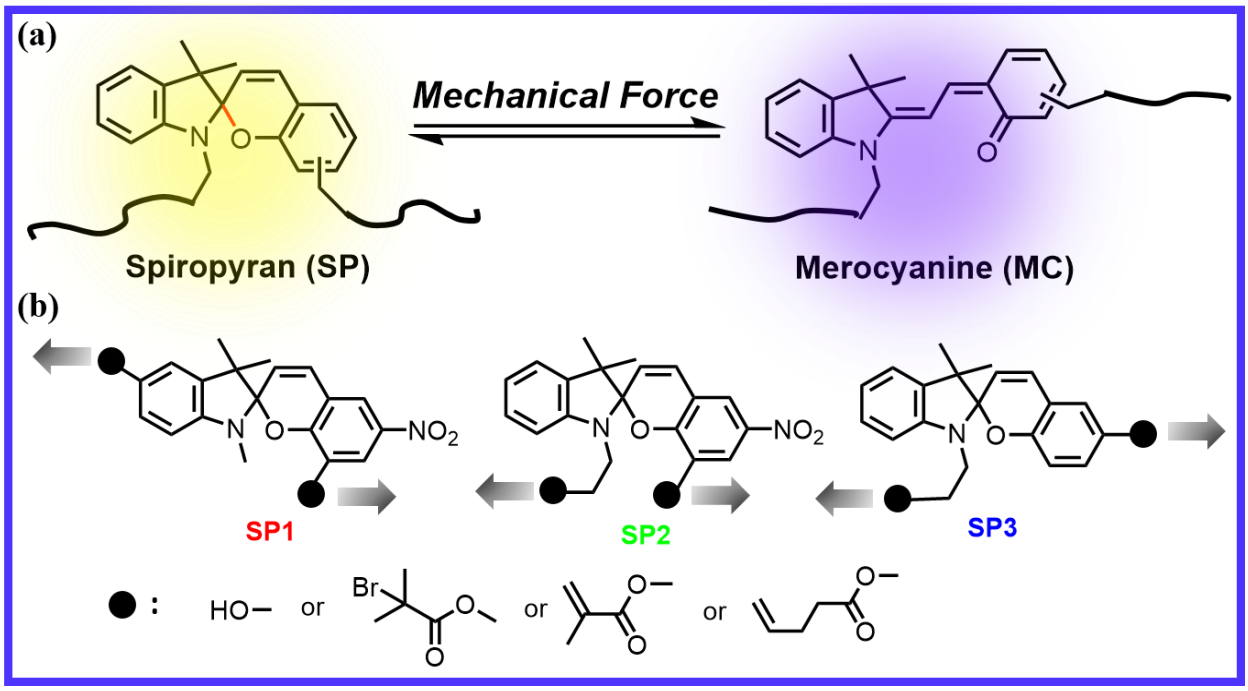

Figure 1-1 (a) Mechanical force-induced ring-opening reaction of spiropyran (SP) to merocyanine (MC); (b) Three types of active SP mechanophores based on the location of attachment. The attachment can be functionalized by hydroxyl group, α-bromoisobutyryl group, methylacryloyl ester group, bis-alkene group.

1.2 Research Objectives

The objective of each chapter is summarized as follows, with a more detailed description of each chapter in the following section "Thesis Organization".

- To give a comprehensive review of spiropyran mechanochemistry, including its application into various polymer systems, impacting factors on mechanoactivation, characterization approaches and challenges, as well as future prospects (Chapter 2)
- To demonstrate the application of SP3 mechanophore into polyacrylates by incorporating divinyl SP3 mechanophore cross-linker into polymethylacrylate (PMA) (Chapter 3)
- To demonstrate the application of SP3 mechanophore into polyolefins by embedding SP3 cross-linker into poly(ethylene-vinyl acetate) (EVA) and poly(ethylene-octene) (EOC) (Chapter 4)
- To demonstrate the application of SP3 mechanophore into acrylic latex coating by incorporating SP3 cross-linker into acrylic latexes (Chapter 5)
- To demonstrate the application of SP3 mechanophore into gas responsive microgels and the CO_2-breathing induced mechanoactivation. (Chapter 6)

1.3 Thesis Organization

This dissertation follows "sandwich" style, consisting of four published articles in peer-reviewed journals (Chapter 3-7) and a review article (Chapter 2) under submission. Except for the reference style and numbering of the figures and tables, the text was copied verbatim from the original manuscript with the reproduction permission from the journals. For clarity purpose, the four published articles, which are "sandwiched" between Literature Review (Chapter 2) and Conclusions (Chapter 7), are about the application of SP mechanophore into various polymer

systems. The other three projects were also summarized in Appendix A-C to provide valuable data, experience and recommendations for future studies.

Chapter 2 is a literature review, presenting spiropyran mechanophore from an engineering prospective. A workflow for SP mechanochemistry, applications in various polymeric systems and impacting factors, as well as characterization techniques are thoroughly discussed. Current limitations and future research directions are briefly highlighted in the end. This review aims to offer deep insight into polymer mechanochemistry and provide approaches to study other mechanophores using the example of SP mechanochemistry in polymers. This paper is under submission.

Chapter 3 reports the synthesis of a new type of spiropyran mechanophore cross-linker, 1'-(2-(methacryloyloxy)ethyl)-3',3'-dimethylspiro[chromene-2,2'-indolin]-6-yl)methyl methacrylate, (SP3), which was incorporated into free radical polymerization of methyl acrylate (MA) as a cross-linker. SP3 cross-linker showed two unique features, which were fast recovery and selective sensitivity to mechanical force (not sensitive to UV). It was also observed that increasing SP content resulted in higher rigidity of the elastomer and lower threshold strain for SP mechanoactivation. Since chain growth polymerization accounts for more than 80% of total polymer products, the combination of divinyl mechanophore cross-linker and chain growth polymerization will lead to the inspirations in engineering applications. This chapter is a

reproduction of an article published in *Polymer*, **2016**, 99, p.521-528 (doi: 10.1016/j.polymer.2016.07.057).

Chapter 4 presents SP-containing polyolefins, poly(ethylene-vinyl acetate) (EVA) and poly(ethylene-octene) (EOC), which were prepared via facile cross-linking by peroxide under hot press. SP3 could not be thermally driven to ring open under high-temperature curing, which was superior to other types of SP mechanophores in polymer processing. In the mechanoactivation of EVA, increasing SP content led to a lower threshold of strain for SP mechanoactivation. Higher SP-to-MC conversion occurred at slower strain rates, indicating SP-to-MC was a rate-dependent reaction. When held at constant strain, MC gradually reverted to SP. Mechanoactivation of EOC was also demonstrated. This work represents the first example of smart polyolefins that feel the force by color changing and provides meaningful insights into expanding mechanochemistry into commercial commodity polymers. This chapter is a reproduction of an article published in *Polymer*, **2017**, 112, p.219-227 (doi:10.1016/j.polymer.2017.02.006)

Chapter 5 reports the preparation of force sensitive acrylic latex coating through the covalent incorporation of SP3 mechanophore. The acrylic latexes were obtained through emulsion copolymerization of butylacrylate (BA), methyl methacrylate (MMA) with vinyltriethoxysilane (VTES) as inter-particle cross-linker and SP3 as intra-particle cross-linker. The mechanoactivation of the SP-containing latex coating was demonstrated. Higher SP content led to higher stress sensitivity and lower threshold stress for SP mechanoactivation. Higher VTES content resulted in

higher critical stress for SP activation but had little effect on stress sensitivity. This is the first example of mechanochromic acrylic latexes and provides a good insight into a variety of acrylic latex-based applications of mechanochemistry in adhesives, protective coatings, and paints. This chapter is a reproduction of an article published in *ACS Applied Materials & Interfaces*, **2017**, 9 (17), p.15156-15163 (doi: 10.1021/acsami.7b04154).

Chapter 6 presents CO_2-breathing induced reversible activation of mechanophore within microgels. The microgels were obtained via soap-free emulsion polymerization (SFEP) of CO_2-switchable monomer 2-(diethylamino)ethyl-methacrylate (DEA) with SP3 as cross-linker. The microgels could be swollen by CO_2 aeration. The swelling force further mechanoactivated SP to MC, causing the emergence of vibrant purple and fluorescence. The transitions were highly reversible, and the initial states of microgels could be recovered by washing off CO_2 with N_2. This work represents the first example of CO_2-breathing activation of mechanophore within microgels. This chapter is a reproduction of an article published in *Macromolecular Rapid Communication*, **2016**, *37* (12), p.957–962. (doi: 10.1002/marc.201600119).

1.4 References

(1) Dai, S.; Ravi, P.; Tam, K. C. *Soft Matter* **2008**, *4* (3), 435.

(2) Lutz, J.-F.; Akdemir, Ö.; Hoth, A. *J. Am. Chem. Soc.* **2006**, *128* (40), 13046.

(3) Zhao, Y. *Macromolecules* **2012**, *45* (9), 3647–3657.

(4) Chen, W.; Du, J. *Sci. Rep.* **2013**, *3*, 2162.

(5) Napoli, A.; Valentini, M.; Tirelli, N.; Müller, M.; Hubbell, J. A. *Nat. Mater.* **2004**, *3* (3), 183–189.

(6) Peng, L.; Feng, A.; Zhang, H.; Wang, H.; Jian, C.; Liu, B.; Gao, W.; Yuan, J. *Polym. Chem.* **2014**, *5* (5), 1751–1759.

(7) Caruso, M. M.; Davis, D. A.; Shen, Q.; Odom, S. A.; Sottos, N. R.; White, S. R.; Moore, J. S. *Chem. Rev.* **2009**, *109* (11), 5755–5798.

(8) Chen, Y.; Spiering, a J. H.; Karthikeyan, S.; Peters, G. W. M.; Meijer, E. W.; Sijbesma, R. P. *Nat. Chem.* **2012**, *4*(7), 559–562.

(9) Davis, D. A.; Hamilton, A.; Yang, J.; Cremar, L. D.; Van Gough, D.; Potisek, S. L.; Ong, M. T.; Braun, P. V; Martínez, T. J.; White, S. R.; Moore, J. S.; Sottos, N. R. *Nature* **2009**, *459* (7243), 68–72.

(10) Jakobs, R. T. M.; Ma, S.; Sijbesma, R. P. *ACS Macro Lett.* **2013**, *2* (7), 613–616.

(11) Lenhardt, J. M.; Black, A. L.; Craig, S. L. *J. Am. Chem. Soc.* **2009**, *131* (31), 10818–10819.

(12) Diesendruck, C. E.; Steinberg, B. D.; Sugai, N.; Silberstein, M. N.; Sottos, N. R.; White, S. R.; Braun, P. V; Moore, J. S. *J. Am. Chem. Soc.* **2012**, *134* (30), 12446–12449.

(13) Peterson, G. I.; Larsen, M. B.; Ganter, M. A.; Storti, D. W.; Boydston, A. J. *ACS Appl. Mater. Interfaces* **2015**, *7* (1), 577–583.

(14) Li, M.; Zhang, Q.; Zhu, S. *Polymer.* **2016**, *99*, 521–528.

Chapter 2 Literature Review

This chapter is based on the review article “Let Spriopyran Help Polymers Feel Force!” which is under submission. To avoid the significant repetitions, the introduction and the future prospects are not included in this section. Minor changes have been made to ensure the consistency of the literature review. This chapter gives a comprehensive review of SP mechanochemistry and its applications into polymers.

Author Contributions

Meng Li and Prof. Shiping Zhu generated the idea of summarizing literature based on SP mechanophore into a review paper. Meng Li finished the manuscript draft of this review, revised by Dr. Yinning Zhou and Prof. Shiping Zhu. Dr. Qi Zhang also provided valuable inputs into the manuscript.

2.1 Abstract

Mechanoresponsive polymers have garnered significant attention in recent years, due to the great potential application in stress/strain sensing and damage warning. Several reviews of mechanochemistry have been published in recent years. In this review, we mainly focus on the most established mechanophore, spiropyran, from an engineering perspective. We present a workflow for SP mechanochemistry, the application in various polymers and impacting factors as

well as characterization techniques. Current limitations and future research directions are briefly highlighted in the end. This review aims to offer deep insight into polymer mechanochemistry and providing study approaches for the other mechanophores.

2.2 Role of SP Mechanophore in Polymers

SP is an effective mechanophore by giving off vibrant colorations and fluorescence upon mechanical loadings. When the C-O bond is cleaved by mechanical force, SP is activated to MC. The closed SP is colorless/yellow and nonfluorescent, whereas the open MC form is blue/red/purple and fluorescent, as shown in Figure 1-1a. To incorporate SP mechanophore into various polymer systems via different chemistries and mechanisms, SP molecule has been functionalized with different functional groups, such as hydroxyl group, α-bromoisobutyryl group, methylacryloyl ester group, and bis-alkene group, as shown in Figure 1-1b. Generally, SP moiety is covalently incorporated into polymers as initiator, cross-linker or monomer.

Initiator. Hydroxyl-containing SP was used as an initiator for ring opening polymerization (ROP) of caprolactone (CL).[1] Functionalized with α-bromoisobutyryl group, SP was applied as atom-transfer radical-polymerization (ATRP) initiator for various polymer systems, including polyacrylates and block copolymers.[2-4]

Monomer. Hydroxyl-containing SP can also be employed as a monomer in step growth polymerization to obtain polyurethane (PU). The step growth polymerization enables controlling mechanophore concentration independently of molecular weight or cross-linking density.[5]

Cross-linker. As a cross-linker for polyacrylates, only a small amount of methylacryloyl ester-containing SP is needed as a stress/strain indicator, with ethylene glycol dimethacrylate (EGDMA) and poly (ethylene glycol) dimethacrylate (PEG) usually added as primary cross-linkers. It is not only because SP mechanophore cross-linker is more complicated to synthesize than the commercially available EGDMA or PEG, but also because only a small amount is sufficient for obvious visual color changing.[2,6] Methylacryloyl ester-containing SP can also be used as co-cross-linker for polyolefins during curing.[7] SP functionalized with bis-alkene group can serve as cross-linker for poly(dimethylsiloxane) (PDMS) system.[8]

2.3 Applied SP Mechanochemistry in Polymers

SP mechanochemistry has been intensively studied in various states of polymers, including bulk polymers, polymer solutions and polymer gels. Based on polymer chemistry, various types of polymers have been chosen for SP mechanophore incorporation, including polyacrylates, polyester, polyolefins, PU, PDMS, and polyamide.

2.3.1 SP-Containing Polymers of Various States

2.3.1.1 Solid Polymers

Mechanoactivation of SP in solid polymeric materials was pioneered by Moore et al. in 2009. SP was covalently incorporated into the backbone of poly(methyl methacrylate) (PMMA) and poly(methacrylate) (PMA) as initiator via ATRP and also into lightly cross-linked PMMA and PMA as a secondary cross-linker via free radical polymerization (FRP). Mechanoactivation of SP in PMA and PMMA bulk polymers was demonstrated via tension and compression, as shown in Figure 2-1a.[2] However, the mechanoactivation in the glassy PMMA under tension test was difficult to achieve. The mechanoactivation in glassy polymers requires large deformation, following the yield point. The glassy polymers usually fail at the low strain before mechanoactivation occurs. Alternative activation methods are called for to apply higher stress to the material for activation before failure. Moore's group later demonstrated that SP-containing PMMA could be mechanically activated by shearing (monotonic torsion) and acoustic sound waves, presented in Figure 2-1b and c.[6,9]

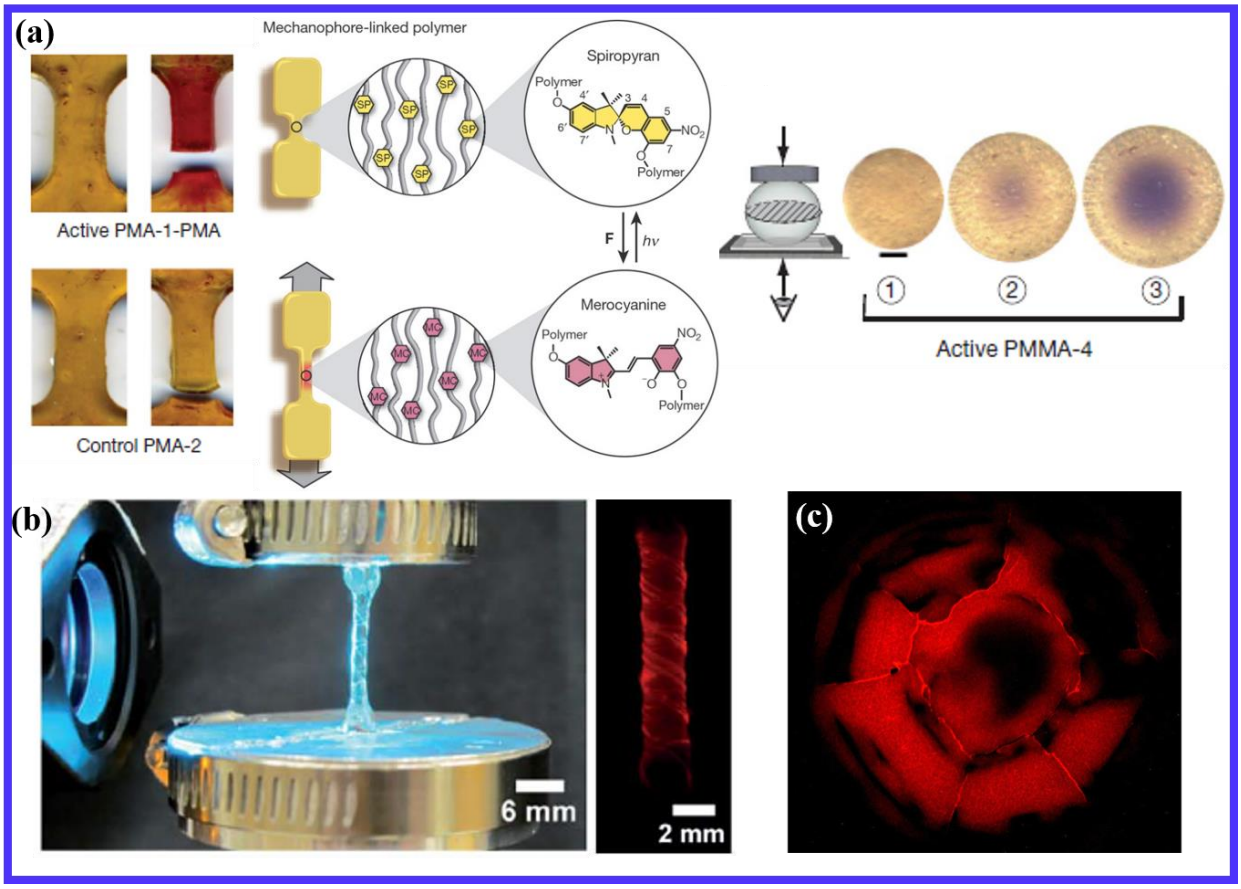

Figure 2-1 Mechanical force induced activation of SP in solid polymers. (a) Mechanoactivation of SP in bulk PMA specimens under stretching and bulk PMMA beads under compression.[2] Copyright 2009, reproduced with the permission from Nature Publishing Group. (b) Mechanoactivation of SP in lightly cross-linked PMMA via torsion and characterized by fluorescence imaging.[6] Copyright 2011, reproduced with the permission from Royal Society of Chemistry. (c) Mechanoactivation of SP-linked polystyrene (PS) films subjected to laser-generated high amplitude acoustic pulses.[9] Copyright 2014, reproduced with the permission from American Chemical Society.

2.3.1.2 Dilute Polymer Solutions

Ultrasonication induced elongation flow can stretch polymer chains and transduce mechanical forces through acoustic cavitation, which describes the sonication induced nucleation, growth and collapse of bubbles in liquid.[10-13] The collapse of bubbles leads to solvodynamic shear forces on the polymer chains, because the chain ends are pulled to the voids created by the imploding bubbles. The forces developed on polymer chains can contribute to mechanoactivation of SP moiety in the backbone. Polymer chains need to be sufficient long for the mechanical force to be focused onto the SP moiety at the center to be mechanically activated,[13-15] which will be introduced in details in Section 4.

Recently, Du's group revealed that mechanoactivation of SP was significantly enhanced in micelles compared to the dissolved counterparts. Self-assembled of poly(*tert*-butyl acrylate-*b*-*N*-isopropylacrylamide) with SP molecule at the center of (SP-(*t*-BA_{88}-b-$NIPAM_{62}$)$_2$) in tetrahydrofuran (THF)/water mixture, the micelles exhibited higher fluorescence intensity than those dissolved in THF under sonication,[4] as shown in Figure 2-2. It was attributed to a synergistic effect of the entangled and swollen polymer chains in the micellar cores, and an improved dielectric constant of the local environment of SP moiety in the micelles.

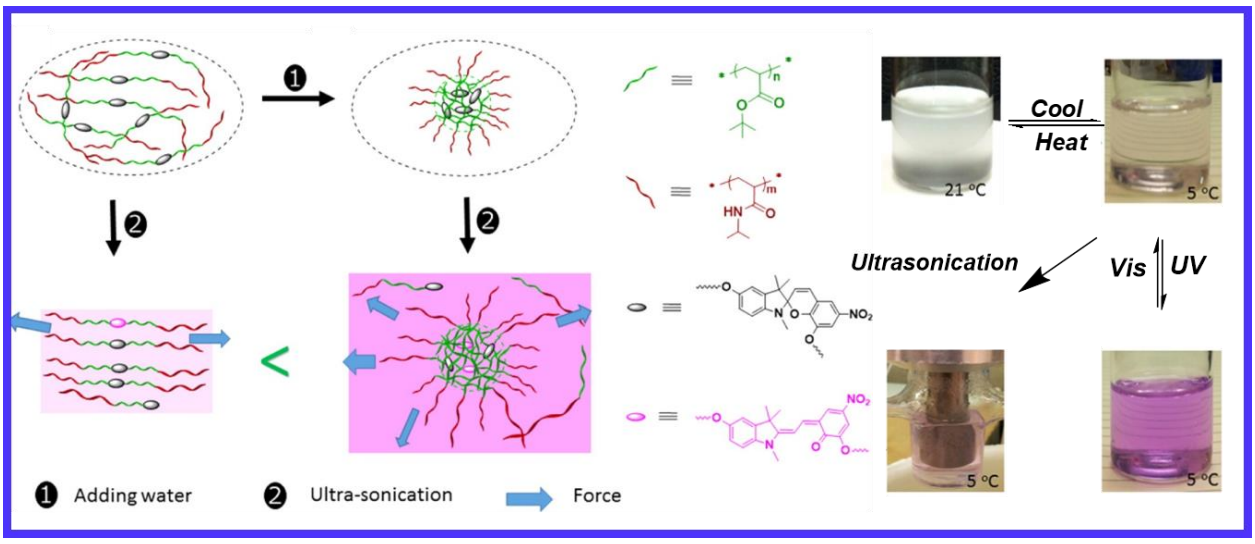

Figure 2-2 Mechanoactivation of SP-(*t*-BA_{88}-b-$NIPAM_{62}$)$_2$ was enhanced within micelles in THF/H_2O mixed solvent compared to those dissolved in THF under sonication.[4] Copyright 2016, reproduced with the permission from American Chemical Society.

2.3.1.3 Polymer Gels

Recently, there has been a new trend in the research of SP mechanoactivation, which is to mechanically activate SP in polymer gels. Swelling force can be used to stimulate the SP mechanoactivation in polymer gels. As is shown in Figure 2-3a, Moore's group initially introduced the concept of solvent-swelling induced mechanoactivation of SP in lightly cross-linked PMMA and demonstrated that swelling force was sufficient to drive the ring-opening reaction of SP-to-MC by excluding the solvent effect.[16] Later, Zhu's group prepared CO_2-switchable poly(2-(diethylamino)ethyl-methacrylate) (PDEA) microgels with SP as cross-linker via soap-free emulsion polymerization and demonstrated CO_2-breathing induced SP mechanoactivation.[17] After

treatment of CO_2, the microgels became swollen due to protonation of the tertiary amine group of PDEA (Figure 2-3b). The swelling force further drove the ring-opening reaction of SP-to-MC in microgels. The emerging purple coloration and fluorescence of the microgel dispersion after CO_2 treatment indicated the activation of MC. Very recently, Zheng's group demonstrated that mechanoactivation of SP in polymer hydrogels could also be achieved directly via tension or compression.[18] A novel poly(acrylamide-*co*-methyl acrylate/spiropyran) (P(AM-*co*-MA/SP)) hydrogel with excellent mechanical properties was developed via micellar-copolymerization method, and mechano-induced color change was demonstrated under a high tensile stress level (tensile stress of 1.45 MPa at the strain of ca. 600%), as shown in Figure 2-3c.

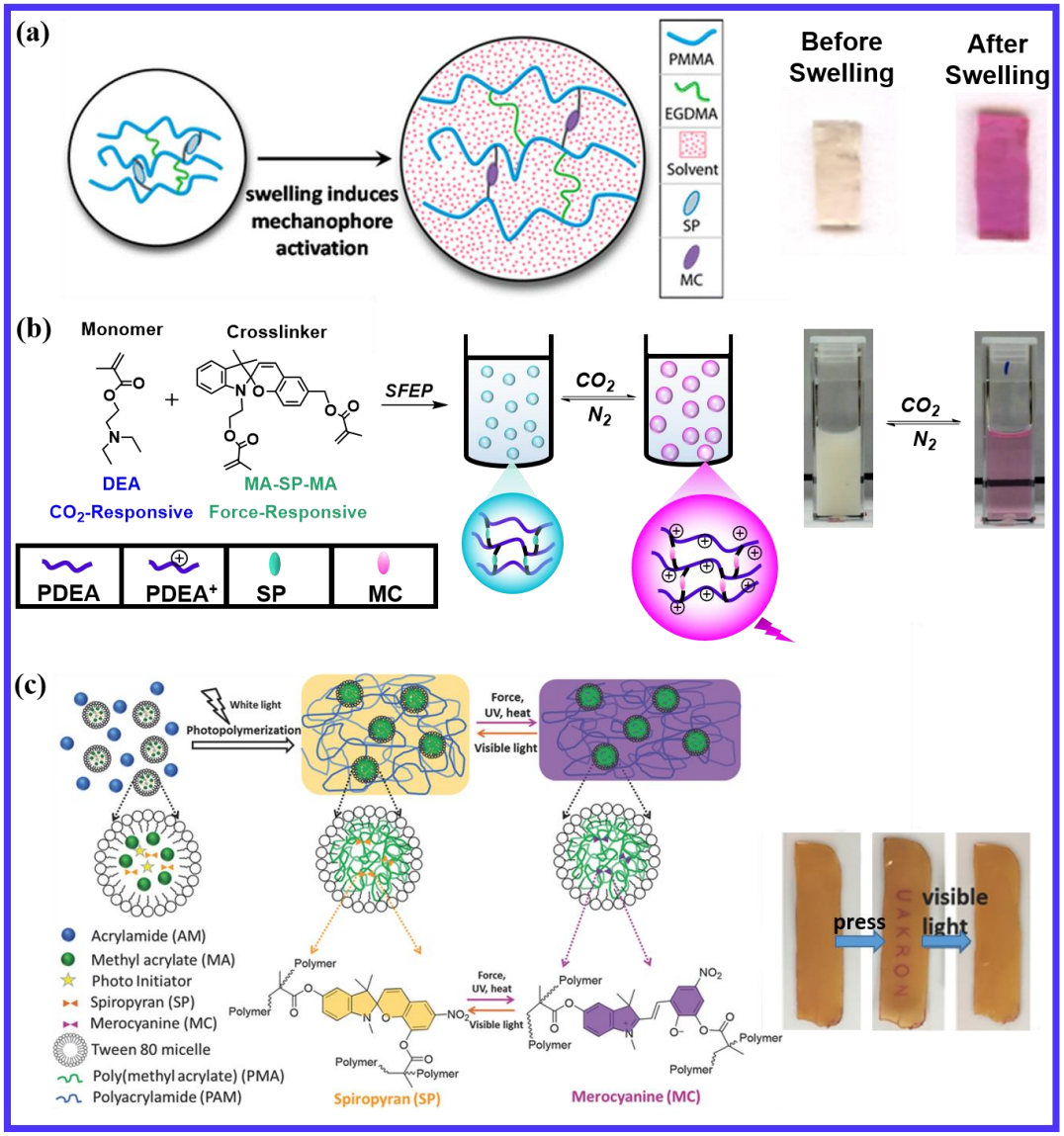

Figure 2-3 SP mechanoactivation within polymer gels. (a) Solvent swelling induced mechanoactivation of SP-cross-linked PMMA gel.[16] Copyright 2014, reproduced with the permission from American Chemical Society. (b) CO_2-breathing induced mechanoactivation of SP within microgel.[17] Copyright 2016, reproduced with the permission from John Wiley and Sons. (c) Stretching/Compression induced activation of SP within stretchable hydrogel.[18] Copyright 2017, reproduced with the permission from John Wiley and Sons.

2.3.2 SP-Containing Polymers of Various Types

2.3.2.1 Polyacrylates

SP mechanophore was initially incorporated into PMMA and PMA as cross-linker or initiator by Moore et al.[2] as shown in Figure 2-1. Thereafter, intensive fundamental studies on SP mechanoactivation behaviors have been carried out based on SP-containing polyacrylates, including PMA, PMMA, poly(ethyl acrylate) (PEA), poly(*n*-butyl acrylate) (PnBA), poly(*iso*-butyl acrylate) (PiBA), poly(*tert*-butyl acrylate) (PtBA), and PDEA, which were prepared via FRP or ATRP.[3,6,9,15,17,19-26] The studies not only enriched fundamental knowledge of mechanochemistry, but also provided valuable information and experience for potentially broadening industrial applications of mechano-responsive polymers. To push one step closer to the real applications, Zhu et al.[27] incorporated SP mechanophore into acrylic latex coating and demonstrated mechanoactivation of latex thin films. Acrylic latexes were prepared using BA and MMA as monomer, vinyltriethoxysilane (VTES) as interparticle cross-linker and SP as intraparticle cross-linker via emulsion polymerization and then cast on to Teflon coated surface to give latex coatings (Figure 2-4). The mechanochromic latex coatings provided good insight into a variety of acrylic latex-based applications of mechanochemistry in adhesives, protective coatings, and paints.

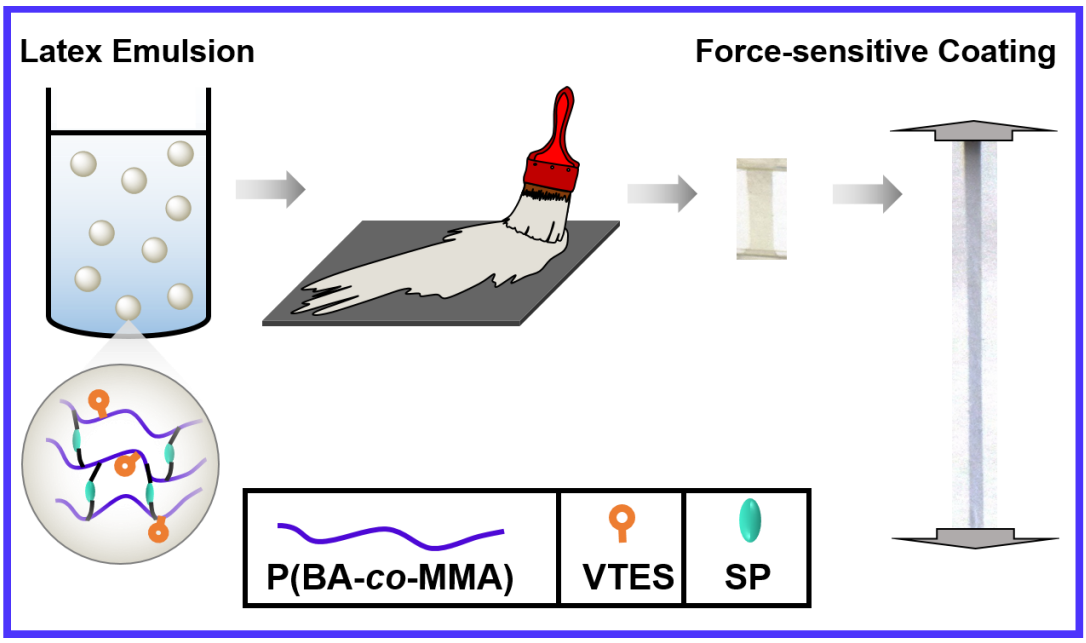

Figure 2-4 Mechanochemically active acrylic latex coating.[27] Copyright 2017, reproduced with the permission from American Chemical Society.

2.3.2.2 Polyesters

As a ductile polyester, polycaprolactone (PCL) has been selected for incorporating SP mechanophore. As is shown in Figure 2-5a, McElhanon et al.[1] synthesized SP-containing PCL with diol-containing SP as initiator via ROP. The mechanoactivation of SP in PCL during straining was illustrated in Figure 2-5b. Boydston's group further advanced the method of preparing SP-containing PCL using 3D printing technology.[28] The computer aided design (CAD) model and the 3D-printed mechanically active PCL are shown in Figure 2-5c-e. Exploiting 3D-printing technology provided the possibility of rapid production of mechanically responsive materials,

which is of great importance for broadening mechanochemistry into potential commercial polymers.

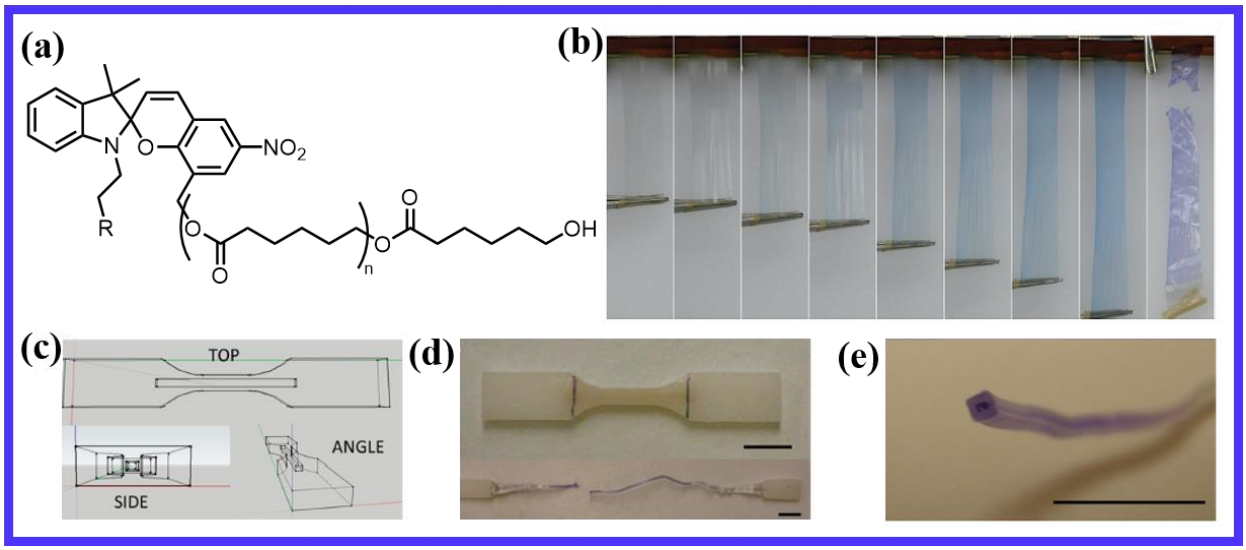

Figure 2-5 Mechanochemically active PCL. (a) Chemical structure of SP-linked PCL;[1] (b) Mechanoactivation of SP in PCL under stretching.[1] Copyright 2010, reproduced with the permission from American Chemical Society. (c-e) CAD model and 3D-printed mechanochemically active PCL.[28] Copyright 2014, reproduced with the permission from American Chemical Society.

2.3.2.3 Polyolefins

As the most commonly and widely used polymer type, polyolefin has more than half of the total polymer consumption in the world. The past decades have witnessed the expanding application of

polyolefins in medical, packaging, sports, cable, wire coatings, etc. Lately, Zhu' group demonstrated the mechanoactivation of SP in polyolefin.[7] As is shown in Figure 2-6, SP was covalently cross-linked into two most widely used commercial polymers, polar poly(ethylene-vinyl acetate) (EVA) and non-polar poly(ethylene octene) (EOC) via free radical mechanism during the curing process, which was carried out under hot press at 160 °C for one hour. The example of color-changing polyolefins in response to mechanical force provided meaningful insights into expanding mechanochemistry into the commercial commodity polymers.

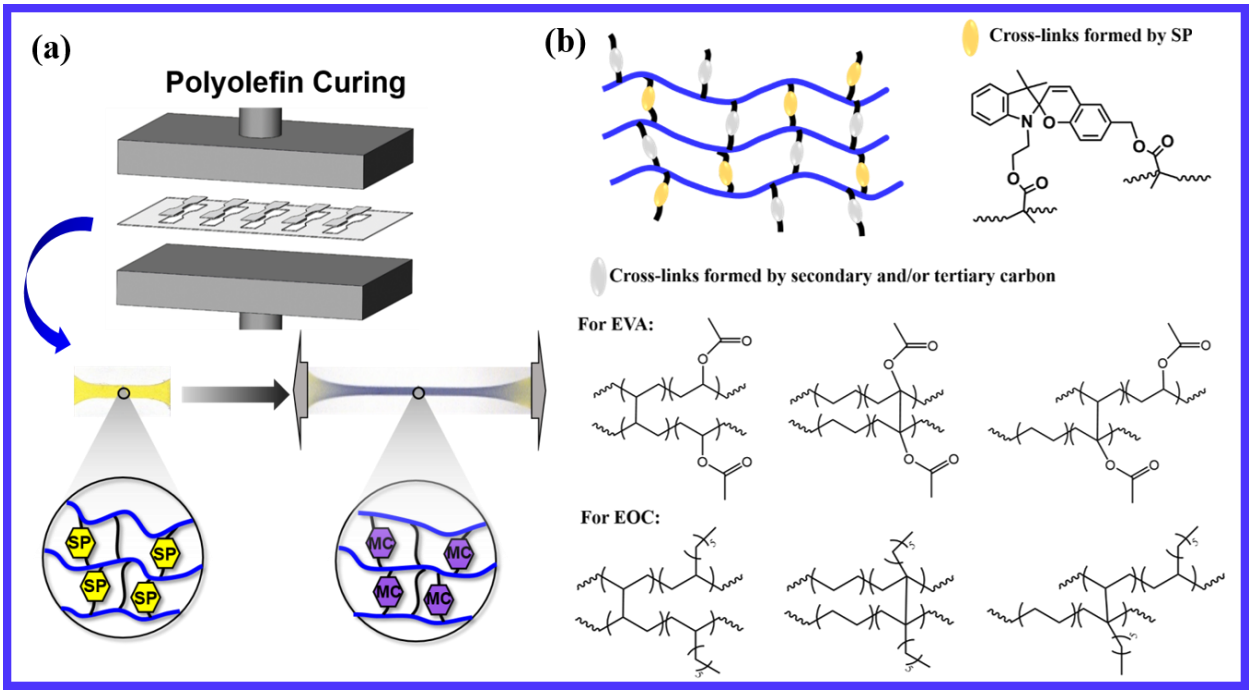

Figure 2-6 (a) Schematic illustration of processing mechanoresponsive polyolefin; (b) Chemical structure of cross-linked EVA and EOC with SP covalently incorporated.[7] Copyright 2017, reproduced with the permission from Elsevier.

2.3.2.4 Polyurethane (PU)

As a ubiquitous engineering polymer, PU exhibits excellent properties, including high abrasion, chemical resistance and advanced mechanical properties. To help PU to feel the force through color changing, Moore et al.[5] synthesized SP-linked PU via step growth polymerization method and demonstrated mechanoactivation of SP-linked PU, as shown in Figure 2-7a. The segmented PU is of particular interest since its elasticity and strength can be well tuned by changing the ratio of hard and soft segments. A typical PU elastomer consists of a polyol, a diisocyanate and a chain extender. The hard segment contains isocyanate and chain extender, and soft segment contains long chain polyols. The advanced engineering properties and adjustable mechanical properties inspired the researchers to incorporate SP mechanophore into segmented PU to study the mechanoactivation behavior in different phases. Moore et al.[29] reported a segmented polyurethane with SP mechanophore in either soft or hard segments (Figure 2-7b).

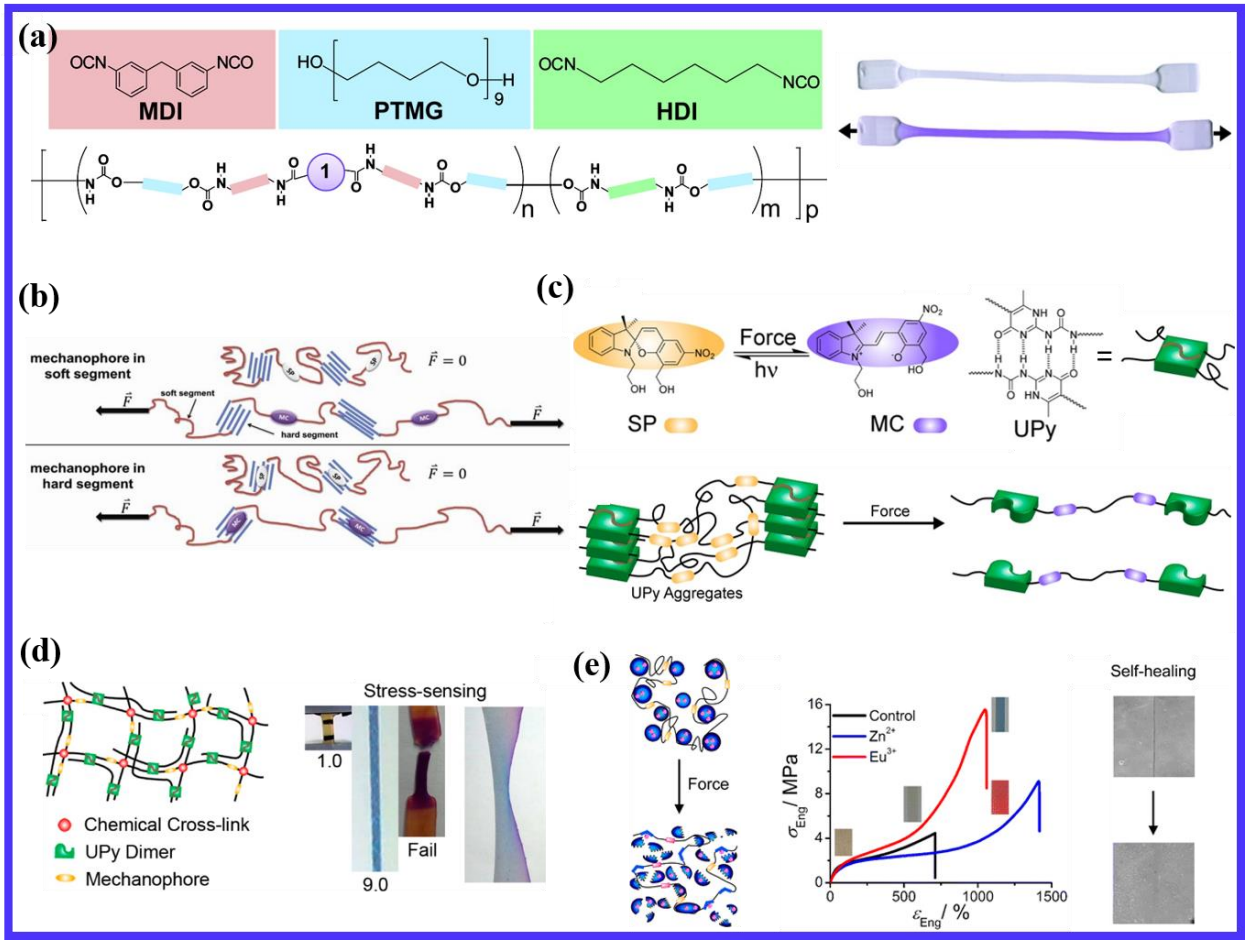

Figure 2-7 Mechanochemically active (a) unsegmented PU.[5] Copyright 2010, reproduced with the permission from American Chemical Society. (b) segmented PU with SP embedded in either soft segments or hard segments.[29] Copyright 2013, reproduced with the permission from American Chemical Society. (c) PU with quadruple hydrogen bonding UPy moieties.[30] Copyright 2013, reproduced with the permission from American Chemical Society. (d) doubly cross-linked PU elastomer (chemical and physical cross-links).[31] Copyright 2014, reproduced with the permission from American Chemical Society. (e) self-healable Zn^{2+}-containing PU.[32] Copyright 2013, reproduced with the permission from American Chemical Society.

To ensure effective mechanoactivation of SP, polymer candidates should possess excellent load-bearing capacity, resilience and defect tolerance. Weng's group has been dedicated to improving the mechanical properties of polymers for better mechanoactivation of SP and have developed several thermoplastic elastomers containing SP moiety. They developed a novel PU containing both covalent SP mechanophore and quadruple hydrogen bonding 2-ureido-4-pyrimidone (UPy) (Figure 2-7c).[30] The effective SP mechanoactivation was due to the superb mechanical properties of the polymer, which was attributed to the fragmentation of hard domains and dissociation of UPy stacks and dimers to dissipate energy during stretching. Later, they also found incorporating UPy at chain ends gave enhanced mechanoactivation of SP, compared to those without UPy.[33] The phenomenon was due to the supramolecular interactions, which could promote chain orientation and strain induced crystallization. Figure 2-7d illustrates the mechanoactivation of SP in a PU elastomer doubly cross-linked by oligo-poly(lactic acid)-capped pentaerythritol (PTT-PLA) as covalent cross-links and UPy as physical cross-links.[31] Weng's group also developed Zn^{2+}-containing polyurethane with SP mechanophore on the backbone, which exhibited damage sensing and self-healing properties (Figure 2-7e).[32] The development of polymers with strong, tough, elastic, self-healing and stress/strain sensing properties is of great importance for fundamental studies and potential applications. Moreover, developing environmentally friendly polymers integrated with damage sensing feature is also one of the most important directions of mechanochemistry. Lately, SP mechanophore was incorporated in waterborne PU, the mechanoactivation of which was investigated by Jia et al.[34]

2.3.2.5 Poly(dimethylsiloxane) (PDMS)

The mechanoactivation of SP in elastomers requires large deformation, which is mostly not recoverable. Craig et al.[8,] reported the covalent incorporation of bis-alkene functionalized SP into the network of PDMS as a cross-linker and characterized the mechanoactivation of SP in PDMS with full shape recovery and high reversibility (Figure 2-8a). The PDMS with repeatable mechanoactivation and full shape recovery renders its possibility in various applications, such as writing panels, soft robots, fluorescent patterning and touch screens (Figure 2-8b-c).[8,35-38]

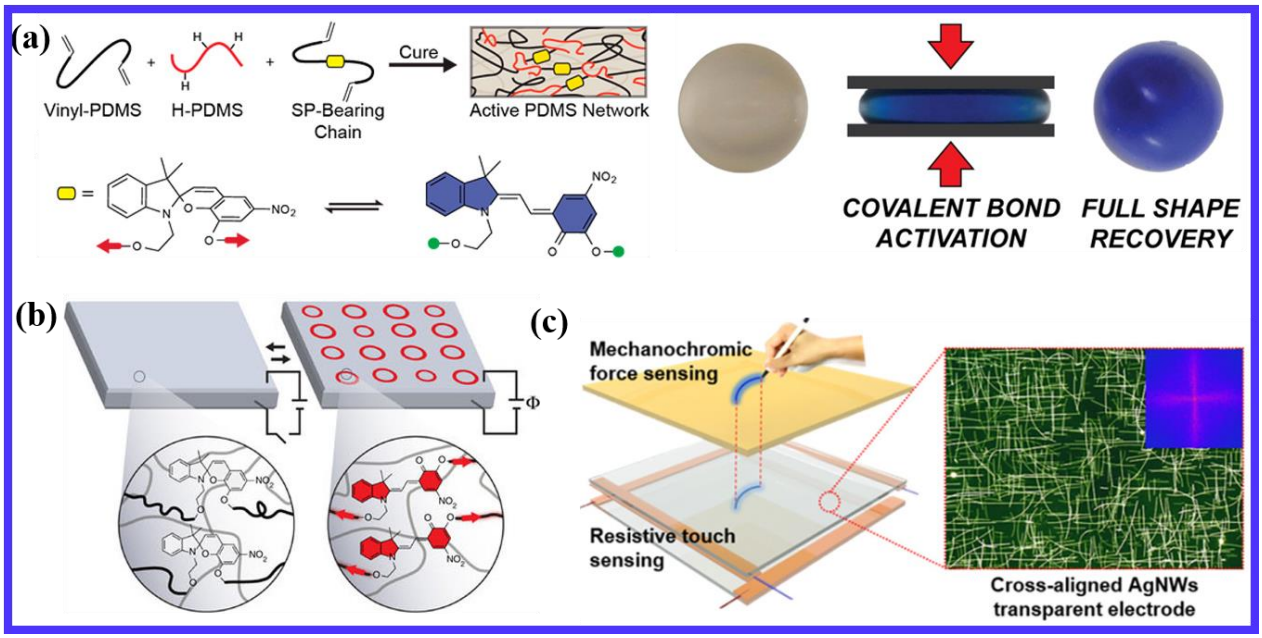

Figure 2-8 Mechanochemically active PDMS. (a) Active PDMS network obtained by incorporating bis-alkene functionalized SP moiety through platinum-catalyzed hydrosilylation, and the mechanoactivation of SP in PDMS with full and repeatable shape recovery.[8] Copyright 2014, reproduced with the permission from American Chemical Society. (b) Electro-mechano-

chemically responsive PDMS for on-demand fluorescent patterning.[38] Copyright 2014, reproduced with the permission from Nature Publishing Group. (c) Force-sensitive mechanochromic touch screen.[37] Copyright 2017, reproduced with the permission from American Chemical Society.

2.3.2.6 Polyamide

The mechanoactivation of SP in polyacrylamide (PAM) is lately achieved by introducing SP-cross-linked PMA microspheres,[18] shown in Figure 2-3c.During gelation process, PAM was connected to SP/PMA microspheres via coupling termination and/or copolymerization of AM and MA. Due to the covalent bonding between PAM and PMA, the macroscopic force on the PAM hydrogel was transmitted into microspheres and eventually to SP molecule for mechanoactivation. Surprisingly, both this work and the mechanoactivation of SP in acrylic latex coating reported by Zhu's group (introduced in 2.3.2.1) revealed a novel design principle, transmission of macroscopic force from outside to inside of SP-containing microgels, which was covalently connected by polymer chains, to mechanically ring open SP to MC.[27] We believe that SP-containing soft microgels can be covalently introduced into a variety of polymers and potentially expand the applications of mechanochemistry.

2.4 Impacting Factors of SP Mechanoactivation

Intensive studies on SP mechanoactivity have been carried out based on SP-containing polymers. In general, most studies focused on the forward reaction of SP-to-MC induced by mechanical loadings and discussed the effect of operating mode (stress/strain, deformation rate, stress

relaxation) and polymer structures (chain length, chain mobility, location of SP in blocks, linking architecture, chain orientation) on SP mechanoactivity. Moreover, the reversion process of MC-to-SP after mechanoactivation has also been investigated in a few literatures. The reversion of MC-to-SP is mainly influenced by chain mobility, residual strain and SP type.

2.4.1 Impacting Factors of Mechanoactivation of SP-to-MC

2.4.1.1 Operation Mode

Stress/Strain. Moore et al.[2] predicted of the selective rupture of spiro C-O bond in SP mechanophore using a modeling method called "COnstrained Geometries simulate External Force" (COGEF) and found that applying force alters the potential energy surface through lowering activation energy barrier to rupture the C-O bond and convert SP to MC. They further confirmed that applying mechanical stress not only lowers activation energy for the forward reaction (SP-to-MC), but also increases the barrier for the reverse reaction (MC-to-SP).[39] Later, Craig et al.[40] studied the force-rate relationship of two SP isomers via single molecule force spectroscopy studies and estimated the threshold stress for SP mechanoactivation on a molecular scale. The threshold stress was approximately 240 pN for ring opening SP1 and 260 pN for SP2 on the time scale of tens of milliseconds, respectively. McElhanon et al.[1] also suggested C-O rupture occurred at a molecular elongation of more than 39% via density functional theory (DFT) and time-dependent DFT calculations.

However, it is difficult to monitor the force felt by SP molecules in the local environment or at a molecular level under the experimental conditions. Sottos et al.[19,20] simulated the local force felt by SP within glassy and rubber polymers via multiscale computational analysis and concluded that microscale force transmission could be interpreted by macroscale stress response. These modeling and theoretical studies laid significant foundations for studying SP mechanoactivation simply using macroscopic stress.

On a macroscopic level of force, when the force is transmitted to C-O bond through polymer chains, SP mechanoactivation starts to occur. There is a threshold stress of SP mechanoactivation, which is the minimum stress to mechanically activate SP in bulk polymers. In literature, the onset of detectable SP activation is usually determined as the moment, at which the activation is significant enough to counteract with the thinning effect.[22] Therefore, critical stress and critical strain for mechanoactivation are defined as the stress and strain when the onset of detectable SP activation occurs. Take mechanoactivation of SP-cross-linked PMMA at 90 °C as an example, the SP-to-MC conversion is minimal in the elastic regime and significantly increases after ca. 10% of strain.[41] Therefore, the critical strain for SP mechanoactivation in this polymer system is estimated to be 10%.

Deformation Rate. The deformation rate has an important effect on the mechanoactivation of SP in three aspects, including SP-to-MC conversion, critical stress for mechanoactivation and time required for initiating activation. (1) SP-to-MC conversion: Higher strain rate leads to higher macroscopic stress, causing greater chain alignment and more force applied across mechanophore. Therefore, greater fluorescence intensity (higher SP-to-MC conversion) was observed for the SP-

linked linear PMA under higher deformation rates.[22] (2) Critical stress: Monotonic torsion experiment of SP-cross-linked PMMA revealed that increasing strain rate increases critical stress for SP to be mechanoactivated by increasing yield stress.[6] The compression test of SP-cross-linked PMMA beads revealed that the threshold stress and yield stress increases linearly with natural log of the strain rate, while the threshold strain remains almost constant.[2] (3) Time for mechanoactivation: Torsional creep experiment of SP-cross-linked PMMA suggested that higher strain rates allow for earlier mechanoactivation. Higher strain rates lead to more force applied across SP moiety, resulting in shorter time required for mechanoactivation initiation. In the torsional creep and monotonic torsion, the time required for mechanoactivation t versus the shearing rate $\dot{r}$ is fitted into a power law relationship, $\mathrm{t} = 0.06 \times \dot{r}^{-0.73}$.[23]

Moreover, when strain rate is increased to a very high level, SP can even be mechanically activated at low strains in glassy polymers. SP could not be mechanically activated in the uniaxial tension test of SP-linked polystyrene (PS) prior to failure (failure stress ca. 60 MPa), while SP mechanoactivation of PS thin film was achieved under laser-generated and high amplitude acoustic pulses, which had a high strain rate (ca. 1×10^7 to $1\times 10^8\ s^{-1}$).[9] The acoustic pulse-generated shockwave mechanically activated SP in PS thin film at a high level of stress but small strains (critical stress ca. 180 MPa). However, high strain rates can lead to an ineligible thermal effect in the glassy polymer. Hooper et al.[42] revealed that thermal effects have a large synergistic effect on the mechanoactivation of SP at high strain rates in solid PMMA. Therefore, the mechanoactivation of SP in glassy polymers under high strain rates cannot be completely distinguished from thermal effects.

However, the time-dependent feature of SP-to-MC reaction is another factor that influences SP mechanoactivation. Silberstein et al.[41] reported a contradictory result with the previously stated evidence. Higher strain rates led to less activation of SP in the uniaxial tension test of SP-cross-linked PMMA at 90 °C. The counterintuitive result was attributed to the time-dependent feature of SP-to-MC reaction feature. Even though lower strain rates result in lower stresses, slower strain rates render more time for SP to convert to MC. The similar trend was also observed in SP-cross-linked polyolefins and acrylic latex coatings.[7,27]

Stress Relaxation. Stress relaxation was mainly affected by stress across mechanophore, time-dependent feature of the SP-to-MC reaction and type of SP mechanophore. (1) Time-dependent feature: A stress relaxation experiment of SP-linked PU was performed by Moore et al.[5] They found that the sample turned increasingly purple when it was held under a constant strain and reached steady-state after 1-2 h. No reversion of MC-to-SP was observed for the SP-linked PU during stress relaxation. Visible light was also applied on the sample when it was held under constant strain. Due to the visible light, MC was reverted to SP, which could be recovered upon removal of the light. All the evidence indicated that SP reached mechanically biased equilibrium when held at constant strain, suggesting that SP-to-MC conversion is a time-dependent process.

(2) Stress-dependent feature: During stress relaxation experiment, however, the stress reduction inevitably affects the SP-to-MC conversion. When the stress is too low, the equilibrium of SP-to-MC conversion is no longer favorable. For the SP-linked PMA, the SP-to-MC conversion continued to proceed until the stress was below ca. 10 MPa.[22] Therefore, the time-dependent

feature only occurs, provided the stress remains high enough. Stress-relaxing experiment of SP-linked PU also confirmed the existence of threshold stress. In the stress relaxing of PU, the SP-to-MC transition rate constants increased linearly with the applied stress, and MC-to-SP reversion rate constants decreased linearly with the stress, when stresses were above the threshold level.[39]

(3) SP type: The type of SP also makes a difference in the SP-MC equilibrium during stress relaxation. Zhu et al.[7] reported fast reversion of SP3-cross-linked polyolefin in the stress relaxation experiment. The plot of the blue intensity vs. time almost overlapped the plot of stress vs. time. Upon held at constant strain, the stress dropped sharply below ca. 9 MPa, probably accounting for the decay of blue coloration. It was also believed that fast reversion might also result from the unique molecular structure of SP3, lacking electron-withdrawing nitro group.

Just as the stress-relaxation has an effect on the mechanical equilibrium of SP and MC, the ring-opening reaction of SP-to-MC also influences the stress relaxation of SP-containing polymer in turn. McElhanon et al.[1] found UV irradiation led to a decrease of 50 kPa in stress of SP-containing PCL, which previously reached a flat baseline of ~ 5.2 MPa in stress under constant 1% of strain (not mechanically activated yet). The light-induced stress relaxation was attributed to lengthening polymer due to the cleavage of C-O bond and ring-opening of SP-to-MC.

2.4.1.2 Polymer Structures and Properties

Chain Length. Polymer chain length plays a crucial role in the ultrasound-induced SP mechanoactivation. Polymer chain length determines whether the ultrasound-induced SP mechanoactivation can occur. Similar to the evidence of other mechanophores activated by sonication reported by Moore, Bielawski and Craig et al.,[14,43-46] Weng et al.[3] found there is a threshold molecular weight for effective mechanoactivation using sonication. SP-linked PnBA was mechanically activated under sonication when M_W > 14 kD, and could not be activated when M_W < 14 kD.

However, which is a better descriptor for mechanical force transduction, molecular weight or polymerization degree? Moore et al.[15] measured the rate constant for the sonication induced SP-to-MC conversion in various polymers, including PMA, PEA and PBA. For the sonication induced mechanoactivation of SP follows the equation, $A_t = B(1 - e^{-kt})$, where A_t is the absorbance at time *t*, *B* is the amplitude and *k* is the rate constant. By plotting *k* as a function of polymerization degree, they revealed that PMA, PEA and PBA all collapsed into a single linear regression, whereas all different linear regressions when *k* was plotted against M_W. The quantitative evidence suggested that polymerization degree is a descriptor of mechanochemical transduction and a determining factor for the mechanoactivity rate, instead of molecular weight.

Chain Mobility. Sufficient chain mobility is required for effective mechanoactivation of SP. Activation of SP in glassy PMMA (T_g = 127 °C) could be achieved at a temperature range of 90-

105 °C or with plasticizer added.[24] At higher temperature than 105 °C, no SP activation was observed because the viscous flow-dominated deformation resulted in lower stress applied on SP moiety. At lower temperature than 90 °C, no mechanoactivation occurred due to insufficient plastic flow. The results suggested that plastic flow is necessary for SP mechanoactivation. Rubber toughening is another alternative to increase plastic deformation to afford SP mechanoactivation in PMMA.[21] Shearing test of cross-linked PMMA also showed that activation of SP occurred after yielding and large plastic flow, suggesting the significance of molecular motion for activation.[6] Torsional creep deformation of SP-cross-linked PMMA coupled with full field fluorescence further confirmed that SP mechanoactivation needs large-scale deformation.[23] It has been concluded the initiation of SP mechanoactivation in glassy polymer occurs after the yield peak even though the stress is much higher than the critical stress to mechanically activate in elastomers.[41]

Location of SP in Blocks. Moore et al.[29] utilized SP mechanophore as a molecular probe of force and orientation by incorporating SP moiety into either soft (SPSS) or hard phase (SPHS) of segmented PU at a low (22 wt%) and a high (40 wt%) content of hard segment. For the PU containing 22 wt% hard segment, the hard and soft segments were miscible, and thus the load was evenly distributed across the hard and soft segments. The same orientation parameters of SP in SPHS and SPSS at 22 wt% hard segment were attributed to the high miscibility of hard and soft segments. However, the phase separation was evident for the PU containing 40 wt% hard segment and SPSS showed higher orientation degree than SPHS due to the higher strain across the soft segments, suggesting that each phase possessed different ability to feel the force.

Linking Architecture. The mechanoactivation behavior of SP also depends on the linking architecture. The mechanoactivation of linear PMMA with SP in the center occurred at much lower strains (strain < 10%) than lightly cross-linked PMMA with SP as a cross-linker (strain > 20%).[24] Moreover, the relative length of primary cross-linker to SP cross-linker also has an effect on SP mechanoactivation behavior. Moore et al.[6] synthesized SP-cross-linked PMMA with three different primary cross-linkers of various length and revealed that the critical stress decreased with longer primary cross-linkers than SP but no further decrease at further length via torsion test.

Chain-orientation. The orientation of SP moiety is of great importance for mechanical activation. The degree of orientation of SP mechanophore-containing linear PMA and PMMA was characterized by an order parameter. When the pre-stretched ratio of SP-embedded PMA was increased, the UV-activated MC gave higher order parameter up to an order of parameter of ca. 0.5.[25] The orientation degree of SP was also higher when activated by mechanical force than UV irradiation. The quantitative results indicated that mechanophores preferentially aligned along the tensile direction. The high orientation degree of SP was also observed in SP-linked PMMA, which was tested under 90 °C and methanol-plasticized, respectively. It was found that the order parameter dropped below 0.1 near failure surface after failure, probably attributed to polymer recoil and relaxation. Therefore, polymer chain alignment plays a significant role in SP mechanoactivation. Using birefringence as an indication of polymer chain alignment, Moore et al.[22] discovered rapid mechanoactivation of SP started when polymer chains aligned along stretching direction. It was also proved that pre-stretching SP-containing polymer before tests improved chain alignment and thus increased mechanoactivation degree.[21]

2.4.2 Impacting Factors of Reversion of MC-to-SP

After the removal of the load, the mechanically activated MC form can be finally reverted to the SP form. The reversion process is a "double-edged sword" for different engineering purposes. On the one hand, we expect SP-containing polymers to have slow reversion so that the persistent coloration will give us warning signals to prevent catastrophic failure from occurring. On the other, the fast recovery of MC-to-SP enables repeatable laboratory experiments within a short period of time and real-time stress sensing purpose. In general, the MC-to-SP reversion mainly depends on the mobility of the local environment, residual strain and SP types.

Mobility. Moore et al.[2] revealed the reversion of MC-to-SP can be affected significantly by the mobility of local environment, reflected by T_g. The reversion of MC-to-SP in elastomeric PMA (T_g = 12 °C) needed 6 h under fluorescent room light, whereas several weeks for glassy PMMA (T_g = 128 °C). For the SP-linked PU ($T_g \approx$ -60 °C) almost disappeared after 1 h in the dark.[5] SP reverts to MC slower in the dark than in the visible light. So it can be concluded that the lower the polymer T_g, the higher mobility the polymer chains, and thus faster reversion of MC-to-SP.

Residual Strain. A comparison of UV-activated and mechanically activated SP-linked PU was carried out by Moore et al.[5] The plot of the fluorescence intensity as a function of time was fitted into a single-exponential decay with a time constant of $\tau \approx 30$ min for the UV-activated sample and $\tau \approx 38$ min for the mechanically activated sample. The slower reversion of mechanoactivated SP in PU was probably attributed to the slow relaxing residual strain remained in the polymer.

SP Type. Zhu et al.[26] discovered that SP3 mechanophore showed a faster reversion than the other two types of SP mechanophore, probably related to the absence of nitro group on 6-position of benzopyran in SP3. The reversion needed ca. 12 min for the SP3-cross-linked PMA to revert to MC, whereas ca. 300 min for the SP2-cross-linked PMA. The plot of the change of green color intensity vs. time was fitted into a sing-exponential decay with a time constant of $\tau \approx 4.7$ min for SP3-cross-linked PMA and $\tau \approx 104$ min for SP2-cross-linked PMA. However, a deep understanding of reversion speed difference between various SP mechanophores must be further explored.

Another noticeable difference on the behavior of color changing upon unloading was also related to SP type. Several studies reported a secondary color change upon relaxation for SP1- and SP2-containing polymers, identified as a transient state.[1,2,5,30,32] The blue/purple transition upon relaxation was probably related to the isomerization about methine bridge.[8] However, no color transition was observed for SP3-containing polymer upon relaxation. SP3-cross-linked PMA turned purple during stretching until failure and persisted after failure.[26] The lack of color transition might also be related to the absence of electron-withdrawing NO_2- group.

2.5 Characterization Methods

The SP is colorless/yellow and non-fluorescent, whereas the activated form, MC state, is purple/blue/red and fluorescent, which can be characterized by RGB analysis, fluorescence imaging and UV-Vis spectroscopy. Each of the methods is introduced as follows.

RGB Analysis The emergence of color is recorded by taking optical images of the SP-containing polymer specimen during stretching or compression experiments, and the optical images are analyzed to obtain the average intensity in Red (R), Green (G) and Blue (B) channel at the region of interest. The RGB ratio can be calculated as rRC=R/(R+G+B), rGC=G/(R+G+B) and rBC=B/(R+G+B), based on Grassmann's law.[47] Mechanoactivation process is directly illustrated via the plot of RGB ratio against strain or stress. As an easy and direct approach to characterize SP mechanoactivation, RGB analysis does not require customized facilities and thus has been widely used in a lot of studies.[2,7,17,26,27]

Fluorescence Imaging In situ fluorescence imaging is achieved by exciting a mechanically activated SP-containing polymer by a 532 nm laser. The resulting fluorescence intensity is recorded and later plotted as a function of stress/strain for mechanoactivation analysis. Compared with RGB analysis, fluorescence imaging appears to be more accurate and utilized extensively in studies.[5,9,23,24,39] Furthermore, fluorescence intensity at various order parameters has been used to investigate the chain orientation feature of SP mechanoactivation.[25,29]

UV-Vis Spectroscopy UV-Vis spectroscopy has been used to study the mechanoactivation of SP-to-MC in bulk polymers via the plot of the intensity at the maximum absorption wavelength (~570 nm) against stress/strain.[5] This method has also been employed in sonication induced mechanoactivation of SP in the polymer solution. Real-time UV-Vis spectroscopy with flow-cell design was used to synchronously quantify the SP-to-MC conversion during sonication of polymers containing SP mechanophore.[15]

2.6 Conclusions

This review has given a comprehensive scope of SP mechanochemistry and its applications in polymers. On one hand, the study of SP mechanochromism provides fundamental knowledge of mechanochemistry, which is of great significance in developing more mechanophores with the desired mechanoresponsiveness, such as stress induced self-strengthening,[48-51] which converts destructive force into constructive functions. On the other hand, the investigation of SP mechanoactivation also gives deep insight and useful guidance in industrial applications in stress/strain sensing and damage warning using SP as a force probe.

2.7 Acknowledgement

The authors sincerely acknowledge the Natural Science and Engineering Research Council (NSERC) (RGPIN-2015-05841) of Canada for supporting this fundamental research through Discovery Grant program. We also thank the Canada Foundation for Innovation (CFI) (200154)

for the equipment and facilities. SZ thanks the Canada Research Chair (CRC) (950-229035) program for supporting his research.

2.8 References

(1) O'Bryan, G.; Wong, B. M.; McElhanon, J. R. *ACS Appl. Mater. Interfaces* **2010**, *2* (6), 1594–1600.

(2) Davis, D. A.; Hamilton, A.; Yang, J.; Cremar, L. D.; Van Gough, D.; Potisek, S. L.; Ong, M. T.; Braun, P. V; Martínez, T. J.; White, S. R.; Moore, J. S.; Sottos, N. R. *Nature* **2009**, *459* (7243), 68–72.

(3) Jiang, S.; Zhang, L.; Xie, T.; Lin, Y.; Zhang, H.; Xu, Y.; Weng, W.; Dai, L. *ACS Macro Lett.* **2013**, *2* (8), 705–709.

(4) Wang, L.-J.; Zhou, X.-J.; Zhang, X.-H.; Du, B.-Y. *Macromolecules* **2016**, *49* (1), 98–104.

(5) Lee, C. K.; Davis, D. A.; White, S. R.; Moore, J. S.; Sottos, N. R.; Braun, P. V. *J. Am. Chem. Soc.* **2010**, *132* (45), 16107–16111.

(6) Kingsbury, C. M.; May, P. A.; Davis, D. A.; White, S. R.; Moore, J. S.; Sottos, N. R.; Ong, M. T.; Braun, P. V.; Martínez, T. J.; White, S. R.; Moore, J. S.; Sottos, N. R.; Luzinov, I.; Minko, S. *J. Mater. Chem.* **2011**, *21* (23), 8381.

(7) Li, M.; Liu, W.; Zhu, S. *Polymer.* **2017**, *112*, 219–227.

(8) Gossweiler, G. R.; Hewage, G. B.; Soriano, G.; Wang, Q.; Welshofer, G. W.; Zhao, X.; Craig, S. L. *ACS Macro Lett.* **2014**, *3*, 216–219.

(9) Grady, M. E.; Beiermann, B. A.; Moore, J. S.; Sottos, N. R. *ACS Appl. Mater. Interfaces* **2014**, *6* (8), 5350–5355.

(10) Suslick, K. S. *Science.* **1990**, *247* (4949), 1439-1445.

(11) Suslick, K. S.; Price, G. J. *Annu. Rev. Mater. Sci.* **1999**, *29* (1), 295–326.

(12) Basedow, A. M.; Ebert, K. H. *Adv. Polym. Sci.* **1977**, *22*, 83–148.

(13) May, P. A.; Moore, J. S. *Chem. Soc. Rev.* **2013**, *42* (18), 7497.

(14) Potisek, S. L.; Davis, D. A.; Sottos, N. R.; White, S. R.; Moore, J. S. *J. Am. Chem. Soc.* **2007**, *129* (45), 13808–13809.

(15) May, P. A.; Munaretto, N. F.; Hamoy, M. B.; Robb, M. J.; Moore, J. S. *ACS Macro Lett.* **2016**, *5* (2), 177–180.

(16) Lee, C. K.; Diesendruck, C. E.; Lu, E.; Pickett, A. N.; May, P. A.; Moore, J. S.; Braun, P. V. *Macromolecules* **2014**, *47* (8), 2690–2694.

(17) Li, M.; Lei, L.; Zhang, Q.; Zhu, S. *Macromol. Rapid Commun.* **2016**, *37* (12), 957–962.

(18) Chen, H.; Yang, F.; Chen, Q.; Zheng, J. *Adv. Mater.* **2017**, 1606900.

(19) Silberstein, M. N.; Min, K.; Cremar, L. D.; Degen, C. M.; Martinez, T. J.; Aluru, N. R.; White, S. R.; Sottos, N. R. *J. Appl. Phys.* **2013**, *114* (2), 23504.

(20) Silberstein, M. N.; Cremar, L. D.; Beiermann, B. A.; Kramer, S. B.; Martinez, T. J.; White, S. R.; Sottos, N. R. *J. Mech. Phys. Solids* **2014**, *63*, 141–153.

(21) Celestine, A.-D. N.; Beiermann, B. A.; May, P. A.; Moore, J. S.; Sottos, N. R.; White, S. R. *Polymer.* **2014**, *55* (16), 4164–4171.

(22) Beiermann, B. A.; Kramer, S. L. B.; May, P. A.; Moore, J. S.; White, S. R.; Sottos, N. R. *Adv. Funct. Mater.* **2014**, *24* (11), 1529–1537.

(23) Degen, C. M.; May, P. A.; Moore, J. S.; White, S. R.; Sottos, N. R. *Macromolecules* **2013**, *46* (22), 8917–8921.

(24) Beiermann, B. A.; Davis, D. A.; Kramer, S. L. B.; Moore, J. S.; Sottos, N. R.; White, S. R. *J. Mater. Chem.* **2011**, *21* (23), 8443.

(25) Beiermann, B. A.; Kramer, S. L. B.; Moore, J. S.; White, S. R.; Sottos, N. R. *ACS Macro Lett.* **2012**, *1* (1), 163–166.

(26) Li, M.; Zhang, Q.; Zhu, S. *Polymer.* **2016**, *99*, 521–528.

(27) Li, M.; Liu, W.; Zhang, Q.; Zhu, S. *ACS Appl. Mater. Interfaces* **2017**, *9* (17), 15156–15163.

(28) Peterson, G. I.; Larsen, M. B.; Ganter, M. A.; Storti, D. W.; Boydston, A. J. *ACS Appl. Mater. Interfaces* **2015**, *7* (1), 577–583.

(29) Lee, C. K.; Beiermann, B. A.; Silberstein, M. N.; Wang, J.; Moore, J. S.; Sottos, N. R.; Braun, P. V. *Macromolecules* **2013**, *46* (10), 3746–3752.

(30) Fang, X.; Zhang, H.; Chen, Y.; Lin, Y.; Xu, Y.; Weng, W. *Macromolecules* **2013**, *46* (16), 6566–6574.

(31) Zhang, H.; Chen, Y.; Lin, Y.; Fang, X.; Xu, Y.; Ruan, Y.; Weng, W. *Macromolecules* **2014**, *47* (19), 6783–6790.

(32) Hong, G.; Zhang, H.; Lin, Y.; Chen, Y.; Xu, Y.; Weng, W.; Xia, H. *Macromolecules* **2013**, *46* (21), 8649–8656.

(33) Chen, Y.; Zhang, H.; Fang, X.; Lin, Y.; Xu, Y.; Weng, W. *ACS Macro Lett.* **2014**, *3* (2), 141–145.

(34) Zhang, Q.; Wang, Y.; Xing, C.; Cai, Y.; Xi, K.; Jia, X. *RSC Adv.* **2017**, *7* (21), 12682–12689.

(35) Brown, C. L.; Barbee, M. H.; Ko, J. H.; Maynard, H. D.; Craig, S. L. *J. Chem. Educ.* **2017**, doi: 10.1021/acs.jchemed.6b00806

(36) Gossweiler, G. R.; Brown, C. L.; Hewage, G. B.; Sapiro-Gheiler, E.; Trautman, W. J.; Welshofer, G. W.; Craig, S. L. *ACS Appl. Mater. Interfaces* **2015**, *7* (40), 22431–22435.

(37) Cho, S.; Kang, S.; Pandya, A.; Shanker, R.; Khan, Z.; Lee, Y.; Park, J.; Craig, S. L.; Ko, H. *ACS Nano* **2017**, *11* (4), 4346–4357.

(38) Wang, Q.; Gossweiler, G. R.; Craig, S. L.; Zhao, X.; Bao, Z. *Nat. Commun.* **2014**, *5*, 4899.

(39) Kim, T. A.; Beiermann, B. A.; White, S. R.; Sottos, N. R. *ACS Macro Lett.* **2016**, *5* (12), 1312–1316.

(40) Gossweiler, G. R.; Kouznetsova, T. B.; Craig, S. L. *J. Am. Chem. Soc.* **2015**, *137* (19), 6148–6151.

(41) Kim, J. W.; Jung, Y.; Coates, G. W.; Silberstein, M. N. *Macromolecules* **2015**, *48* (5), 1335–1342.

(42) Hemmer, J. R.; Smith, P. D.; van Horn, M.; Alnemrat, S.; Mason, B. P.; de Alaniz, J. R.; Osswald, S.; Hooper, J. P. *J. Polym. Sci. Part B Polym. Phys.* **2014**, *52* (20), 1347–1356.

(43) Kean, Z. S.; Black Ramirez, A. L.; Yan, Y.; Craig, S. L. *J. Am. Chem. Soc.* **2012**, *134* (31), 12939–12942.

(44) Wiggins, K. M.; Syrett, J. A.; Haddleton, D. M.; Bielawski, C. W. *J. Am. Chem. Soc.* **2011**, *133* (18), 7180–7189.

(45) Brantley, J. N.; Wiggins, K. M.; Bielawski, C. W. *Science.* **2011**, *333* (6049).

(46) Kryger, M. J.; Munaretto, A. M.; Moore, J. S. *J. Am. Chem. Soc.* **2011**, *133* (46), 18992–18998.

(47) *Colorimetry*; Schanda, J., Ed.; John Wiley & Sons, Inc.: Hoboken, NJ, USA, 2007.

(48) Ramirez, A. L. B.; Kean, Z. S.; Orlicki, J. A.; Champhekar, M.; Elsakr, S. M.; Krause, W. E.; Craig, S. L. *Nat. Chem.* **2013**, *5* (9), 757–761.

(49) Wang, J.; Piskun, I.; Craig, S. L. *ACS Macro Lett.* **2015**, *4* (8), 834–837.

(50) Kean, Z. S.; Niu, Z.; Hewage, G. B.; Rheingold, A. L.; Craig, S. L. *J. Am. Chem. Soc.* **2013**, *135* (36), 13598–13604.

(51) Zhang, H.; Gao, F.; Cao, X.; Li, Y.; Xu, Y.; Weng, W.; Boulatov, R. *Angew. Chemie Int. Ed.* **2016**, *55* (9), 3040–3044.

Chapter 3 Mechanoactivation of Spiropyran in Polymethylacrylate

This chapter is based on the manuscript entitled "Photo-inactive divinyl spiropyran mechanophore cross-linker for real-time stress sensing", which was published on *Polymer*, **2016**, 99, p.521-528 (doi: 10.1016/j.polymer.2016.07.057). The permission of this reproduction is granted by Elsevier. This chapter shows the successful functionalization of the third type of spiropyran mechanophore (SP3) into divinyl cross-linker and the incorporation of SP3 into polymethylacrylate (PMA). The unique responsiveness to mechanical force and UV irradiation has been well investigated.

Author Contributions

Meng Li generated the original idea jointly with Prof. Shiping Zhu and Dr. Qi Zhang. Meng Li carried out all the experiments and prepared the manuscript drafts, which was revised by Prof. Shiping Zhu and Dr. Qi Zhang.

3.1 Abstract

In this work, we study the mechanical activation of a new type of spiropyran mechanophore cross-linker, (1'-(2-(methacryloyloxy)ethyl)-3',3'-dimethylspiro(chromene-2,2'-indolin)-6-yl)methyl methacrylate (MA-SP3-MA) in poly methyl acrylate (PMA), prepared via free radical polymerization. Compared with other SPs, SP3 mechanophore shows two unique features. First, the films exhibit good sensitivity towards mechanical force but not to UV irradiation. Second, the

merocyanine (MC)-to-SP reversion in PMA films after relaxation was very fast. Further, the mechanical activation can be repeated for three times but with diminishing of peak color, caused by the damage of overstrained polymer chains. We also observe that increasing SP content leads to stiffer and more rigid elastomer as well as earlier threshold strain for activation point of SP to MC but has little effect on threshold stress for SP activation. This work offers inspirations towards mechanophore design for polymeric materials to broaden the scope of potential applications of mechanophores.

3.2 Introduction

In the past few decades, we have witnessed the prosperity of smart materials due to their potential applications in many areas.[1] There are numerous types of stimuli-responsive polymers developed in response to changes of various stimuli, such as, pH,[2] temperature,[3] light,[4,5] ultrasound,[6] redox agents,[7,8] and voltage.[9,10]

However, one of the most critical responses is to monitor mechanical failures of structural materials, such as stress fraction, fatigue and hysteresis within polymeric materials by giving off early warnings to avoid further development of catastrophic failure. An appealing effective approach is to incorporate chemically labile functional groups, which are responsive to exogenous mechanical forces ("mechanophore"). The responses can vary based on different polymer mechanochemistry , such as selective scission of polymer chains,[11] release of small molecules,[12]

mechanically induced electrocyclic ring openings,[13,14] and cycloreversion,[15,16] as well as isomerization.[13] A great effort has been made to develop mechano-responsive polymeric systems due to their promising applications in force sensing,[13,17–23] self-reinforcement,[24] mechano-catalysis,[25] small molecule releases for further chemical activation.[26,27]

Optical change in response to mechanical stimulation is most direct and easy way for stress/strain sensing within materials. The mechanically induced signals include color change, fluorescence emission and luminescence.[13,19,28–34] Spiropyrans are great candidates for damage/stress sensing within polymers in terms of mechanochromism. When the force is applied along C-O bond, the closed SP form undergoes electro cyclic ring-opening to yield an open merocyanine (MC) form, which is fluorescent and purple colored. There can be a few possible points for attachment on SP molecules to enable efficient force transduction across the C-O bond. So far there have been three types of SPs reported in the literature, as shown in Figure 3-1.

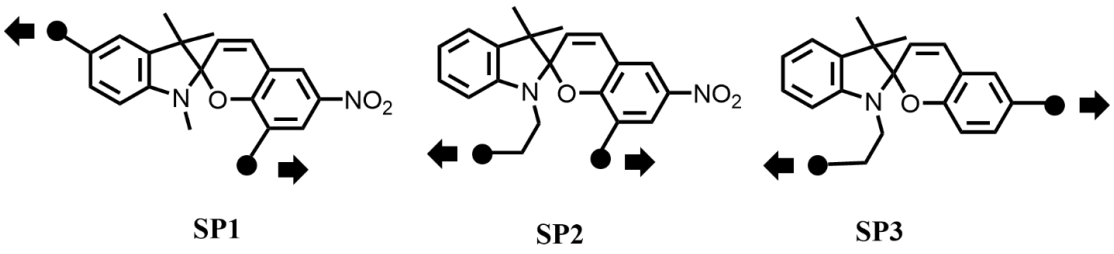

Figure 3-1 Three types of SPs employed as mechanophores

SP1 mechanophore was initially incorporated into elastic poly(methyl acrylate), glassy poly(methyl methacrylate), ductile polyurethane by Moore's group.[13,18,19,33,35–39] SP2 mechanophore was introduced into poly (ε-caprolactone),[23] elastic poly (dimethylsiloxane) (PDMS) by Craig's group,[21,40,41] and thermoplastic elastomer of polystyrene-*b*-poly(*n*-butylacryalte)-SP-poly(*n*-butylacryalte)-*b*-polystyrene by Weng's group.[42–46] Recently, Boydston et al. reported 3D-printing of mechanochromic poly(ε-caprolactone) polymers containing a new type of spiropyran, SP3.[47] Due to the absence of electron-withdrawing group $–NO_2$ in the spiropyran, SP3 exhibited unique feature of being selectively mechanical sensitive but not UV sensitive, while SP1 and SP2 are dual mechanical- and light-responsive. The sensitivity to mechanical activation but not to UV enabled SP3 sensing forces in outdoor materials without being interfered by exposure of sunlight. Furthermore, it took only 30 s for SP to revert back to MC for SP3 type. The fast recovery provides potentials in real-time monitoring of stress/strain within materials in practice.

However, the application of SP3 mechanophore is limited because diol-containing 2-(6-(hydroxymethyl)-3',3'-dimethylspiro(chromene-2,2'-indolin)-1'-yl)ethanol (HO-SP3-OH**)** can only be applied in step growth polymerization. Herein, we further functionalized it with methacrylol ester to yield divinyl-containing MA-SP3-MA cross-linker, which can be employed in chain growth polymerization, accounting for more than 80% of total polymer products. Although the derivatization of MA-SP3-MA from HO-SP3-OH does not seem to be complicated or fancy in terms of chemistry, this divinyl SP3 cross-linker has a lot to offer in terms of broadening the mechanophore application in polymeric materials, which is the significance of this paper. The

combination of mechanophore and chain growth polymerization will lead to inspirations in engineering applications, such as acrylic and vinyl coatings, polyolefinic plastics and elastomers, and functional gel materials.

As a demonstration in this work, MA-SP3-MA was incorporated as cross-linker in free radical polymerization of methyl acrylate (MA). We also prepared methacrylol ester functionalized SP2 (MA-SP2-MA) for comparison. The responses of SP3- and SP2- containing PMA films were characterized under UV and mechanical activation. To compare the MC-to-SP reversion time of SP3 and SP2 mechanophores, coloration decay as a function of time was studied. Due to the unique features of SP3 over its counterpart, the mechanical activation of SP3-containg PMA films was then focused on and systematically studied. Mechanical activation during tensile tests and cyclic mechanical activation were investigated. To gain an insight of the effect of SP3 content on mechanical activation and mechanical properties of films, a series of detailed studies were conducted. Threshold strain, threshold stress, stress-strain curves, stress at certain strain and glass transition temperature (T_g) were compared among the films containing different SP content.

3.3 Experimental Methods

3.3.1 Chemicals

2, -3, -3-Trimethyl-3*H*-indole (98%, Aldrich), 2-bromoethanol (95%, Aldrich), salicylaldehyde (98%, Aldrich), formaldehyde (37 wt%, Sigma-Aldrich), piperidine (≥ 99.5%, Aldrich), 4-(dimethylamino) pyridine (≥ 99%, Aldrich), triethylamine (≥ 99.5%, Sigma) and methacryloyl chloride (97%, Aldrich) were used as received.

Methyl acrylate (MA, 99%, Aldrich) and ethylene glycol dimethacrylate (EGDMA, 98%, Aldrich) were passed through a short column filled with inhibitor remover to remove monomethyl ether hydroquinone prior to use. Benzoyl peroxide (BPO, ≥ 98%, Sigma-Aldrich), *N*, *N*-dimethylaniline (DMA, ≥ 99.5%, Aldrich) were used as received. All the other chemicals were used directly as received.

3.3.2 Characterization

See the Supporting Information for descriptions of instrumentation of NMR spectra, mass spectrometry, FT-IR (ATR) and DSC.

3.3.3 Polymer preparation

Synthesis of MA-SP3-MA and MA-SP2-MA The SP-based mechanophore MA-SP3-MA were prepared from an esterification of HO-SP3-OH,[47] and (1'-(2-(methacryloyloxy)ethyl)-3',3'-dimethyl-6-nitrospiro(chromene-2,2'-indolin)-8-yl)methyl methacrylate (MA-SP2-MA) from 2-(8-(hydroxymethyl)-3',3'-dimethyl-6-nitrospiro(chromene-2,2'-indolin)-1'-yl)ethanol (HO-SP2-OH).[23] Scheme 3-1 shows the synthetic route. HO-SP3-OH (0.56 g, 1.66 mmol), triethylamine (0.046 g, 0.46 mmol) and 4-dimethylaminopyridin (0.056 g, 0.46 mmol) were dissolved in dry $CHCl_3$ (25 mL) and charged into a round bottom flask with a magnetic stirring bar. A solution of methacryloyl chloride (0.49 g, 4.65 mmol) in $CHCl_3$ (10 mL) was added dropwise for over 15min, when the reaction was kept in ice bath. The reaction was allowed to proceed for 12 h at room temperature. The reaction mixture was then washed by 0.1 M HCl solution, 10 wt% Na_2CO_3 solution, water and brine, successively. The oil phase was collected, dried over anhydrous Na_2SO_4 and concentrated by rotary evaporation. The pure product was obtained by chromatography eluting with ethyl acetate/hexane (1:6) to afford MA-SP3-MA (0.32 g, 40.7%). With the same procedure, we also synthesized MA-SP2-MA (0.43 g, 45.2%).

For **MA-SP3-MA:** ^{1}H NMR (200 MHz, $CDCl_3$) δ 7.24-6.60 (m, 8H), 6.15 (s, 1H), 6.10 (s, 1H), 5.73 (d, J=10.2 Hz, 1H), 5.58 (s, 1H), 5.57 (s, 1H), 5.09 (s, 2H), 4.31 (t, 6.0 Hz, 2H), 3.72-3.23 (m, 2H), 1.97 (s, 3H), 1.93 (s, 3H), 1.31 (s, 3H), 1.16 (s, 3H). ^{13}C NMR (200 MHz, $CDCl_3$) δ 167.31, 154.12, 147.16, 136.28, 130.27, 129.29, 127.86, 127.64, 127.24, 125.80, 121.77, 119.96,

119.36, 118.39, 115.19, 106.52, 104.74, 66.18, 62.97, 52.31, 42.44, 25.86, 20.07, 18.42. MS (ESI): ($M+H^+$) calculated for $C_{29}H_{32}NO_5$, calculated for, 474.2; found, 474.3.

For **MA-SP2-MA**: ^{1}H NMR (200 MHz, $CDCl_3$) δ 8.57 (s, 1H), 8.41 (s, 1H), 7.43-6.82 (m, 5H), 6.59 (s, 1H), 6.58 (s, 1H), 6.27 (s, 1H), 6.01 (s, 1H), 5.75 (d, *J*= 2 Hz, 1H), 5.32 (s, 2H), 3.80 (t, *J*=2.6 Hz, 2H), 3.50 (m, 2H), 2.20 (s, 3H), 2.08 (s, 3H), 1.54 (s, 3H), 1.28 (s, 3H).^{13}C NMR (200 MHz, $CDCl_3$) 166.68, 164.33, 151.31, 150.33, 145.84, 139.38, 135.53, 134.42, 133.04, 132.51, 131.34, 129.28, 127.70, 126.74, 124.59, 123.75, 122.56, 122.40, 121.86, 112.03, 109.44, 63.70, 61.09, 50.05, 48.02, 28.39, 20.29, 18.35. MS (ESI): ($M+H^+$) calculated for $C_{29}H_{31}N_2O_7$, 519.2; found, 519.3. See the Supporting Information for the detailed results of NMR and mass spectrometry.

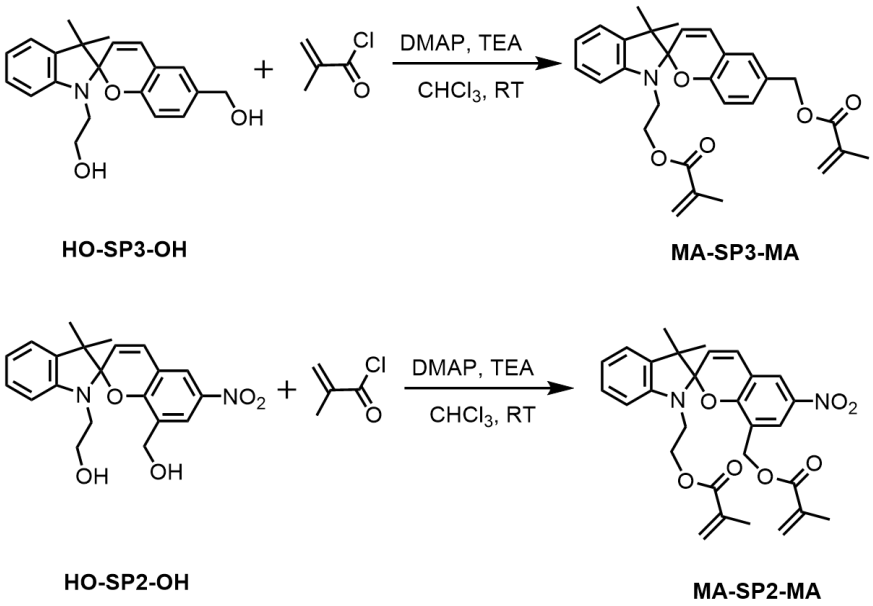

Scheme 3-1 Synthesis of cross-linker MA-SP3-MA and MA-SP2-MA

Free Radical Polymerization of MA with MA-SP-MA Cross-linked poly(methyl acrylate) (PMA) films with varying MA-SP3-MA content were prepared by free radical polymerization. EGDMA was added as additional cross-linker in order to keep the total cross-linker content constant at ~1 mol% with respect to the monomer MA. The MA-SP3-MA contents for the polymerization runs were 0, 0.05, 0.11, 0.27, 0.52 mol%, respectfully. For comparison, a MA-SP2-MA cross-linked PMA film containing 0.27 mol% of MA-SP2-MA was also prepared. To simplify sample names, the type of SP used is indicated by the first letter and the mol% of SP is indicated by the following number (e.g. A52 is comprised of 0.52 mol% of MA-SP3-MA, and B27 is comprised of 0.27 mol% of MA-SP2-MA).

A typical procedure was as follows, BPO (0.062 mmol, 15.02 mg), MA (0.01 mol, 0.86 g), MA-SP3-MA (0.053 mmol, 25 mg) and EGDMA (0.050 mmol, 9.7 mg) were mixed in a vial capped by a rubber stop and the mixture was subsequently flushed with N_2 for 30 min. DMA (4.46 μl, 0.051 mmol) was then added and well mixed. The mixture was then quickly transferred via cannula into a degassed PTFE mold sealed by a rubber cap. After injection, the mold was gently tapped in order to remove trapped bubbles. The viscosity of mixture increased due to gel effect. The mold was kept under the room temperature (~23 °C). After polymerization for more than 24 hours, the polymer films were easily removed from mold and heated overnight at 40 °C in the vacuum oven to remove unreacted residual monomer. The film masses before (M_1) and after vacuum drying (M_2) were used to determine the monomer conversion by gravimetric method. The polymer films

were then put in vials filled with toluene, which were shaken for 24 h to further remove sol polymers (oligomeric, linear and slightly branched chains). The films were then removed from vials, further washed with toluene, dried in an oven and weighed (M_3). The ratio of M_3/M_2 was determined as gel content.

3.3.4 UV Irradiation

The light source utilized in the UV irradiation of polymer films was a 18.4 W hand-held mineral light lamp (Upland, CA 91786, USA). The wavelength for UV irradiation was 366 nm.

3.3.5 Tensile Tests

The films were then cut into smaller strips for mechanical testing. The dimension of the strips was 15 mm × 2 mm × 0.48 mm (length, width and thickness). Uniaxial tensile tests were carried out on TA Instruments Dynamic Mechanical Analyzer 2980 with the loading rate of 6 N/min up to 18 N at room temperature (~23 °C). It is approximately equivalent to 12 mm/min at strain rate. The strain was defined as $\varepsilon=(L-L_0)/L_0$, where L_0 and L are the distance between grips before and after stretching. The initial grip distance L_0 for all tests was 5.6 mm. An engineering stress was defined as $\sigma_{Eng}=F/S_0$, where F is the loading on the grips and S_0 is the cross section area before stretching. Herein, all the stress discussed is engineering stress unless stated otherwise. Each reported value is based on the average of 5 repeated measurements.

Cyclic uniaxial tensile tests were conducted using an Instron 3366 Benchtop Universal Mechanical Testing system (Instron Corporation; Canton, MA) with the crosshead speed of 30 mm/min up to 62 mm in displacement (270 % strain) at room temperature (~23 °C). The dimension of the strips used for cyclic tensile tests was 50 mm × 2.5 mm × 0.48 mm (length, width and thickness). The initial grip distance L_0 is 23 mm. For all the cycles, the strains were calculated using L_0.

During tensile tests, pictures were captured by NIKON D7000 with a NIKKOR 18-105 mm 1:3.5-5.6G ED lens under ambient room light. The pictures were taken every 5 seconds from the starting point of each tensile test. The RGB value was obtained by analyzing pictures in Adobe Photoshop CS6 Software. RGB ratios of the gauge were calculated by Grassmann's law:[48] rRC=R/(R+G+B), rGC=G/(R+G+B) and rBC=B/(R+G+B). rRC, rGC and rBC are the ratios of red, green and blue component of RGB. R, G and B are the average intensity of red, green and blue channels in the region of interest. The change in of intensity drRC, drGC and drBC was obtained by subtracting the initial rRC, rGC and rBC value, respectively from the ratio at each point.

3.4 Results and Discussion

3.4.1 Polymer Film Preparation

Figure S3-1 ~ S3-6 show NMR results and MS of MA-SP3-MA and its counterpart MA-SP2-MA, which confirmed the successful synthesis. The divinyl monomers were used as cross-linkers for the preparation of PMA films via free radial polymerization. Table 3-1 summarizes the five SP3-containing films with varying SP3 content and one SP2-containing film. In each sample preparation, the combination of SP and EGDMA made up ~1 mol% cross-linker content in the film. For example, A27 film contained 0.27 mol% MA-SP3-MA and 0.75 mol% EGDMA with respect to MA content. In a typical experiment, BPO was added as initiator and DMA was added to lower the initiation temperature.[13] After polymerization for more than 24 hours, all monomer conversions reached higher than 97% and all the runs yielded smooth polymer films with almost no trapped bubbles. The gel contents of polymer films were no less than 97%.

Table 3-1 Composition and conversion data of the synthesized polymer

Polymer	SP Type	SP : EGDMA (mol%:mol%)	Conversion	Gel Content
A0	**MA-SP3-MA**	0:1.0	98%	97%
A5	**MA-SP3-MA**	0.05:0.95	98%	99%
A11	**MA-SP3-MA**	0.11:0.90	97%	99%
A27	**MA-SP3-MA**	0.27:0.75	98%	97%
A52	**MA-SP3-MA**	0.52:0.50	98%	98%
B27	**MA-SP2-MA**	0.27:0.75	98%	98%

3.4.2 Photochromism, Mechanochromism and Kinetics Study

To investigate the photochromism properties, A27 and B27 film were exposed to an irradiation of 366 nm light generated from a UV lamp for 30 min. Optical images were taken after the UV irradiation, shown as Figure 3-2a. For B27, a vibrant purple coloration was observed, while for A27 no color change was observed. The observation agreed with the literature that SP3 type mechanophore had no photochromism.[47] It was attributed to the absence of the electron-withdrawing $–NO_2$ group on 6-position of benzopyran and thus there was only negligible amount of excited MC state induced by UV irradiation.[49–51]

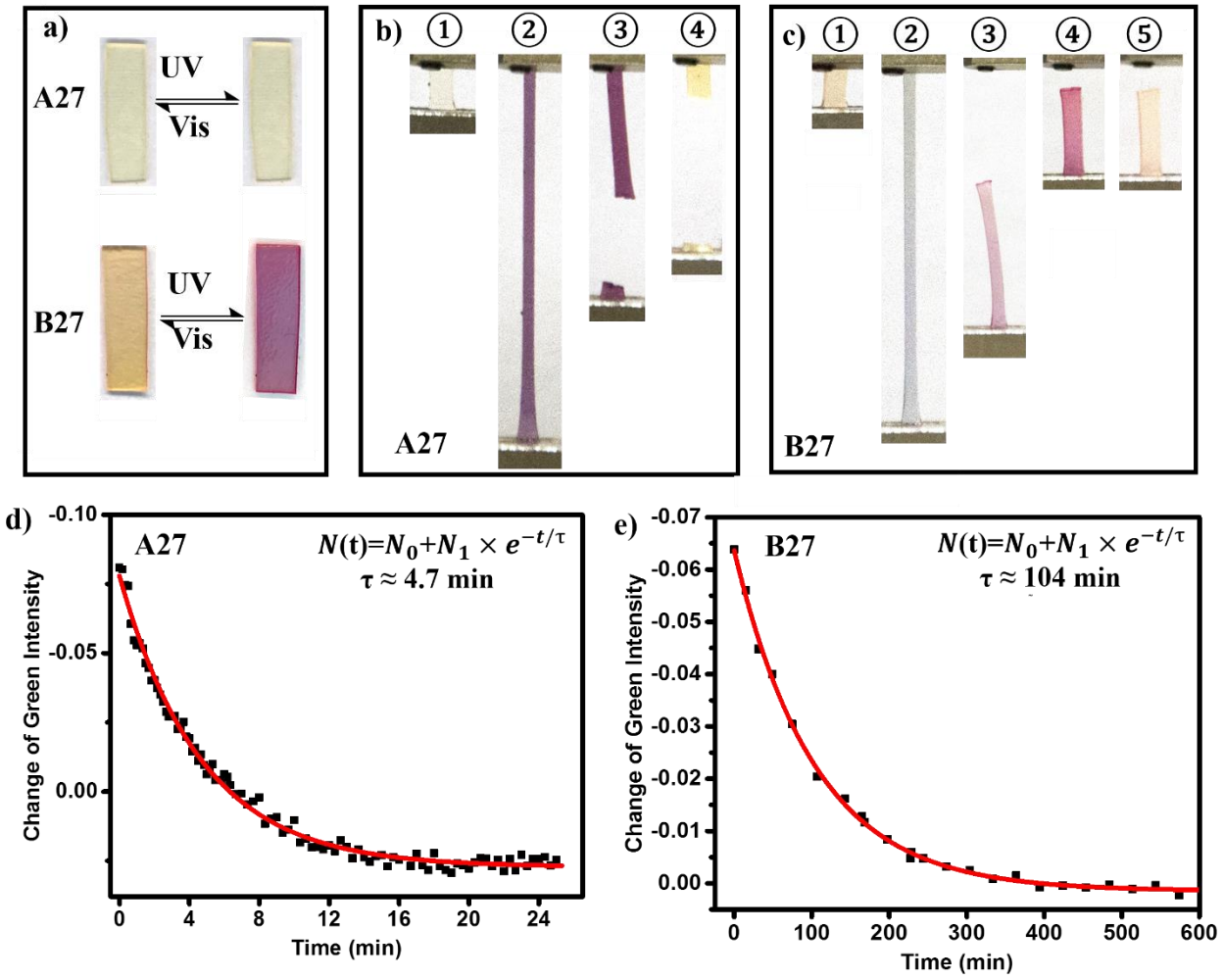

Figure 3-2 a) Optical images of photochromism in A27 and and B27; b) Optical images of A27 film ① before stretching, ② when stretched, ③ right after failure and ④ 12 min after failure; c) Optical images of B27 film ① before stretching, ② when stretched, ③ right after failure, ④ 5 min after failure, ⑤ 300 min after failure; d) Change of green intensity decay of mechanically activated A27 film fitting single exponential decay $N(t)=N_0+N_1e^{-t/\tau}$ with $\tau\approx4.7$ min; e) Change of green intensity decay of mechanically activated B27 film fitting single exponential decay $N(t)=N_0+N_1e^{-t/\tau}$ with $\tau\approx104$ min

Mechanical activation behaviors were studied based on A27 and B27 films. Optical images of the polymer films were taken during uniaxial tensile tests. As shown in Figure 3-2b, the initial A27 film was pale yellow because of the covalently embedded spiropyran.[21] It turned vibrant purple when stretched. The purple coloration gradually deepened during elongation until failure and persisted after failure. The characteristic purple coloration substantiated the mechanical activation of SP-to-MC transition. After failure, the purple intensity of A27 film gradually decreased and completely reversed to initial yellow color in approximately 12 min. For a comparison, as shown in Figure 3-2c, B27 film turned blue when stretched and immediately turned purple upon failure, which agreed with the previous report.[21] The purple coloration deepened when the films relaxed to the original length and reached most intensive after 5 min. Then the purple coloration gradually disappeared and turned to almost initial pale yellow color after around 300 min. The failure strains for A27 and B27 were both ~350%. The failure stresses for A27 and B27 were ~19 MPa and ~20 MPa, respectively. Therefore, the negligible variations of failure strain and stress between the two films were not the main reasons for the big difference in MC-to-SP reversion time. Moreover, all the operations in this work were performed with exposure to the constant ambient fluorescent room light (FRL) at room temperature, unless stated otherwise.

To gain further insight of the time required for the MC-to-SP reversion within A27 and B27 without loading, optical images of the films were taken and utilized for analyzing MC-to-SP transition kinetics. The time upon A27 failure was set to zero. The slight difference in color intensity caused by varying thickness was negligible during 25 min coloration decay because it

took only 30 s for A27 to recover its original length. Optical images of the mechanically activated region were captured every 10 s over 30 min and RGB value was obtained by analyzing the images in Photoshop Software. The mean green intensity ratio was used to analyze MC-to-SP reversion kinetics because it has the largest window of changing among the three channels. The mean green intensity change in the region of interest (drGC) was plotted against time, which fitted to a single exponential decay $N(t)=N_0+N_1e^{-t/\tau}$ with $\tau\approx4.7$ min, shown in Figure 3-2d. The curve shows that under room temperature and FRL, open MC form needed around 12 min to revert back to the closed SP form favourable at equilibrium for SP3 type mechanophore.

The same procedure for analyzing SP2 closing kinetics was also performed on B27 film for comparison. Upon failure, the mechanically induced blue coloration immediately shifted to purple coloration due to the isomerization of the methane bridge of MC.[21] Unlike SP3-containing A27 film, the purple intensity of B27 first underwent a significant increase over 5 min of relaxation and then started to drop, as shown in Figure 3-2c (③, ④ and ⑤). The increase in purple intensity was probably attributed to the gradual accumulation of the MC isomers favourable at equilibrium. The varying thickness during relaxation might also account for the coloration increase because it took around 3 min for B27 film to recover its original length after failure. The time at the highest purple coloration was defined as time zero. The fitted exponential decay curve of drGC over time was similar to that of A27 film, except for a much longer time constant, $\tau\approx104$ min, shown in Figure 3-2e. The curve shows that at least 300 min was required for the open MC form to revert back to the closed SP form under room temperature and FRL for SP2 type mechanophore. Also as a

reference, the SP1-containing PMA needed about 6 h for recovery.[13] The reason for the MC-to-SP reversion rate difference between SP3 and SP2 as well as SP1 is to be explored in our future work.

Clearly, SP3 has two unique features as stress/strain indicator. On the one hand, due to the selectivity towards mechanical activation but no sensitivity to UV irradiation, SP3 cross-linker provides possibilities for stress and damage sensing of polymeric materials in outdoor application. On the other hand, SP3 shows its potential in real-time stress/strain sensing. The most ideal scenario is real-time stress/strain sensing without intensive bright light illumination to "reset", in which purple coloration is induced by loading and the coloration completely disappears upon unloading. Compared to SP1 and SP2, SP3 mechanophore had a much higher rate of recovery without the assistance of bright light illumination. Shortly after relaxation under ambient light, SP3 mechanophore can be reused as a stress/ strain indicator. Considering the advanced properties, SP3-containing PMA films were focused on in this work and their mechanical activation during elongation was further studied in a great detail.

3.4.3 Mechanical Activation vs Stretching

We then characterized the mechanical properties and the mechanochemical reactivity of the polymer films. A27 was taken as an example to present the mechanical activation of SP3. The stress-strain curves of uniaxial stretching of A27 film were recorded by a Dynamic Mechanical Analyzer with the loading rate of 6 N/min up to 18 N at room temperature (~23 °C). In order to

analyze SP activation during elongation, optical images of the A27 film were captured by NIKON D7000 every 5 s during tensile experiments and RGB value was obtained by analyzing images in Photoshop. The representative optical images of A27 film under varying strain were shown in Figure 3-3a. The stress and the change of intensity in three channels (drRC, drGC and drBC) were plotted against strain, shown as Figure 3-3b. The polymer film was deformed up to the failure at ~352% strain. For drRC, it first underwent a slight decrease at lower strain and a big increase at strain hardening region. For drBC, it slowly increased at lower strain and largely increased at strain hardening region. Compared with drRC and drBC, drGC had a larger changing window and thus it was selected to analyze SP-to-MC conversion. The profile of drGC slowly decreased at lower strain and sharply dropped at strain hardening region. Strain threshold of mechanical activation of SP to MC (ε_{sp}) was estimated to be 259%, which was determined by the crossover point of two tangent lines. It shows when A27 film was stretched to more than 259% strain, it started to turn purple, indicating the SP-to-MC transition. During further elongation, the purple coloration deepened. Upon fracture, the purple color persisted.

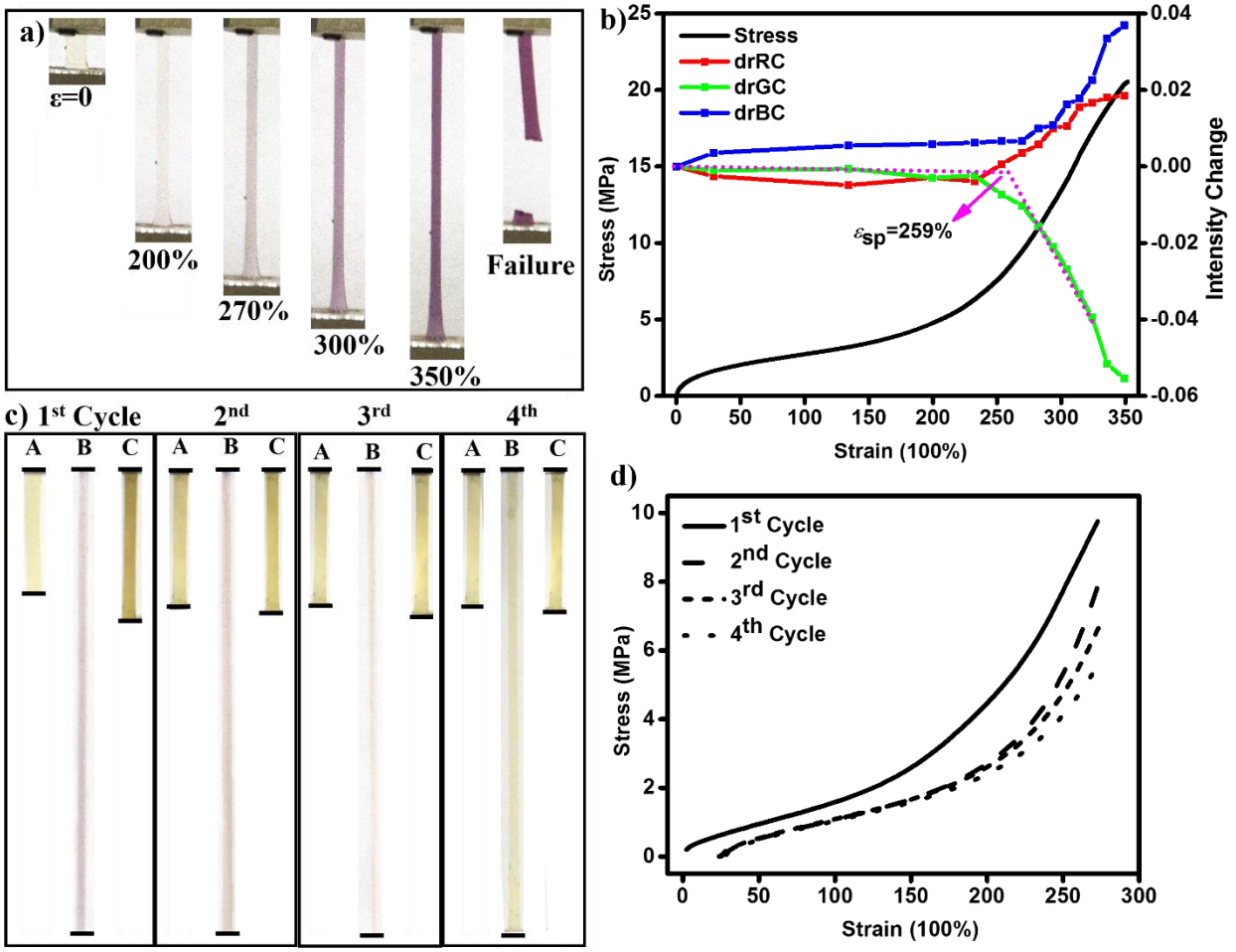

Figure 3-3 a) Optical images of the A27 film during the tensile experiment; b) Stress and change of intensity in red, green and blue channel as a function of strain; c) Optical images of A27 film with 4 cycles of stretching to 270 % strain and relaxing under ambient light. The initial **A27** film was pale yellow (A), turned purple when stretched (B), turned dark yellow in 10 s after released (C). After 10 min of relaxation under ambient conditions, **A27** film was "reset" to pale yellow form; d) Stress-strain curves of 4 cyclic stretching until 270% strain. (Herein, strain was defined as as $\varepsilon=(L-L_0)/L_0$, where L_0 is the initial gauge distance. The starting strain of 2nd cycle is 24% caused by irreversible deformation.)

The mechanical-induced activation of SP in the polymer films was repeated for 4 cycles. Figure 3-3c shows 4 cycles of stretching and relaxation of A27 film. The film showed pale yellow (A), turned purple when stretched (B) and turned to dark yellow in 10 s after unloading (C). The film was "reset" to the original pale yellow after 10 min of relaxation under ambient FRL (2nd cycle A) and reactivated again. Compared to the previous reports on SP1 and SP2,[13,21] it took shorter time for SP3 cross-linker to "reset" from excited MC state to colorless SP form without the assistance of bright light illumination. However, a sharp decrease in purple coloration intensity induced by mechanical activation in each cycle as compared to the first one was observed. In the 4^{th} cyclic activation, there was almost no mechanical induced purple coloration.

To assess whether the diminishing of color was due to photooxidation, the same cyclic activation of A27 film was repeated in the dark. Almost the same extent of purple intensity decrease compared to the initial cycle was observed. Therefore, photooxidation is not the reason to account for the color loss. The thermal MC-to-SP reversion could also be eliminated since the time scale is much longer than the experiment. To gain a deeper insight of possible reasons that contribute to the loss of peak color, the stress-strain curves of 4 cyclic stretching A27 film were plotted in Figure 3-3d. The stress at 270 % strain dropped from 9.6 MPa to 5.3 MPa over the 4 cyclic stretch. It was due to the breaking of the overstressed polymer chains. Hence, it can be concluded that the sharp decrease in peak color was mainly due to the stress decrease caused by permanent damage of overstressed chains. The cyclic stretch of A27 films were repeated for 3 times, in all of which films

were broken at grips during the 5th cyclic stretch. Therefore, further cyclic stretch could not be performed.

3.4.4 Mechanical Activation vs SP content

To confirm that complete consumption of the monomers and cross-linkers, polymers films were put in toluene and shaken for 24 h to extract sol materials, including unreacted monomer, cross-linker, oligomer, linear and slightly branched polymers. The mass differences between before and after washing with toluene were all less than 3%. FTIR spectroscopy of the prepolymerization solution (a mixture of BPO, MA, MA-SP3-MA and DMA) and ATR of the polymer films A0, A5, A11, A27 and A52 were also characterized, as shown in Figure S3-7. It is evident that after polymerization the absorbance band at around 1718 cm^{-1} corresponding to C=C stretching disappeared. Therefore, it can be concluded that MA-SP3-MA act as an effective cross-linker in the polymer networks.

To provide deeper insight, we investigated the effect of SP content incorporated in the polymer film on the mechanical activation. Tensile tests were performed on the five SP3 cross-linked PMA films A0, A5, A11, A27 and A52 and the corresponding optical images during stretching were captured every 5 s for RGB analysis. In all the tensile tests, the purple coloration deepened with the continuous elongation and persisted upon failure. The change of green intensity (drGC) was plotted against strain for five PMA films with varying SP3 content, as shown in Figure 3-4a. The

strain threshold ε_{sp} decreased with the increasing SP content. This trend shows that for the polymer film with a higher SP content, a lower onset strain was required for SP-to-MC transition. Threshold strain ε_{sp} provides direct and helpful engineering information of the starting point of SP-to-MC conversion in the polymers. However, varying threshold strain ε_{sp} does not give clear insight of onset point of SP ring opening in terms of its fundamental mechanism. Then the change of green intensity (drGC) as a function of engineering stress was depicted as shown in Figure 3-4b. Threshold stress σ_{sp} was introduced to describe the stress needed for the onset of SP-to-MC conversion, determined by the similar way to ε_{sp}. Within experimental errors, the threshold stress σ_{sp} of all four PMA films ranged from 6.7 MPa to 7.1 MPa.

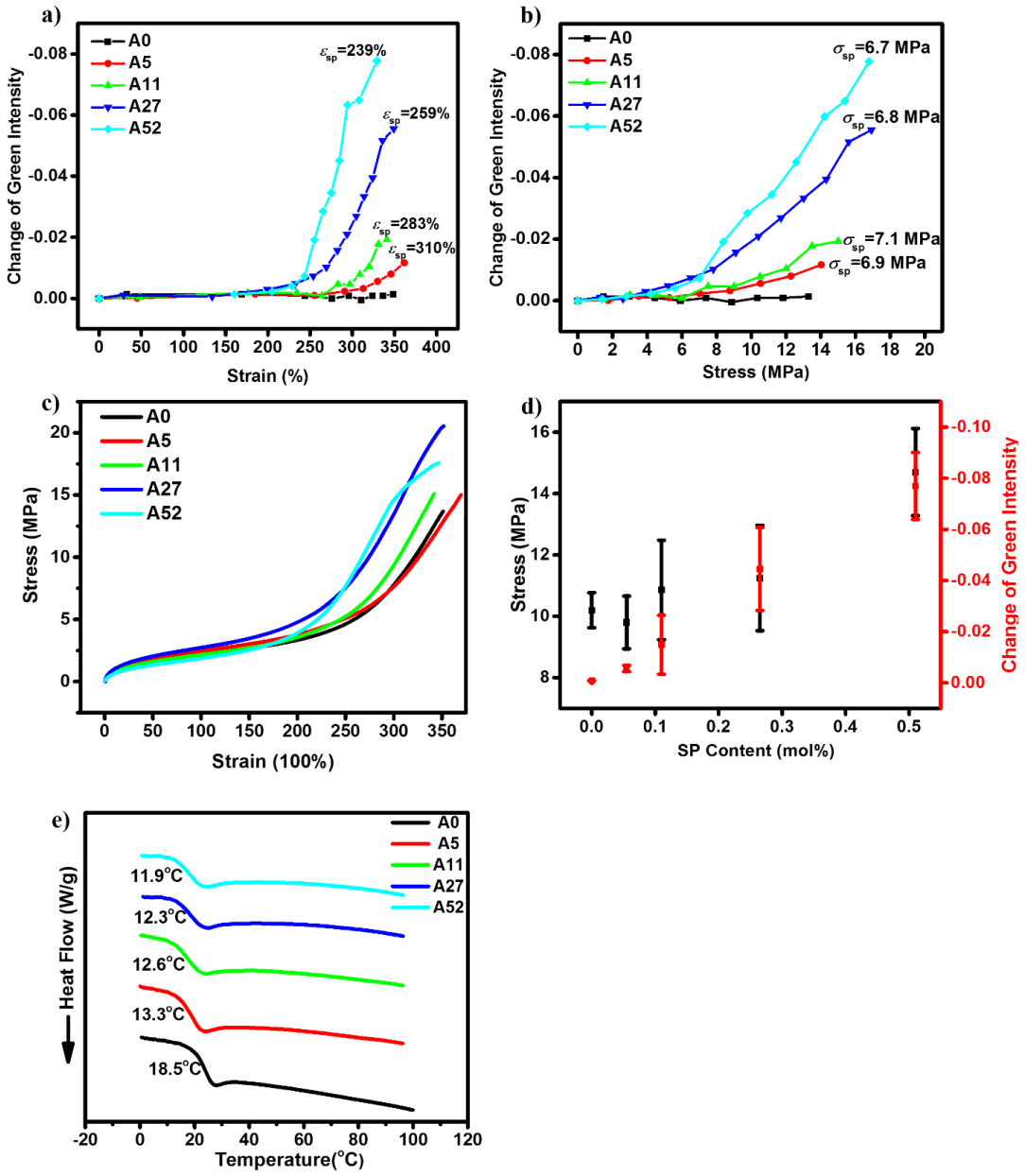

Figure 3-4 a) Change of green intensity as a function of strain for A0-A52; b) Change of green intensity as a function of stress for A0-A52; c) stress as a function of strain for **A0**-**A52** (variability in stress was 0.57~1.72 MPa and variability in drGC was 0.0012~0.016, shown as error bars in the figure); d) Stress and change of green intensity of **A0**-**A52** as a function of SP content at 329% strain; e) DSC data showing the glass transition temperature of **A0**-**A52**.

The stress/strain curves for five PMA films were shown in Figure 3-4c. All the stress/strain curves were similar. However, the stress under certain strain varies among the five samples. Therefore, we studied the mean stress and the mean change of green intensity (drGC) as a function of SP content at a certain strain, as shown in Figure 3-4d. Herein, 329% strain was selected as certain strain, which was after the strain threshold (the highest ε_{sp} is 310%) and before the strain at failure (the lowest strain at failure is 341%) of all samples. The value of stress at 329% strain was ~10 MPa for the PMA films containing lower SP content (0~0.11 mol%), while it increased to ~14.7 MPa for the film containing 0.52 mol% SP. The absolute value of drGC increased with the increasing SP content, suggesting that the higher SP content, the more purple coloration. The purple color intensity was directly proportional to the amount of excited MC state. On one hand, a higher SP content used in preparation of the polymer film could offer more MC state. On the other, a higher SP-to-MC conversion would occur in response to a higher stress of the film with higher SP content. Both factors contributed to the deeper purple coloration in the polymer films with higher SP contents. The higher stress for the films with higher SP content might be attributed to the higher rigidity caused by the bulkier molecular structure of SP in **MA-SP3-MA** than ethylene glycol unit in EGDMA.

To analyze the effect of SP content on T_g of the polymers, DSC of five PMA films were characterized, as shown in Figure 3-4e. There was a decrease of T_g with the increasing SP content. A possible explanation is that T_g is dependent on free volume. The bulky SP groups in the network

prevented close packing of PMA primary chains and thus yielded more free volumes, in comparison to the ethylene glycol group in EGDMA. In other words, SP-crosslinked part is less dense than EGDMA-crosslinked part. Therefore, lower T_g was observed for PMA films containing higher SP content. In general, **MA-SP3-MA** is an effective and efficient cross-linker for free radical polymerization of acrylates with cross-linking.

3.5 Conclusion

In summary, we designed and synthesized the divinyl mechanophore **MA-SP3-MA** ((1'-(2-(methacryloyloxy)ethyl)-3',3'-dimethylspiro(chromene-2,2'-indolin)-6-yl)methyl methacrylate) from its diol derivative **HO-SP3-OH**. It was employed as an effective cross-linker in the free radical polymerization of MA. The polymer samples prepared with **SP3** showed sensitivity towards mechanical activation without the interference of UV irradiation. The MC-to-SP reversion kinetics studies showed that the **SP3**-containing polymer films required only ~12 min for SP to revert to MC, which is 24 times faster than **SP2** type and 29 times faster than **SP1** type. Besides, the mechanical activation of **SP3** in polymers was repeatable for three times with a decrease of peak color caused by the damage of overstressed polymer chains. Moreover, increasing **SP3** content results in more rigid, stiffer, lower T_g of the elastomer and earlier threshold strain for SP activation but has almost no effect on threshold stress for SP activation. The threshold stress to mechanically activate SP to MC ranged from 6.7 MPa to 7.1 MPa.

This work has demonstrated the mechanochromic behavior of the synthesized SP mechanophore cross-linker. It broadens the application of SP mechanophore in chain growth polymerization, accounting for the majority of polymer products. It also provides potentials for applications of real-time stress sensing within outdoor polymeric materials. This work offers inspiration of mechanophore design for polymeric materials.

3.6 Acknowledgement

The authors sincerely acknowledge the Natural Science and Engineering Research Council (NSERC) of Canada for supporting this fundamental research through Discovery Grant program. We also thank the Canada Foundation for Innovation (CFI) for the equipment and facilities. SZ thanks the Canada Research Chair (CRC) program for supporting his research.

3.7 References

(1) Yoshida, M.; Lahann, J. *ACS Nano* **2008**, *2* (6), 1101–1107.

(2) Dai, S.; Ravi, P.; Tam, K. C. *Soft Matter* **2008**, *4* (3), 435.

(3) Lutz, J.-F.; Akdemir, O.; Hoth, A. *J. Am. Chem. Soc.* **2006**, *128* (40), 13046–13047.

(4) Zhao, Y. *Macromolecules* **2012**, *45* (9), 3647–3657.

(5) Yan, Q.; Xin, Y.; Zhou, R.; Yin, Y.; Yuan, J. *Chem. Commun. (Camb).* **2011**, *47* (34), 9594-9596.

(6) Chen, W.; Du, J. *Sci. Rep.* **2013**, *3*, 2162.

(7) Napoli, A.; Valentini, M.; Tirelli, N.; Müller, M.; Hubbell, J. A. *Nat. Mater.* **2004**, *3* (3), 183–189.

(8) Ma, N.; Li, Y.; Xu, H.; Wang, Z.; Zhang, X. *J. Am. Chem. Soc.* **2010**, *132* (2), 442–443.

(9) Peng, L.; Feng, A.; Zhang, H.; Wang, H.; Jian, C.; Liu, B.; Gao, W.; Yuan, J. *Polym. Chem.* **2014**, *5* (5), 1751–1759.

(10) Yan, Q.; Yuan, J.; Cai, Z.; Xin, Y.; Kang, Y.; Yin, Y. *J. Am. Chem. Soc.* **2010**, *132* (27), 9268–9270.

(11) Piermattei, A.; Karthikeyan, S.; Sijbesma, R. P. *Nat. Chem.* **2009**, *1* (2), 133–137.

(12) Berkowski, K. L.; Potisek, S. L.; Hickenboth, C. R.; Moore, J. S. *Macromolecules* **2005**, *38* (22), 8975–8978.

(13) Davis, D. A.; Hamilton, A.; Yang, J.; Cremar, L. D.; Van Gough, D.; Potisek, S. L.; Ong, M. T.; Braun, P. V; Martínez, T. J.; White, S. R.; Moore, J. S.; Sottos, N. R. *Nature* **2009**, *459* (7243), 68–72.

(14) Lenhardt, J. M.; Black, A. L.; Craig, S. L. *J. Am. Chem. Soc.* **2009**, *131* (31), 10818–10819.

(15) Kolb, H. C.; Finn, M. G.; Sharpless, K. B. *Angew. Chem. Int. Ed. Engl.* **2001**, *40* (11), 2004–2021.

(16) Rostovtsev, V. V; Green, L. G.; Fokin, V. V; Sharpless, K. B. *Angew. Chem. Int. Ed. Engl.* **2002**, *41* (14), 2596–2599.

(17) Lee, C. K.; Beiermann, B. A.; Silberstein, M. N.; Wang, J.; Moore, J. S.; Sottos, N. R.; Braun, P. V. *Macromolecules* **2013**, *46* (10), 3746–3752.

(18) Kingsbury, C. M.; May, P. A.; Davis, D. A.; White, S. R.; Moore, J. S.; Sottos, N. R. *J. Mater. Chem.* **2011**, *21* (23), 8381.

(19) Beiermann, B. A.; Davis, D. A.; Kramer, S. L. B.; Moore, J. S.; Sottos, N. R.; White, S. R. *J. Mater. Chem.* **2011**, *21* (23), 8443.

(20) Karthikeyan, S.; Sijbesma, R. P. *Macromolecules* **2009**, *42* (14), 5175–5178.

(21) Gossweiler, G. R.; Hewage, G. B.; Soriano, G.; Wang, Q.; Welshofer, G. W.; Zhao, X.; Craig, S. L. *ACS Macro Lett.* **2014**, *3*, 216–219.

(22) Grady, M. E.; Beiermann, B. A.; Moore, J. S.; Sottos, N. R. *ACS Appl. Mater. Interfaces* **2014**, *6* (8), 5350–5355.

(23) O'Bryan, G.; Wong, B. M.; McElhanon, J. R. *ACS Appl. Mater. Interfaces* **2010**, *2* (6), 1594–1600.

(24) Ramirez, A. L. B.; Kean, Z. S.; Orlicki, J. A.; Champhekar, M.; Elsakr, S. M.; Krause, W. E.; Craig, S. L. *Nat. Chem.* **2013**, *5* (9), 757–761.

(25) Jakobs, R. T. M.; Ma, S.; Sijbesma, R. P. *ACS Macro Lett.* **2013**, *2* (7), 613–616.

(26) Larsen, M. B.; Boydston, A. J. *J. Am. Chem. Soc.* **2013**, *135* (22), 8189–8192.

(27) Diesendruck, C. E.; Steinberg, B. D.; Sugai, N.; Silberstein, M. N.; Sottos, N. R.; White, S. R.; Braun, P. V; Moore, J. S. *J. Am. Chem. Soc.* **2012**, *134* (30), 12446–12449.

(28) Caruso, M. M.; Davis, D. A.; Shen, Q.; Odom, S. A.; Sottos, N. R.; White, S. R.; Moore, J. S. *Chem. Rev.* **2009**, *109* (11), 5755–5798.

(29) Black, A. L.; Lenhardt, J. M.; Craig, S. L. *J. Mater. Chem.* **2011**, *21* (6), 1655–1663.

(30) Beyer, M. K.; Clausen-Schaumann, H. *Chem. Rev.* **2005**, *105* (8), 2921–2948.

(31) Ariga, K.; Mori, T.; Hill, J. P. *Adv. Mater.* **2012**, *24* (2), 158–176.

(32) Chung, C.-M.; Roh, Y.-S.; Cho, S.-Y.; Kim, J.-G. *Chem. Mater.* **2004**, *16* (21), 3982–3984.

(33) Lee, C. K.; Davis, D. A.; White, S. R.; Moore, J. S.; Sottos, N. R.; Braun, P. V. *J. Am. Chem. Soc.* **2010**, *132* (45), 16107–16111.

(34) Chen, Y.; Spiering, a J. H.; Karthikeyan, S.; Peters, G. W. M.; Meijer, E. W.; Sijbesma, R. P. *Nature chemistry*. **2012**, *4*(7), 559–562.

(35) Potisek, S. L.; Davis, D. A.; Sottos, N. R.; White, S. R.; Moore, J. S. *J. Am. Chem. Soc.* **2007**, *129* (45), 13808–13809.

(36) Degen, C. M.; May, P. A.; Moore, J. S.; White, S. R.; Sottos, N. R. *Macromolecules* **2013**, *46* (22), 8917–8921.

(37) Beiermann, B. A.; Kramer, S. L. B.; May, P. A.; Moore, J. S.; White, S. R.; Sottos, N. R. *Adv. Funct. Mater.* **2014**, *24* (11), 1529–1537.

(38) Beiermann, B. A.; Kramer, S. L. B.; Moore, J. S.; White, S. R.; Sottos, N. R. *ACS Macro*

Lett. **2012**, *1* (1), 163–166.

(39) Lee, C. K.; Diesendruck, C. E.; Lu, E.; Pickett, A. N.; May, P. A.; Moore, J. S.; Braun, P. V. *Macromolecules* **2014**, *47* (8), 2690–2694.

(40) Wang, Q.; Gossweiler, G. R.; Craig, S. L.; Zhao, X. *Nat. Commun.* **2014**, *5*, 4899

(41) Gossweiler, G. R.; Brown, C. L.; Hewage, G. B.; Sapiro-Gheiler, E.; Trautman, W. J.; Welshofer, G. W.; Craig, S. L. *ACS Appl. Mater. Interfaces* **2015**, *7* (40), 22431–22435.

(42) Jiang, S.; Zhang, L.; Xie, T.; Lin, Y.; Zhang, H.; Xu, Y.; Weng, W.; Dai, L. *ACS Macro Lett.* **2013**, *2* (8), 705–709.

(43) Hong, G.; Zhang, H.; Lin, Y.; Chen, Y.; Xu, Y.; Weng, W.; Xia, H. *Macromolecules* **2013**, *46* (21), 8649–8656.

(44) Fang, X.; Zhang, H.; Chen, Y.; Lin, Y.; Xu, Y.; Weng, W. *Macromolecules* **2013**, *46* (16), 6566–6574.

(45) Chen, Y.; Zhang, H.; Fang, X.; Lin, Y.; Xu, Y.; Weng, W. *ACS Macro Lett.* **2014**, *3* (2), 141–145.

(46) Zhang, H.; Chen, Y.; Lin, Y.; Fang, X.; Xu, Y.; Ruan, Y.; Weng, W. *Macromolecules* **2014**, *47* (19), 6783–6790.

(47) Peterson, G. I.; Larsen, M. B.; Ganter, M. A.; Storti, D. W.; Boydston, A. J. *ACS Appl. Mater. Interfaces* **2015**, *7* (1), 577–583.

(48) *Colorimetry*; Schanda, J., Ed.; John Wiley & Sons, Inc.: Hoboken, NJ, USA, 2007.

(49) Keum, S.-R.; Lee, K.-B.; Kazmaier, P. M.; Buncel, E. *Tetrahedron Lett.* **1994**, *35* (7), 1015–1018.

(50) Keum Myung-Jin, S.-R. L. *Bull.Korean.Chem. Soc.* **1999**, *20* (12), 1464–1468.

(51) Aramaki, S.; Atkinson, G. H. *J. Am. Chem. Soc.* **1992**, *114* (2), 438–444.

(52) Sheng, Y.; Leszczynski, J.; Garcia, A. A.; Rosario, R.; Gust, D.; Springer, J. *J. Phys. Chem. B* **2004**, *108* (41), 16233–16243.

3.8 Supporting Information

Characterization

Nuclear Magnetic Resonance (NMR): ^{1}H and ^{13}C NMR spectra were recorded on a Bruker AV 200 (200MHz) spectrometer with $CDCl_3$ as the solvent at 293 K. The chemical shifts were referenced to residual peaks of ^{1}H peak at 7.26 ppm and ^{13}C peak at 77.26 ppm, respectively.

Mass Spectrometry (MS): Low-resolution mass spectrometry was performed on Micromass Quattro Ultima (LC-ESI/APCI Triple Quadrupole Mass Spectrometer) with an electrospray ionization (ESI) source.

FTIR Spectroscopy: FTIR spectroscopy (Thermal NICOLET 6700) was utilized to characterize the prepolymer solution and identify the characteristic absorbance band of C=C. For FTIR measurement, a dilute prepolymer (a mixture of BPO, MA, **MA-SP3-MA** and DMA) in chloroform solution (1 wt%) was directly casted on to a KBr disc and dried under infrared lamp. The film was then placed in the specimen holder of the spectrophotometer. Spectrum was recorded by scanning 64 times at a resolution of 2 cm^{-1} using a DTGS (deuteriotriglycine sulfate) KBr Detector. The background was collected and subtracted to remove the water and CO_2 absorbances from the spectrum. The obtained wavenumber ranged from 400 to 4000 cm^{-1}. The FIIR characterization was repeated for 3 times.

Due to elasticity of the obtained polymer films, it was difficult to obtain polymer powder for FTIR characterization. Instead, Attenuated Total Reflectance (ATR, Thermal NICOLET 6700) was employed to characterize polymer films **A0**, **A5**, **A11**, **A27** and **A52** to estimate the consumption of C=C bond. For ATR analysis, the polymer films (~0.5 mm in thickness) were placed directly onto the stage. The spectra were obtained by scanning 64 times at a resolution of 0.5 cm^{-1} with DTGS KBr Detector. Subtracting the background, all the spectra were recorded with a wavenumber from 525 to 4000 cm^{-1}.

Contrast to FTIR sampling by transmission, ATR technique is for characterization of polymer surfaces. The typical penetration depth of the IR beam into the sample ranges from 0.5μm to 5 μm.

To demonstrate the inside of polymer films, ATR characterization of each sample was repeated 3 times with a thin layer cut at cross-section (~0.2 mm in thickness).

Differential Scanning Calorimetry (DSC): TA Instruments Differential Scanning Calorimetry 2910 was employed for thermal analysis of polymer film **A0**, **A5**, **A11**, **A27** and **A52**. For DSC characterization, 6 mg of polymer sample was placed in nonhermetically sealed aluminum pans, which was heated at 10 °C/min from room temperature to 200 °C, held at 200 °C for 0.5min, cooled at 5 °C/min to -20 °C, held at -20 °C for 5 min, and heated to 200 °C at 10 °C/min. For each polymer sample, three DSC spectra were recorded. The obtained data were analyzed by TA Universal Analysis software. Glass transition temperature (T_g) of polymers were determined by the cross point of two tangent lines above and below the transition region.

Supporting Figures

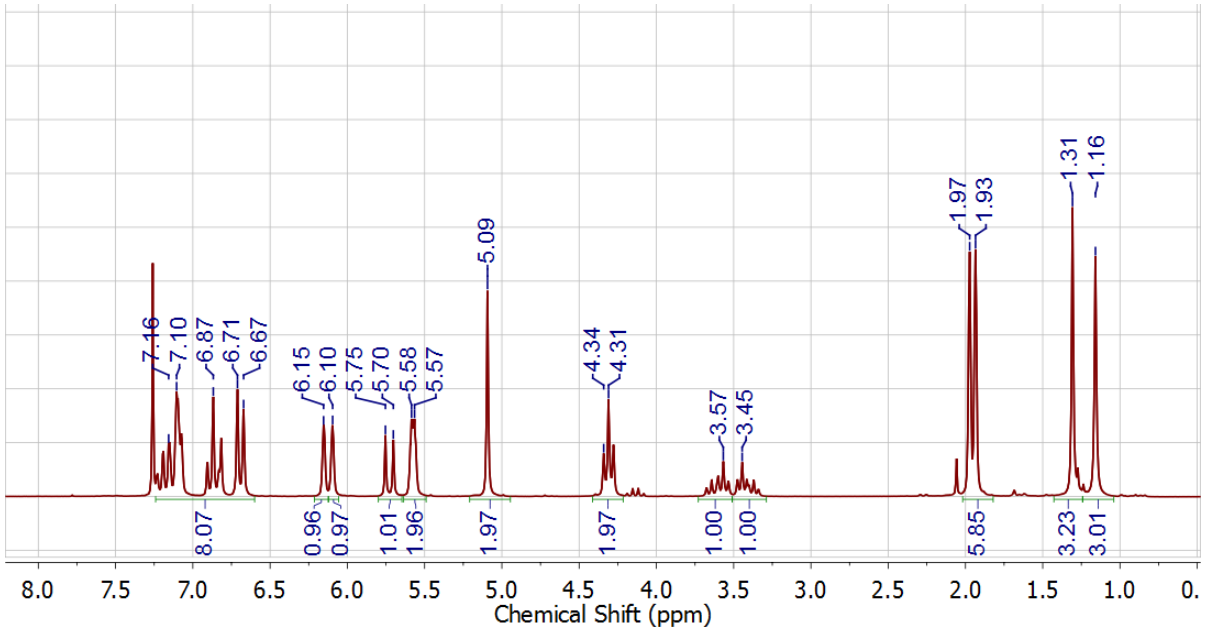

Figure S3-1 ^{1}H NMR spectrum of MA-SP3-MA in $CDCl_3$

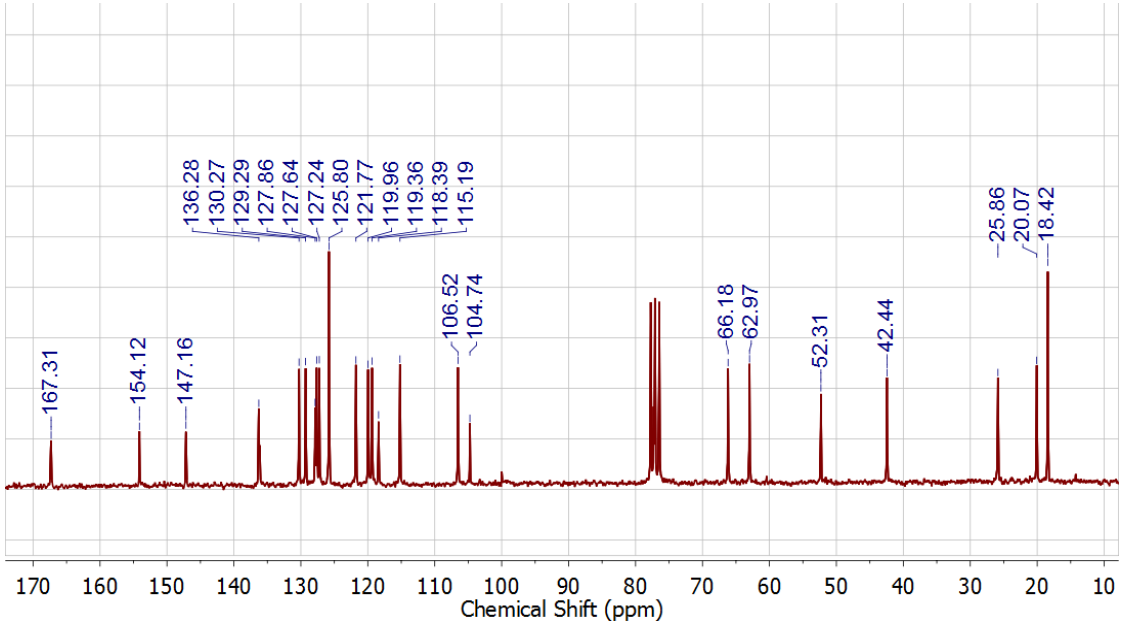

Figure S3-2 ^{13}C NMR spectrum of MA-SP3-MA in CDCl3

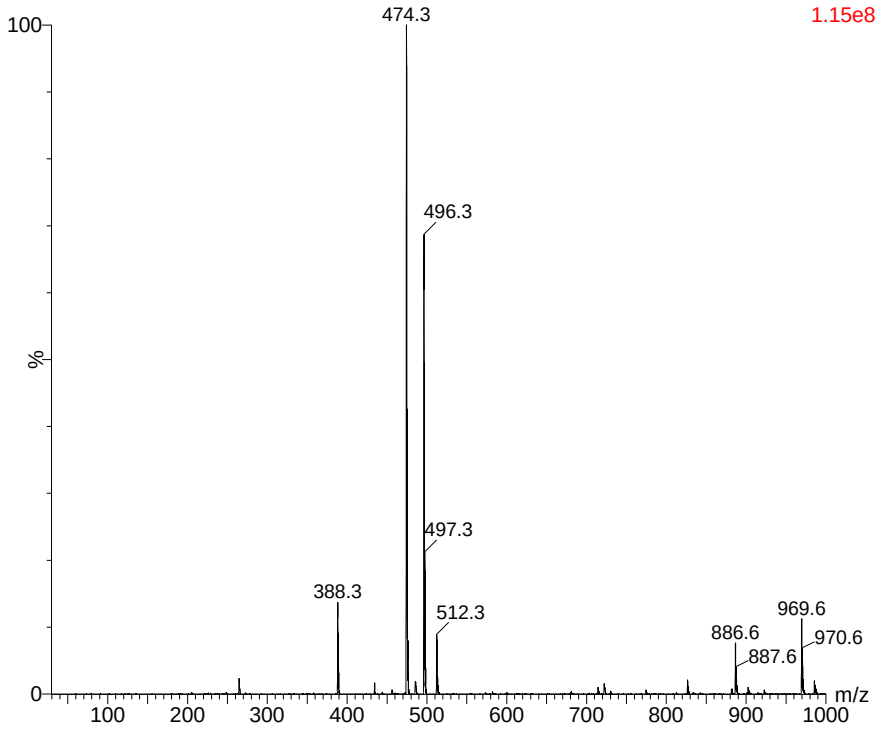

Figure S3-3 Mass spectrometry of MA-SP3-MA

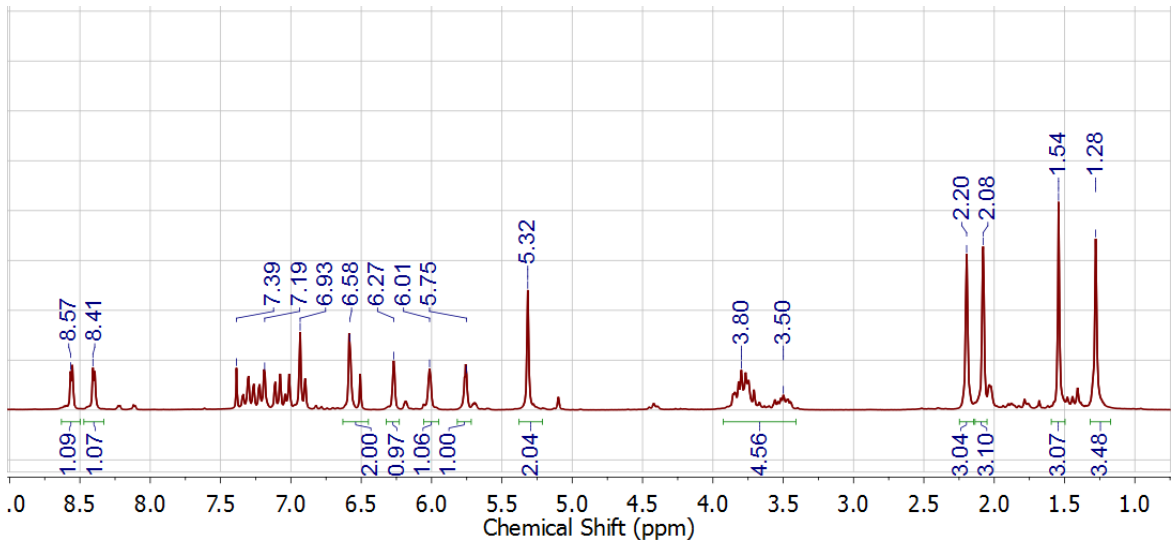

Figure S3-4 ^{1}H NMR spectrum of MA-SP2-MA in $CDCl_3$

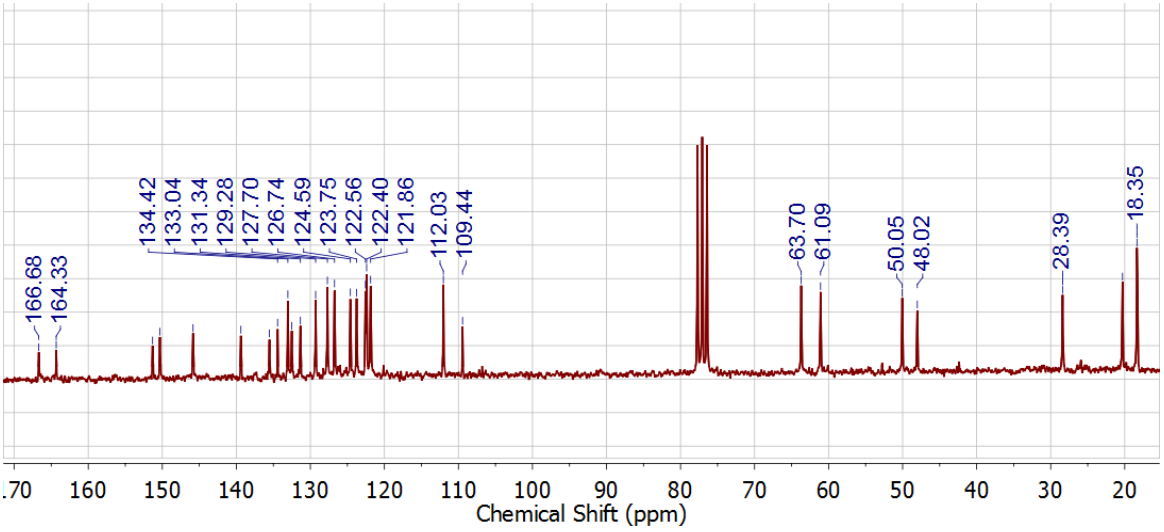

Figure S3-5 ^{13}C NMR spectrum of MA-SP2-MA in $CDCl_3$

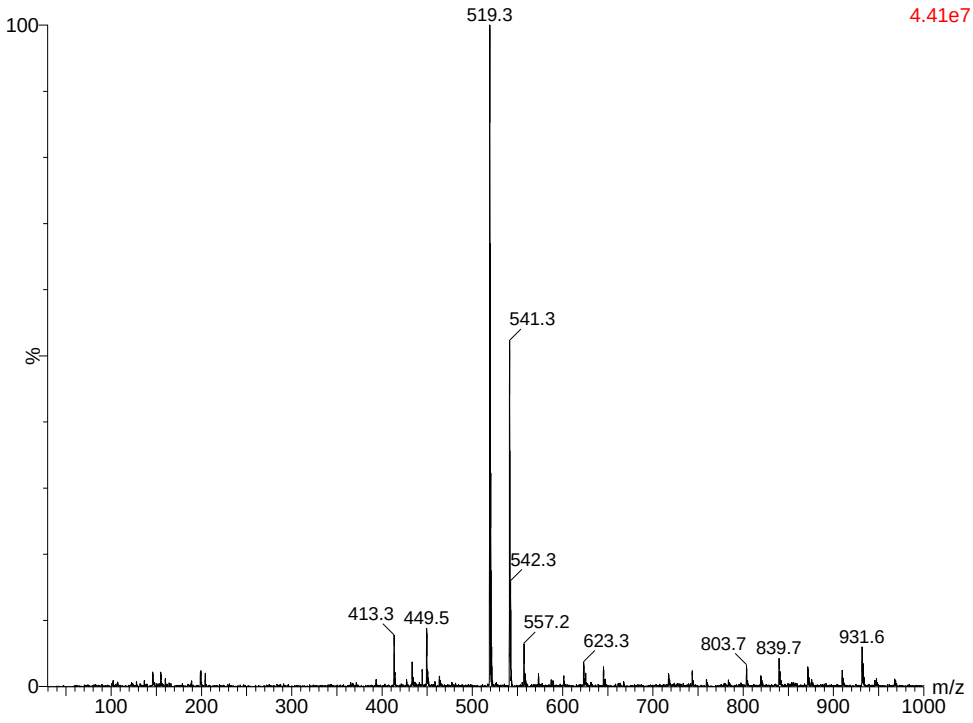

Figure S3-6 Mass spectrometry of MA-SP2-MA

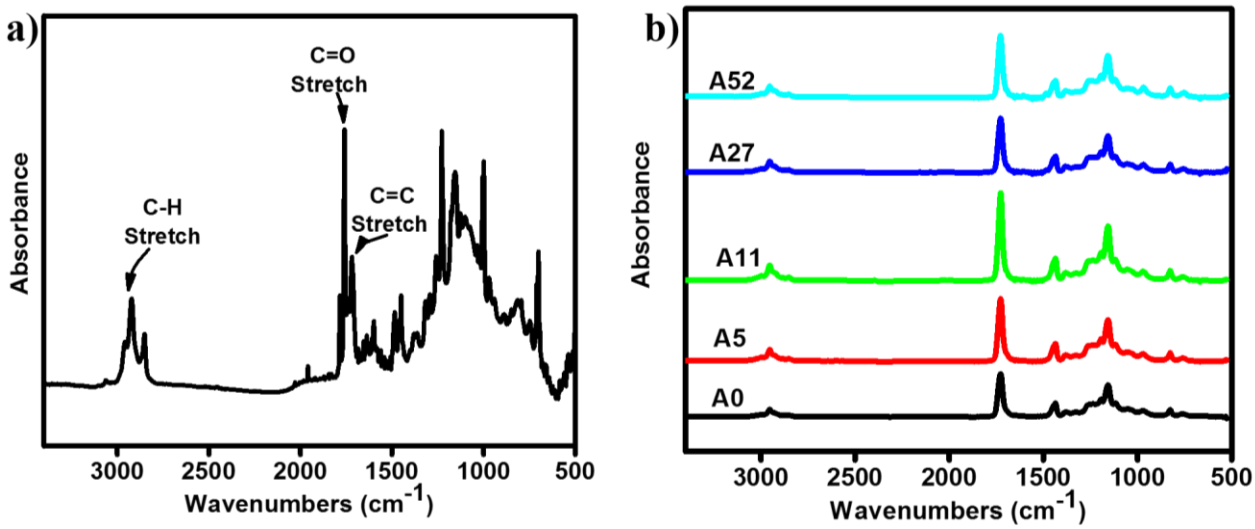

Figure S3-7 a) FTIR spectroscopy of prepolymerization solution; b) ATR of polymer

Chapter 4 Mechanoactivation of Spiropyran in Polyolefins

This chapter is based on the manuscript entitled "Smart Polyolefins Feeling the Force: Color Changeable Poly(Ethylene-Vinyl Acetate) and Poly(Ethylene-Octene) in Response to Mechanical Force", published on *Polymer*, **2017**, 112, p.219-227 (doi:10.1016/j.polymer.2017.02.006). The permission of this reproduction is granted by Elsevier. The significance of this work represents the first example of mechanoresponsive polyolefin through color changing. It also provides deep insight into the application of mechanophore into commercial polymers

Author Contributions

Meng Li and Dr. Weifeng Liu jointly generated the original idea of incorporating spiropyran mechanophore into polyolefins. Meng Li performed all the experiments and prepared the manuscript draft, which was revised by Dr. Weifeng Liu and Prof. Shiping Zhu.

4.1 Abstract

Spiropyran (SP) mechanophore cross-linker was covalently incorporated into two widely used polyolefins, poly(ethylene-vinyl acetate) (EVA) and poly(ethylene-octene) (EOC), through facile cross-linking by peroxide under hot press. It was found that (1'-(2-(methacryloyloxy)ethyl)-3',3' dimethylspiro(chromene-2,2'-indolin)-6-yl)methyl methacrylate (SP3) could not be thermally

driven to merocyanine (MC) in polyolefins during high temperature cross-linking, which is superior to other types of SP mechanophores used for polymer processing. The force-induced ring-opening reaction of SP-to-MC was demonstrated on SP3-cross-linked EVA. It was found that increasing the SP content resulted in earlier activation and that more MC was driven from SP at a slower strain rate. When held at constant strain, MC gradually reverted to SP. The mechanoactivation of SP was also investigated for SP3-cross-linked EOC. This work represents the first example of color-changeable polyolefins in response to mechanical force and demonstrates the feasibility of applying mechanophores to widely-used commercial polyolefins for stress sensing.

4.2 Introduction

Over the past few years, there has been an increasing interest in mechanoresponsive smart materials, which can transfer mechanical stimuli into other forms of energy.[1–3] To prevent the catastrophic damage or failure of materials, it is crucial to monitor stress fraction, fatigue, and hysteresis. The most prevalent method to design and develop force sensitive material is to incorporate a mechanoresponsive motif ("mechanophore"), containing a labile bond that is subject to change under mechanical force. Among all the mechanochemistry, some allow for direct visual warnings through color changing, fluorescence emission and light-emitting.[4–6]

Regarding color-changeable materials in response to mechanical force, employing colorimetric mechanophore spiropyran (SP) in polymer was pioneered by Sottos, Moore, and their co-workers.[4,5,7–12] SP, covalently incorporated into a polymer, undergoes electrocyclic-ring-opening reaction when subjected to stress and yields a purple/blue colored fluorescent merocyanine (MC) form. Bis(adamantly)-1,2-dioxetane was reported to have the feature of mechanoluminescence by Sijbesma, Meijer, and their co-workers.[6,13] These mechanophores allow for stress visualization with high spatial and temporal features, facilitating the prevention of catastrophic failure.

Prior work has demonstrated incorporating SP mechanophores into poly(methyl acrylate),[4,5,10,14] poly(methyl methacrylate),[4,8,9,12,14] poly(urethane),[15] poly(dimethylsiloxane),[16–18] poly(ε-caprolactone),[19] and carefully designed elastomers such as polystyrene-b-poly(n-butylacryalte)-SP-poly(n-butylacryalte)-b-polystyrene.[20,21] Recently, Meng et al. introduced SP mechanophore into CO_2-breathing microgels.[22] However, incorporation of mechanophores into polyolefins for stress/ strain sensing has not been reported. Polyolefins are most commonly and widely used and account for over half of the total polymers consumed around the world. In past decades, we have witnessed the ever-expanding application of polyolefins in our daily life, such as medical, packaging, sports, cable, wire coatings and so on. Rendering the most widely used polyolefins with mechanical force sensitivity has many potential applications, and thus deserves to be investigated. Therefore, we propose to incorporate SP mechanophore into polyolefins to demonstrate the idea.

To test the idea, we chose poly(ethylene-vinyl acetate) (EVA) as a platform because of its excellent flexibility, resilience, toughness and crack resistance.[23] Also, its relatively high polarity is speculated to render high compatibility with SP mechanophore. A non-polar polyolefin, poly(ethylene-octene) (EOC) was also selected as another candidate for SP mechanophore incorporation due to its excellent elasticity, good tear resistance, and long shelf life.[24] In this work, the preparation of mechanoresponsive polyolefins was achieved by cross-linking EVA or EOC using peroxide, during which SP mechanophore cross-linker was added as co-cross-linker. Scheme 4-1 illustrates the network of cross-linked EVA and EOC, consisting of two types of cross-links. One type of cross-links is formed by the termination of macroradicals (tertiary carbon and/or secondary carbon), and the other type is formed by free radical addition reaction and/or copolymerization of dimethyacrylate-containing SP cross-linker.[23,25,26] Covalently cross-linked into the polymer network, SP co-cross-linker indicates stress/strain by giving off purple/blue color during the deformation of polyolefins.

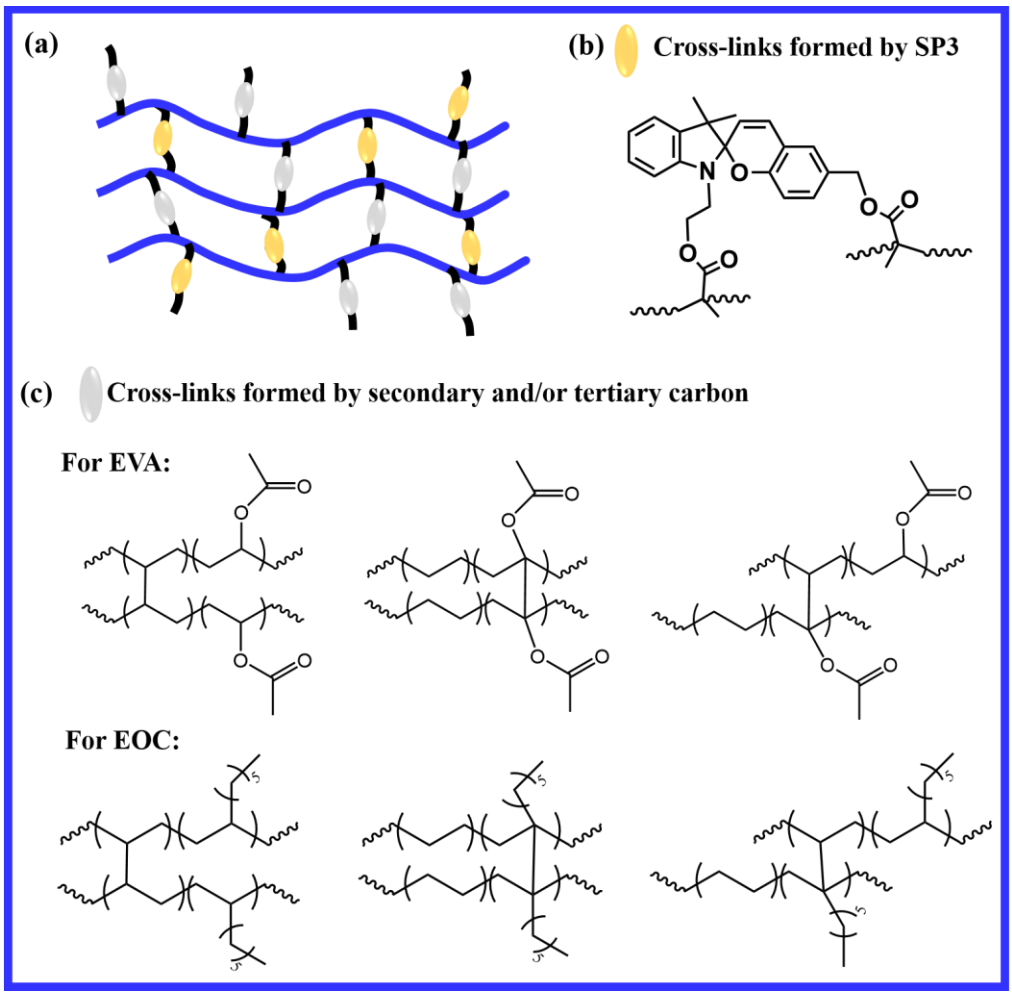

Scheme 4-1 (a) EVA and EOC polymer network containing both SP cross-links and cross-links from secondary and/or tertiary carbon of EVA and EOC; (b) Chemical structure of the SP3 cross-links; (c) Chemical structure of the cross-links formed by secondary and/or tertiary carbon of EVA and EOC.

So far, there have been three types of SP mechanophore cross-linkers, including 1',3',3'-trimethyl-6-nitrospiro(chromene-2,2'-indoline)-5',8-diyl bis(2-methylacrylate) (SP1),[4] (1'-(2-

(methacryloyloxy)ethyl)-3',3'-dimethyl-6-nitrospiro(chromene-2,2'-indolin)-8-yl)methyl methacrylate (SP2), and SP3,[27] shown in Figure 4-1. Both SP1 and SP2 are sensitive to UV irradiation and mechanical force, while SP3 is sensitive to mechanical force but not to UV due to the lack of the electron-withdrawing nitro group.[27,28] In this work, SP3-containing polyolefins were systematically investigated because unlike its counterpart no thermally driven SP-to-MC conversion was observed for SP3 under high temperature curing. The mechanical activation of SP3 under the uniaxial tensile test of EVA was studied. The effects of SP3 content, strain rate and stress relaxation on the mechanical activation of SP3 in EVA were investigated in detail. Mechanical activation of SP3-cross-linked EOC was also discussed. To the best of our knowledge, it is the first time that mechanophore is incorporated into polyolefins for stress/strain indication, which is of great importance for broadening the application of mechanochemistry and gaining insight into the force distribution in engineering polymers upon straining.

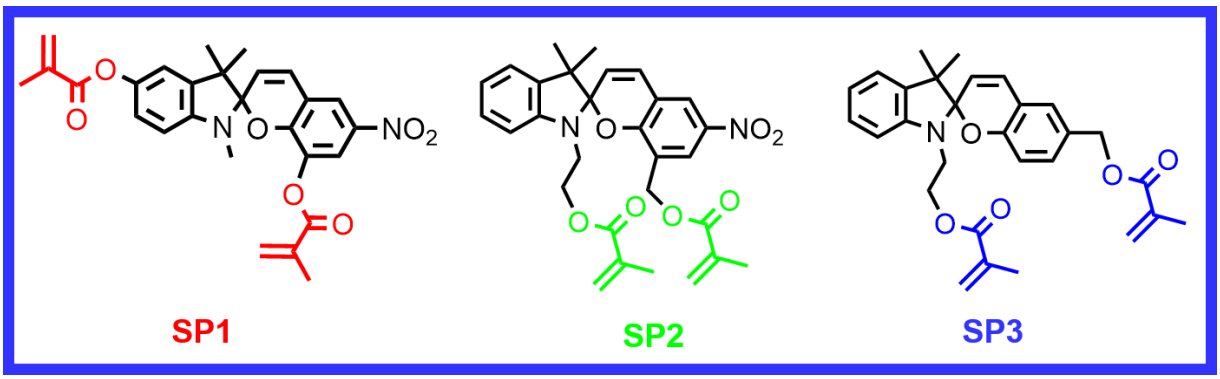

Figure 4-1 Three types of SP mechanophore cross-linkers.

4.3 Experimental Methods

4.3.1 Chemicals

EVA (25 wt% vinyl acetate content; melt index, 19 g/ 10 min under the load of 2.16 kg; density, 0.941 g/cm^3) and dicumyl peroxide (DCP, 98%) were purchased from Aldrich. EOC (melt index, 0.5 g/10 min under the load of 2.16 kg; density, 0.863 g/cm^3) was purchased from Dow. All the chemicals were used as received unless stated otherwise. SP3 and SP2 were synthesized *via* the methods described by Meng et al.[27]

4.3.2 Sample Preparation

Five samples of cross-linked EVA containing various SP3 contents were prepared using a hot press. DCP was used as initiator and SP mechanophore was added as co-cross-linker. The SP contents in the five runs were 0 mg, 8 mg, 16 mg, 32 mg and 48 mg, respectively, in 1 g of EVA. SP2-cross-linked EVA and SP3-cross-linked EOC was prepared by the same method. To simplify polymer names, SP content and type are indicated by the numbers before and after "SP", e.g. EVA-16SP3 contained 16 mg SP3 in 1 g EVA.

A typical cross-linking procedure is as follows. 1 g EVA, 20 mg DCP and 16 mg SP3 were well mixed in 5 mL toluene at 100 °C for 30 min. The solvent was evaporated from the mixture in a

vacuum oven over night. A hot press (CARVER, Model 4389, Wabash, USA) was then used for curing EVA samples. The cross-linkable EVA was compression molded using dog-bone shaped molds (Figure 4-S1) and cured for 1 h at 160 °C under 4000 psi. The molds were then cooled down to room temperature and the cross-linked EVA specimens were easily removed from molds for the later characterization. The preparation of the SP-cross-linked EOC follows the same procedure as above.

4.3.3 Characterization

Differential Scanning Calorimetry (DSC): The crystallization temperature (T_c), melting temperature (T_m) and enthalpy of crystallization (ΔH_c) were determined using TA Instruments Differential Scanning Calorimetry 2910 system. For DSC characterization, polymer samples weighing 7~10 mg were used. The polymer samples were heated at 10 °C/min from room temperature to 100 °C, held at 100 °C for 5 min, cooled at 5 °C/min to -50 °C, held at -50 °C for 5 min, and then reheated to 100 °C at 10 °C/min and cooled down at 5 °C/min to -50 °C. The curves obtained were analyzed by TA Universal Analysis software. The T_c, T_m, and ΔH_c was determined from the second cycle.

Sol Extraction: Extraction of sol fraction was carried out by boiling toluene. The cross-linked EVA or EOC specimens were immersed in toluene, which was brought to reflux for 72 h to remove sol contents. The specimens were then dried in an oven for overnight. The masses of specimens

before and after extraction, M_1 and M_2, were weighed. Gel content was calculated as the mass ratio M_2/M_1.

Tensile Tests: Measurements were performed on an Instron 3366 Benchtop Universal Mechanical Testing system (Instron Corporation; Canton, MA) at room temperature (~23 °C). The crosshead speed was 30 mm/min. The dimensions of the specimens can be referred to the mold dimensions as shown in Figure S4-1. To avoid slippage and damage from the clamps, small pieces of thick rubber were used to "sandwich" the sample at the region of the clamps. All the stress results reported in this paper are engineering stress. Each engineering stress-strain curve was based on three repeated measurements. The effect of different strain rates (30, 60 and 120 mm/min) was also studied. Stress relaxation experiments of cross-linked EVA were carried out by stretching the specimens at 60 mm/min to 462 % strain and holding for one hour. All the experiments were performed under the same ambient fluorescent room light at room temperature.

RGB Color Analysis: Mechanical activation of SP-to-MC was analyzed using RGB color analysis. Optical images were taken by a NIKON D7000 camera with a NIKKOR 18-105 mm 1:3.5-5.6G ED lens. A white board was used as the background under ambient room light conditions. During each tensile test, photos were taken every 2 seconds as the samples were strained. The photos were analyzed in Adobe Photoshop CS6 Software. After the background was white balanced, the average intensity of red (R), green (G) and blue (B) channel at the region of interest was obtained and used for calculating RGB ratio. According to Grassmann's law,[26] RGB ratio was calculated as

rRC=R/(R+G+B), rGC=G/(R+G+B) and rBC=B/(R+G+B). The intensity change in each channel, drRC, drGC and drBC were obtained by subtracting the initial RGB ratio from the RGB ratio at each point, respectively.

4.4 Results and Discussion

4.4.1 Mechanochromism of SP cross-linked EVA

4.4.1.1 SP-cross-linked EVA

The recipes of SP cross-linked EVA are summarized in **Table 4-1**. In a typical experiment, cross-linking of EVA was performed using peroxide via the free radical mechanism. In Run 2-6, DCP was added as initiator, and SP3 was added as co-cross-linker. The content of SP was regulated at a range of 0 ~ 48 mg with a fixed EVA and DCP content. To select the best SP cross-linker candidate, SP2 was also separately incorporated into EVA for comparison in Run 7. After cross-linking in the hot press at 160 °C for one hour, all runs yielded smooth specimens.

To confirm effective cross-linking of the samples, the gel content of SP-cross-linked EVA was estimated via sol extraction experiment. The gel content was 86% for the nascent EVA cross-linked by DCP only, and increased to ~95% for SP-cross-linked EVA, due to the increase of total

cross-linker content caused by SP incorporation. It can be concluded that SP was effectively cross-linked into the EVA network during the hot press curing process.

DSC was employed to study thermal properties of uncured and cured EVA. The T_c of EVA was 49.4 °C before curing, whereas decreased to ~ 45 °C after curing. Cross-linking resulted in a decrease of T_c. Moreover, cross-linking also resulted in crystallinity decrease in the express of ΔH_c decrease. The T_m of EVA was not affected by cross-linking. The further incorporation of SP3 or SP2 during cross-linking had virtually little effect on T_c or ΔH_c.

Table 4-1 Recipes, gel content and thermal properties of uncured and cured EVA

Run	Polymer	EVA: DCP: SP (g: g: g)	Gel Content (100%)	T_c (°C)	ΔH_c (J/g)	T_m (°C)
1	EVA (uncured)	1: 0: 0	-	49.4	68.3	75.5
2	EVA-0SP3	1: 0.02:0	86	44.5	36.2	75.6
3	EVA-8SP3	1: 0.02: 0.008	94	44.9	34.7	75.5
4	EVA-16SP3	1: 0.02: 0.016	95	44.6	33.3	75.2
5	EVA-32SP3	1: 0.02: 0.032	97	44.2	33.4	75.4
6	EVA-48SP3	1: 0.02: 0.048	96	45.4	33.6	75.1
7	EVA-48SP2	1: 0.02: 0.048	94	46.2	33.5	75.9

Optical images of EVA with and without SP co-cross-linker after curing are shown in Figure 4-2. Prior to curing, all of the mixtures of EVA with SP2 and EVA with SP3 exhibited transparent and almost no color. After curing, the neat EVA cross-linked by DCP only was colorless, whereas those cross-linked by SP appeared to be colored. SP2-cross-linked EVA exhibited dark red, indicating it was a mixture of the yellow SP form and the red MC form. The similar phenomenon was also reported for SP1-containing PMMA.[5] This might be attributed to the thermally driven ring-opening reaction of SP-to-MC under the high temperature of 160 °C during the curing process.

However, this MC form in the SP2-cross-linked EVA could not be driven back to SP form even under illumination of visible light at elevated temperature. Interestingly, the SP3-cross-linked EVA exhibited yellow coloration, suggesting the majority of spiropyran stayed in the closed SP form.[16] With the increasing SP3 content, the yellow color intensity increased due to more covalently embedded spiropyran in the network. The thermal inactive feature of SP3 compared to SP1 and SP2 was probably due to the lack of electron withdrawing group $–NO_2$. It was the molecular structural difference that caused the difference and made SP3-cross-linker a good candidate for high-temperature processing, which largely saves the effort of using visible light illumination for MC-to-SP reversion. Considering the SP3's feature of insensitivity to high temperature over its counterpart in this system, SP3-cross-linked EVA was focused on in this work, and its mechanoactivation was further investigated in depth.

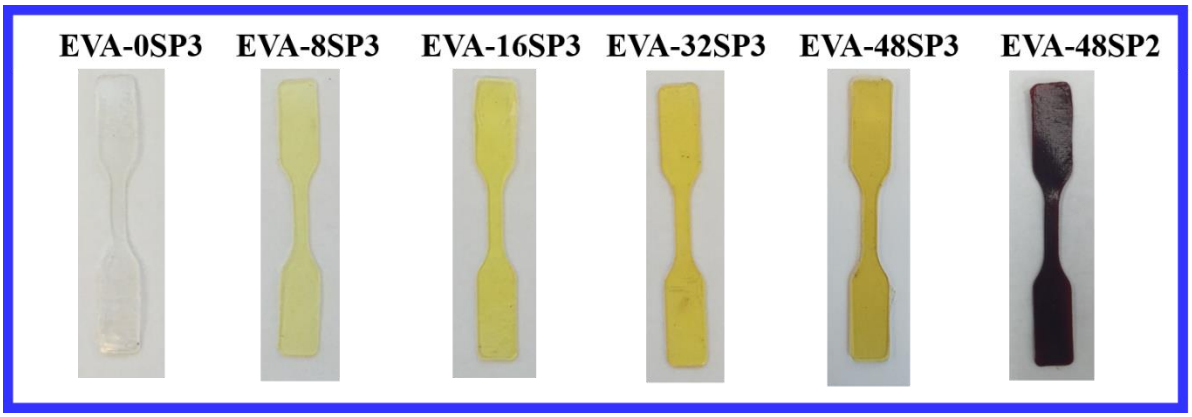

Figure 4-2 Optical images of the SP3-cross-linked and SP2-cross-linked EVA specimens

4.4.1.2 Mechanical Activation under Uniaxial Stretching

The mechanical properties and mechanoactivation were studied via the uniaxial tensile tests. EVA-48SP3 was taken as an example to demonstrate SP3 mechanoactivation in EVA. The dog-bone-shaped specimen was stretched at a constant strain rate of 30 mm/min until failure. During elongation, digital images of the gauge section were captured every 2 s. The RGB ratio was calculated via the method, as described previously in Experimental Methods.

The representative optical images of the EVA-48SP3 specimen during uniaxial stretching in Figure 4-3a reveal the emergence of blue color with increasing elongation. The appearance of blue color during elongation indicated the ring-opening reaction of SP. Prior to curing, EVA with SP3 physically incorporated did not show any blue coloration after deformation. Only after curing, when SP mechanophore was covalently incorporated into EVA network, the mechanoactivation could be observed after stretching. The isomerization of SP-to-MC was induced by the force-induced cleavage of C-O bond. It is conclusive that it was the mechanical force that accounted for the force-induced blue coloration.

As the specimen was further elongated, the blue color became deeper. Upon fracture at the failure strain of ~ 544%, the blue color persisted and then quickly disappeared within ~30 s. The corresponding changes of intensity in the red (drRC), green (drGC) and blue channels (drBC), as well as stress, are plotted in Figure 4-3b as a function of strain. EVA-48SP3 showed a nearly linear

reduction in red and green intensity, and a linear increase in blue intensity. Since the color of the mechanically activated specimen appeared blue, drBC was used for the color change analysis.

The emerging point of the blue color was at ~ 175% strain (Figure 4-3a) even though the profile of drBC appeared to increase since the starting point (Figure 4-3b). The increase in drBC before ~175 % strain was due to the "loss" of yellow intensity caused by the reduction of thickness during elongation. Since yellow is the complementary color of blue, the seeming increase of drBC in the early strain was attributed to the decrease of yellow. After ~175 % strain, the continuous increase of drBC resulted from the actual emerging blue color. It would be helpful to quantify the percentage of mechanoactivation of SP by assuming full activation by UV irradiation. However, it could not be achieved for the SP3 type due to its unique feature, which is sensitive to mechanical force but not to UV irradiation. The selective sensitivity feature of SP3 enables stress/strain sensing in outdoor materials.[27]

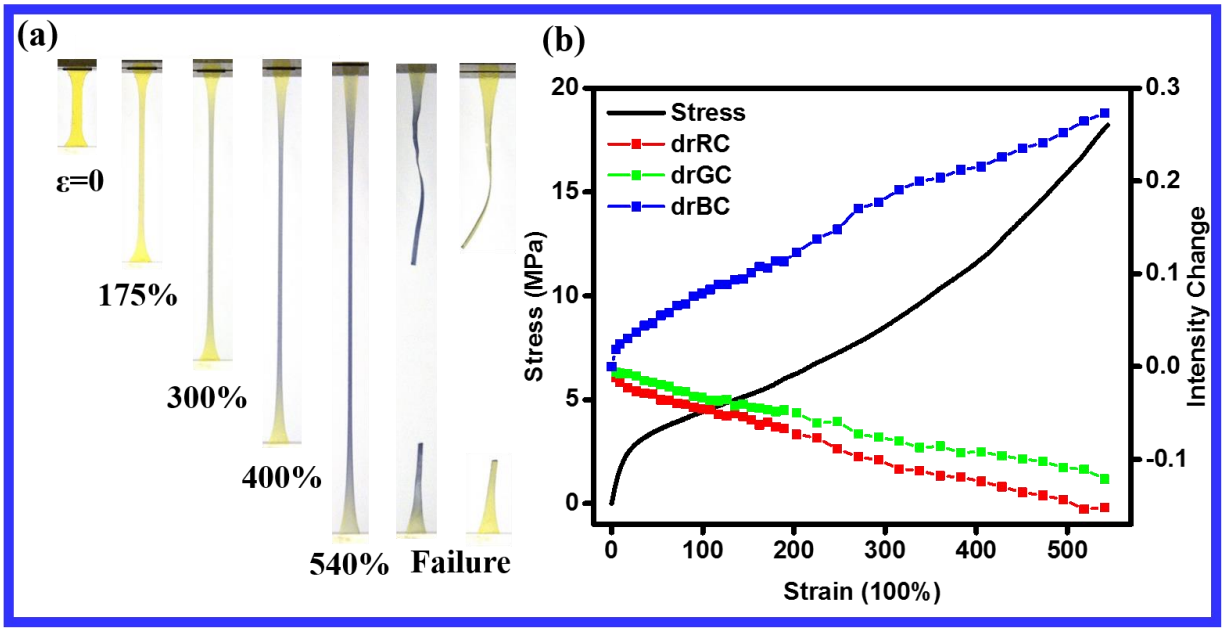

Figure 4-3 (a) Optical images of EVA-48SP3 during the tensile test at strain indicated by the numbers below. After fracture, the blue color disappeared within ~30 s. (b) Engineering stress, change of intensity in drRC, drGC and drBC as a function of strain.

4.4.1.3 Effect of SP3 Content on Mechanical Activation

The effect of SP3 content incorporated into the polymer network on the mechanoactivation was then studied. Uniaxial tensile tests were performed on four SP3-cross-linked EVA specimens (EVA-8SP3, EVA-16SP3, EVA-32SP3 and EVA-48SP3) and the nascent EVA cross-linked by DCP only (EVA-0SP3). The strain rate was 30 mm/min, during which optical images were taken for RBG analysis.

Digital images of stretched specimens containing varying SP content at 530 % strain are shown in Figure 4-4a. Mechanically induced ring-opening reaction of the yellow SP to the blue MC appeared to be more evident for specimens containing higher SP content (EVA-32SP3 and EVA-48SP3) than those with lower SP content (EVA-8SP3 and EVA-16SP3). The difference in the onset strain of color change among these samples was obvious. The onset strain of EVA-48SP3, EVA-32SP3, EVA-16SP3 and EVA-8SP3 were ~175%, ~275%, ~705% and ~850%, respectively (See Figure S4-2 through S4-5 in Supporting Information). Therefore, it can be concluded that increasing SP content led to earlier mechanoactivation.

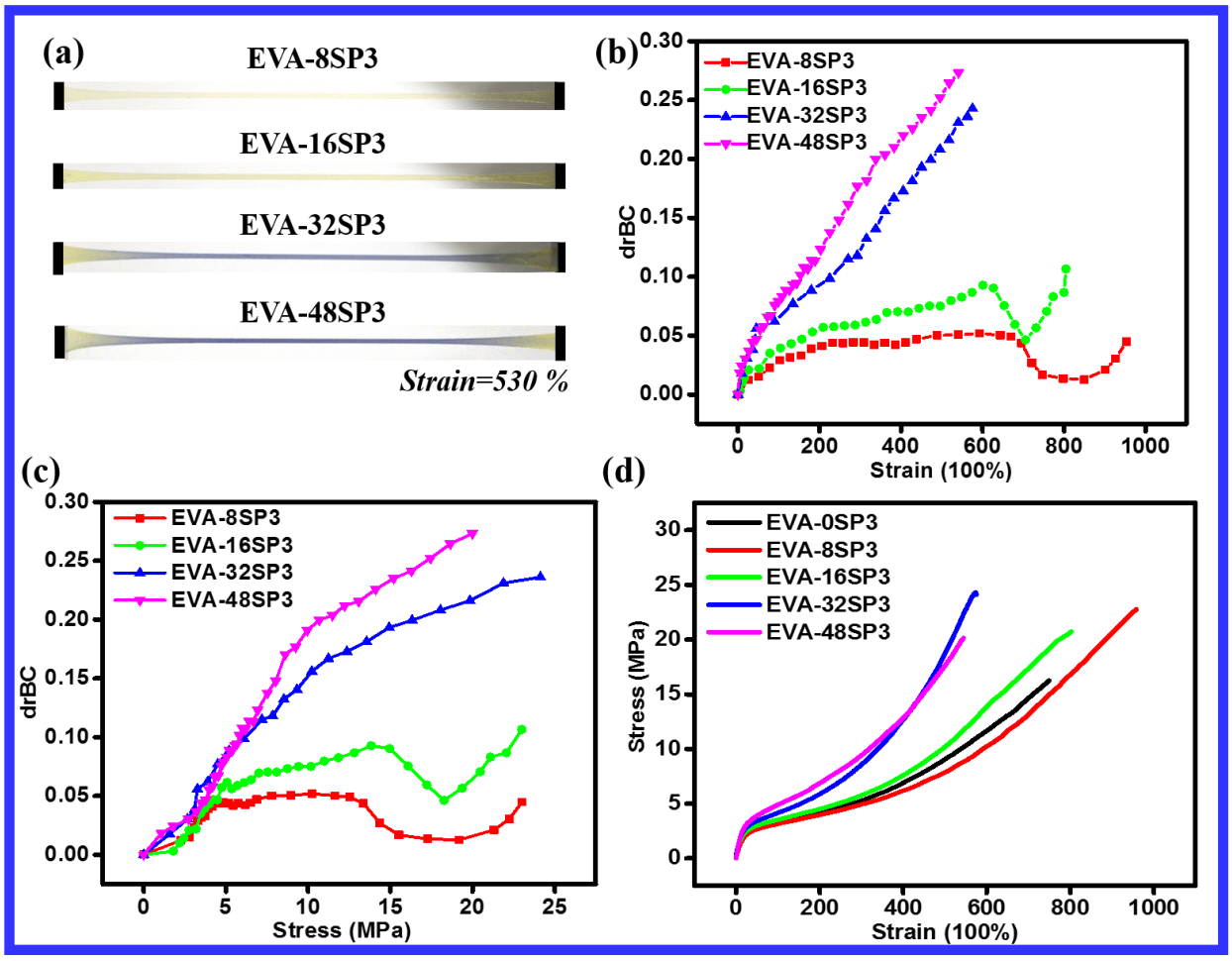

Figure 4-4 (a) Optical images of four elongated SP3-cross-linked EVA specimens at 530 % strain; (b) The drBC as a function of strain for the four SP3-cross-linked EVA specimens; (c) The drBC as a function of engineering stress for the four SP3-cross-linked EVA specimens; (d) Engineering stress as a function of strain for the four SP3-cross-linked EVA and nascent EVA specimens

The drBC of the four EVA samples containing various amounts of SP was plotted against strain in Figure 4-4b and stress in Figure 4-4c. The mechanical activation of SP-cross-linked EVA

exhibited the following trends: (1) The drBC at a given strain was greater for the EVA specimen containing higher SP content, (2) The drBC at a given stress was greater for the EVA specimen containing higher SP content. It is because more MC was obtained from the higher content of SP, which was initially contained in the EVA. There was a sharp drop in blue intensity at higher strain/stress levels for EVA-8SP3 and EVA-16SP3. As shown in Figure S4-4, EVA-16SP3 specimen first showed a decrease in yellow color intensity between 0 and 650 % strain, resulting in the increase in drBC. After 650 % strain, the yellow color deepened probably due to the whitening effect, leading to the sharp drop in drBC as shown in Figure 4-4b and 4-4c. The visible blue color started to emerge after 705 % strain, contributing to the final increase of drBC. The similar result was also observed for EVA-8SP3 (Figure S4-5). However, the whitening effect did not influence those containing high SP content. The profile of drBC increased over the whole range of elongation for EVA-32SP3 and EVA-48SP3, because the blue coloration emerged much earlier than the whitening effect. For the samples of EVA-32SP3 and EVA-48SP3, the curve of drBC vs. strain appeared almost linear, while drBC vs. stress showed a fast linear increase, followed by a slower linear increase.

The stress-strain curves of the four SP3-cross-linked EVA and nascent EVA samples cross-linked by only DCP are shown in Figure 4-4d. All five cross-linked EVA samples followed the same trend. However, the stress at a certain strain appeared higher for those with higher SP content (EVA-32SP3, EVA-48SP3) than those with lower SP content (EVA-0SP3, EVA-8SP3, EVA-16SP3). The higher stiffness could be the result of the synergistic effects of incorporating bulky spiropyran and a higher cross-linking density.

A possible explanation for the SP mechanoactivation and deformation behavior is as follows. The SP mechanophore played a role of both cross-linker and stress indicator in the EVA network. At an early strain (0 ~ 3 %), the stress-strain behavior exhibited an ideal Hooke's elasticity. At this stage, no SP-to-MC conversion occurred due to the low stress. After this point, the collective slips resulted in the fragmentation of crystallites.[29] The stress was then mainly distributed on the cross-linker, leading to a high SP-to-MC conversion rate. At further elongation, the disentanglement and straightening of the main chain led to the chain orientation and crystallization, which could bear more stress, and thus, lowered the stress on the cross-linker. This might account for a slower SP-to-MC conversion rate and thus a slower linear increase of drBC at higher stress levels. By incorporating SP mechanophore into a polymer network as a cross-linker, therefore, we can obtain visual indication of the stress applied on the cross-linker during deformation, which can further help mapping stress on polymer chains on a molecular level.

4.4.1.4 Effect of Strain Rate on Mechanical Activation

Uniaxial stretching tests under different strain rates (30, 60 and 120 mm/min) were conducted on EVA-48SP3 to study the effect of deformation rate on mechanoactivation of SP. As shown in Figure 4-5 a-c, the SP mechanoactivation had the following trends: (1) The drBC at a certain strain level was greater under slower strain rates. (2) The drBC at a certain stress level was also higher at slower strain rates. (3) The three engineering stress-strain curves completely overlapped. SP-to-

MC conversion appeared to be higher at slower strain rate even though the presumable force applied onto the cross-linker was almost identical. It is because the slower strain rate rendered more time for the ring-opening reaction of SP-to-MC. The experimental results suggested the SP mechanoactivation was a rate-dependent reaction, which agreed with previous reports.[9,11,30] The drBC is re-plotted against time in Figure 4-5d. Since SP-to-MC conversion is induced by stress, the rate of SP-to-MC conversion was greater at higher strain rates (or higher stress rates).

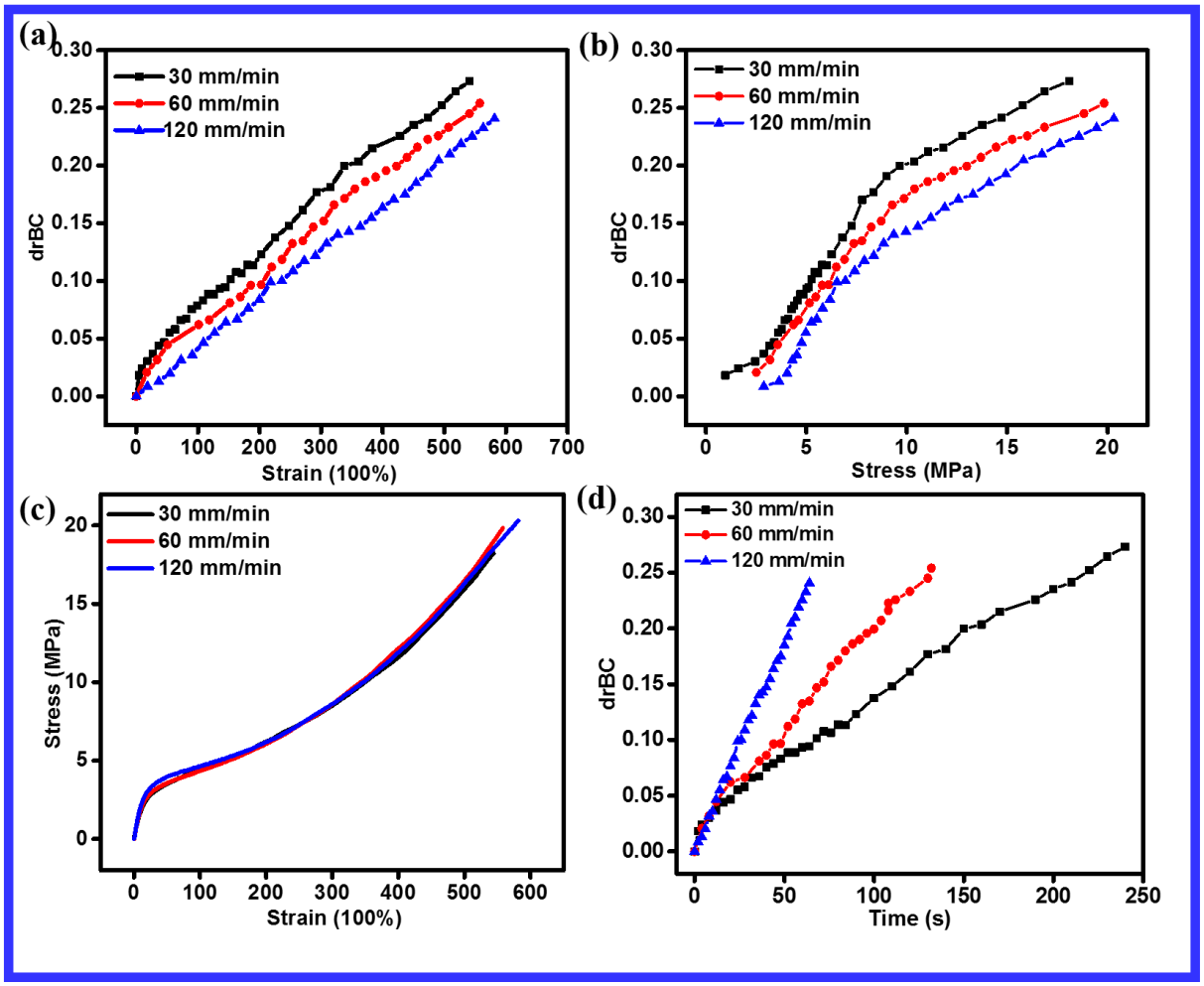

Figure 4-5 EVA-48SP3 specimen under uniaxial tension at different strain rate. (a) The drBC vs. strain; (b) The drBC vs. stress; (c) Stress vs. strain; (d) The drBC vs. time.

4.4.1.5 Mechanical Activation under Stress Relaxation

Typical stress relaxation experiments of the EVA-48SP3 specimen were performed, during which mechanoactivation of SP was monitored. The specimen was stretched at 60 mm/min up to 462% strain and held for one hour. Optical images of the specimen were captured every minute during stress relaxation. Representative images of the specimen at a given time are shown in Figure 4-6a. The onset of stretching was set as time "0". Stress vs. time and drBC vs. time are shown in Figure 4-6b and Figure 4-6c, respectively. Upon stress relaxation, both stress and drBC dropped over time. This observation at first seemed to contradict with literature results, in which more MC was driven from SP as the stress decayed at a constant strain.[10,11] However, further investigation led us to a deeper understanding of SP mechanoactivation. Two possible factors were influencing the SP-to-MC conversion. First, SP-to-MC conversion was both time-dependant and stress-dependant (related to the location of SP). In the literature, SP was in the center of linear poly(methyl acrylate) and polyurethane.[10,11] During stress relaxation, the stress applied on SP was still above the threshold stress for SP-to-MC conversion. Meanwhile, more time was rendered to enable more SP-to-MC conversion. Therefore, the time-dependent feature of SP appeared to be dominant. In this work, SP served as a cross-linker in EVA, which carried most of the force upon straining. When held at constant strain, the force on the cross-linker started to drop because the force was more evenly distributed onto the gradually oriented main chains. The decreased force on SP led to the blue color fading despite more time rendered for the conversion of SP-to-MC. Hence, the force-dependent feature in influencing the ring opening of SP might be the main factor in this case. Moreover, the type of SP mechanophore also makes a difference in MC-to-SP

reversion rate.[27] The fast reversion feature of SP3 might also synergistically contribute to the fading of blue coloration. Interestingly, the curves of drBC vs. time and stress vs. time coincided when put together. The blue color almost instantaneously reflected the force applied to the specimen, suggesting the high potential of the SP3 cross-linker in real-time stress-sensing in polyolefin systems.

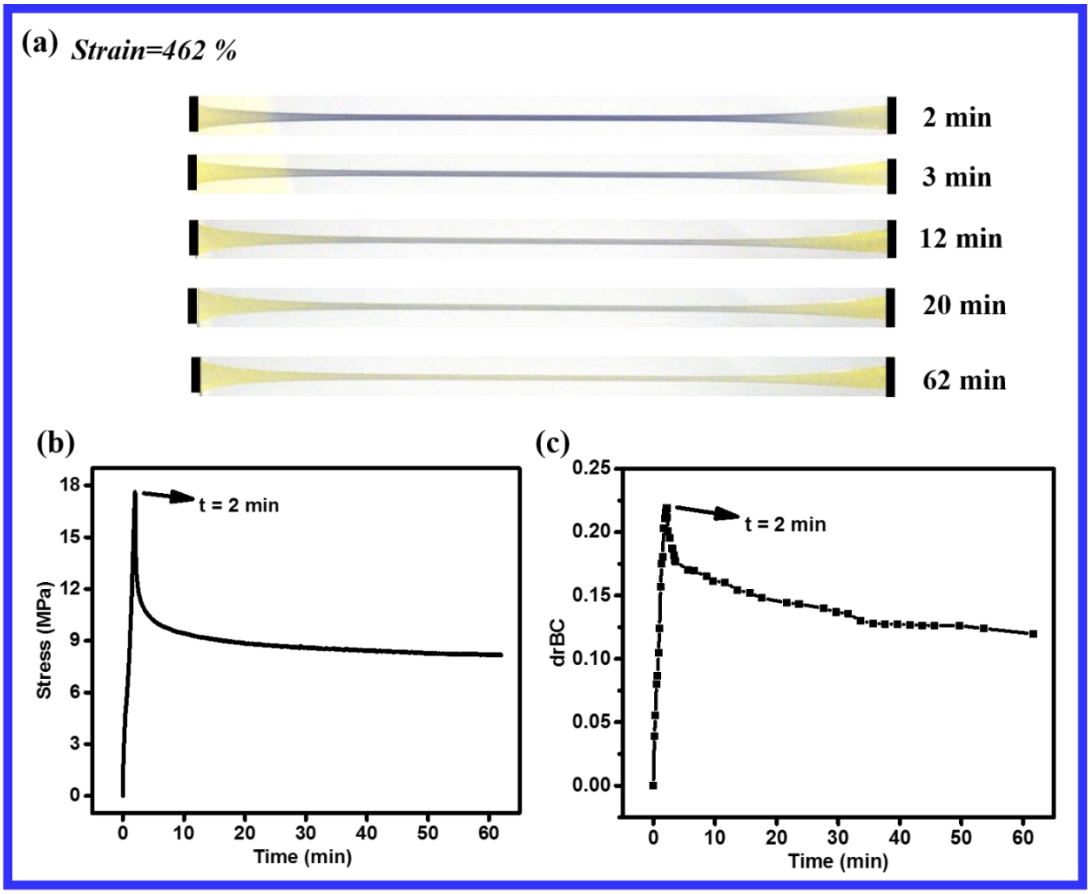

Figure 4-6 (a) Optical images of EVA-48SP3 held at 462% strain during stress relaxation; (b) Engineering stress of EVA-48SP3 held at 462 % strain vs. time; (c) The drBC of mechanically activated EVA-48SP3 held at 462 % strain vs. time.

4.4.2 Mechanochromism of SP Cross-linked EOC

Having demonstrated the SP mechanoactivation in the polar polyolefin, EVA, we wondered if SP mechanophore cross-linker could be covalently incorporated in other non-polar polyolefin systems for stress/strain sensing. Our choice was one of the most important and widely used polyolefin thermoplastic elastomer, EOC. The cross-linking procedure of EOC in the presence of SP3 using DCP was similar to the procedure of cross-linking EVA. The chosen EOC-32SP3 contained 32 mg of SP3, the amount of which was sufficiently small to minimize phase separation between EOC and SP3, and yet large enough to show the vibrant blue coloration during deformation. A uniaxial tensile test of EOC-32SP3 was conducted at a strain rate of 30 mm/min, during which digital images were taken every 2 s. The representative images of the specimen at different levels of strain are shown in Figure 4-7a and the stress vs. strain curve is plotted in Figure 4-7b. After ~ 600 % strain, the blue color emerged, indicating the mechanoactivation of SP-to-MC. The blue color deepened during further elongation up to fracture. Therefore, SP3 cross-linker could also be incorporated into a non-polar polyolefin system like EOC for stress/strain sensing by color changing.

However, there was an inevitable issue for covalently incorporating SP into EOC. It was the poor compatibility between the polar SP cross-linker and the non-polar EOC. After cured in the hot press, the EOC-32SP3 showed unevenly distributed yellow regions, suggesting that SP3 was not

evenly cross-linked in the network. The emerging blue color turned out to be uneven during deformation. To improve the compatibility between SP and non-polar polyolefin materials, design and preparation of an SP cross-linker with lower polarity must be explored in future work.

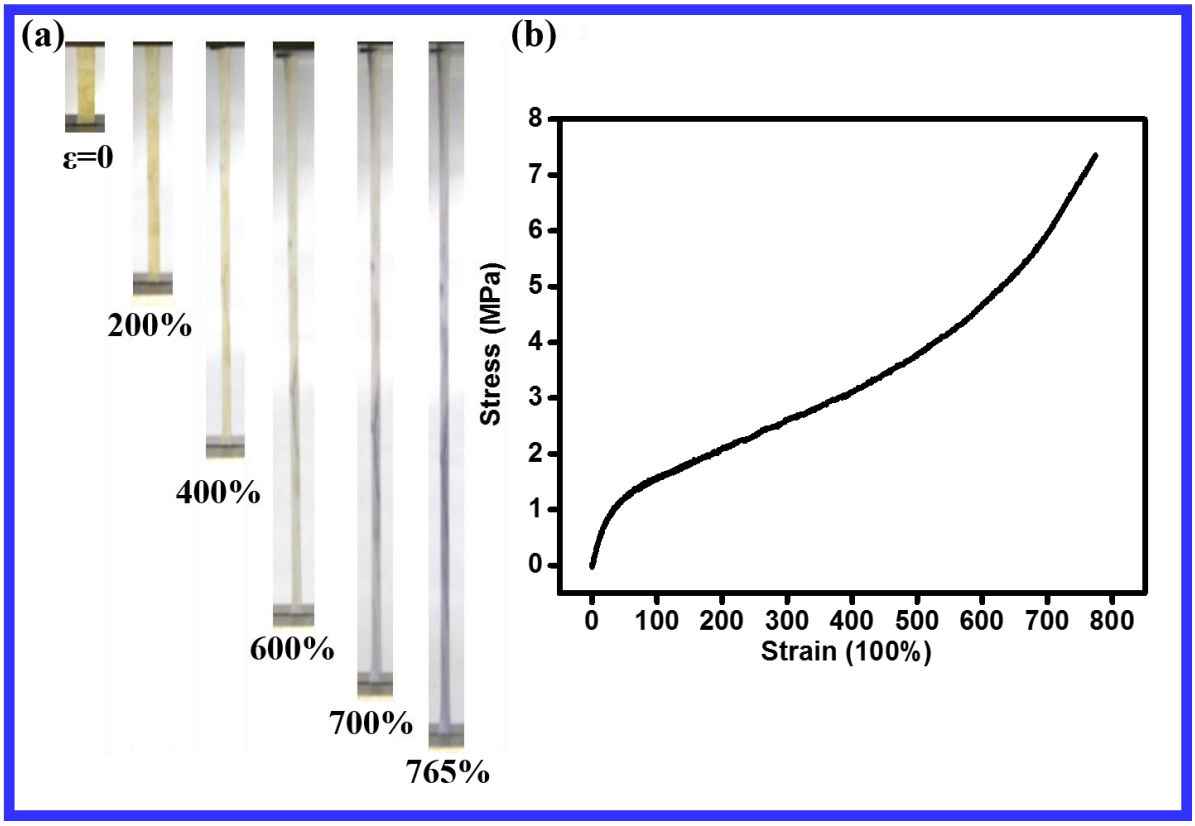

Figure 4-7 (a) Digital images of EOC-32SP3 under uniaxial tensile test; (b) Stress vs. strain of EOC-32SP3.

4.5 Conclusions

In conclusion, we have developed a facile method to covalently incorporate an SP mechanophore cross-linker into commercially available polyolefins such as EVA and EOC by simply curing them under hot press. The mechanoactivation of SP mechanophore in these two polyolefin systems has been successfully demonstrated. The SP3 type mechanophore cross-linker exhibited its excellent feature of insensitivity to high temperature processing in this system to other types of SP mechanophores, that is, SP was not thermally driven to MC for SP3-cross-linked polyolefin during high-temperature curing. With the RGB method, the blue color intensity was shown to increase during deformation. It was revealed that higher SP content led to earlier mechanoactivation and greater blue color intensity at certain levels of strain/stress. The blue color at certain levels of strain/stress appeared to be more intensive at slower strain rates, indicating SP-to-MC conversion was a rate-dependent reaction. When held at a constant strain, the MC form reverted to the SP form possibly due to the decreased stress and fast reversion feature of SP3. For the SP-cross-linked EOC, it also exhibited blue coloration during deformation. However, the compatibility of SP and EOC need to be improved.

The present contribution represents the first example of smart polyolefins that feel the force by color changing, opening the possibilities of applying SP mechanophore into widely used polyolefin materials. This work also provides an insight of choosing SP3 type over other SP mechanophores for high-temperature polymer processing. Last but not least, this study not only gives a fundamental understanding of mechanoactivation response of SP in polyolefins but also provides

an effective approach to study the force distribution on polyolefin network at a molecular level during deformation.

4.6 Acknowledgement

The authors sincerely acknowledge the Natural Science and Engineering Research Council (NSERC) of Canada for supporting this fundamental research through Discovery Grant program. We also thank the Canada Foundation for Innovation (CFI) for the equipment and facilities. SZ thanks the Canada Research Chair (CRC) program for supporting his research.

4.7 References

(1) Ramirez, A. L. B.; Kean, Z. S.; Orlicki, J. A.; Champhekar, M.; Elsakr, S. M.; Krause, W. E.; Craig, S. L. *Nat. Chem.* **2013**, *5* (9), 757–761.

(2) Caruso, M. M.; Davis, D. A.; Shen, Q.; Odom, S. A.; Sottos, N. R.; White, S. R.; Moore, J. S. *Chem. Rev.* **2009**, *109* (11), 5755–5798.

(3) Weder, C. *J. Mater. Chem.* **2011**, *21* (23), 8235.

(4) Davis, D. a; Hamilton, A.; Yang, J.; Cremar, L. D.; Van Gough, D.; Potisek, S. L.; Ong, M. T.; Braun, P. V; Martínez, T. J.; White, S. R.; Moore, J. S.; Sottos, N. R. *Nature* **2009**, *459* (7243), 68–72.

(5) Beiermann, B. A.; Davis, D. A.; Kramer, S. L. B.; Moore, J. S.; Sottos, N. R.; White, S. R. *J. Mater. Chem.* **2011**, *21* (23), 8443.

(6) Chen, Y.; Spiering, a J. H.; Karthikeyan, S.; Peters, G. W. M.; Meijer, E. W.; Sijbesma, R. P. *Nature chemistry*. July 2012, pp 559–562.

(7) Grady, M. E.; Beiermann, B. A.; Moore, J. S.; Sottos, N. R. *ACS Appl. Mater. Interfaces* **2014**, *6* (8), 5350–5355.

(8) Lee, C. K.; Diesendruck, C. E.; Lu, E.; Pickett, A. N.; May, P. A.; Moore, J. S.; Braun, P. V. *Macromolecules* **2014**, *47* (8), 2690–2694.

(9) Degen, C. M.; May, P. A.; Moore, J. S.; White, S. R.; Sottos, N. R. *Macromolecules* **2013**, *46* (22), 8917–8921.

(10) Beiermann, B. A.; Kramer, S. L. B.; May, P. A.; Moore, J. S.; White, S. R.; Sottos, N. R. *Adv. Funct. Mater.* **2014**, *24* (11), 1529–1537.

(11) Lee, C. K.; Davis, D. A.; White, S. R.; Moore, J. S.; Sottos, N. R.; Braun, P. V. *J. Am. Chem. Soc.* **2010**, *132* (45), 16107–16111.

(12) Kingsbury, C. M.; May, P. A.; Davis, D. A.; White, S. R.; Moore, J. S.; Sottos, N. R. *J. Mater. Chem.* **2011**, *21* (23), 8381.

(13) Chen, Y.; Sijbesma, R. P. *Macromolecules* **2014**, *47* (12), 3797–3805.

(14) Beiermann, B. A.; Kramer, S. L. B.; Moore, J. S.; White, S. R.; Sottos, N. R. *ACS Macro Lett.* **2012**, *1* (1), 163–166.

(15) Lee, C. K.; Davis, D. a; White, S. R.; Moore, J. S.; Sottos, N. R.; Braun, P. V. *Journal of the American Chemical Society*. November 17, 2010, pp 16107–16111.

(16) Gossweiler, G. R.; Hewage, G. B.; Soriano, G.; Wang, Q.; Welshofer, G. W.; Zhao, X.; Craig, S. L. *ACS Macro Lett.* **2014**, *3*, 216–219.

(17) Wang, Q.; Gossweiler, G. R.; Craig, S. L.; Zhao, X. *Nat. Commun.* **2014**, *5* (May), 4899.

(18) Gossweiler, G. R.; Brown, C. L.; Hewage, G. B.; Sapiro-Gheiler, E.; Trautman, W. J.; Welshofer, G. W.; Craig, S. L. *ACS Appl. Mater. Interfaces* **2015**, *7* (40), 22431–22435.

(19) O'Bryan, G.; Wong, B. M.; McElhanon, J. R. *ACS Appl. Mater. Interfaces* **2010**, *2* (6), 1594–1600.

(20) Jiang, S.; Zhang, L.; Xie, T.; Lin, Y.; Zhang, H.; Xu, Y.; Weng, W.; Dai, L. *ACS Macro Lett.* **2013**, *2* (8), 705–709.

(21) Hong, G.; Zhang, H.; Lin, Y.; Chen, Y.; Xu, Y.; Weng, W.; Xia, H. *Macromolecules* **2013**, *46* (21), 8649–8656.

(22) Li, M.; Lei, L.; Zhang, Q.; Zhu, S. *Macromol. Rapid Commun.* **2016**, *37* (12), 957–962.

(23) Stelescu, M. D.; Manaila, E.; Craciun, G.; Zuga, N. *Polym. Bull.* **2012**, *68* (1), 263–285.

(24) Svoboda, P.; Petr. *Polymers (Basel).* **2015**, *7* (12), 2522–2534.

(25) Dikland, H. G.; van der Does, L.; Bantjes, A. *Rubber Chem. Technol.* **1993**, *66* (2), 196–212.

(26) Murgic, Z. H.; Jelenic, J.; Murgic, L. *Polym. Eng. Sci.* **1998**, *38* (4), 689–692.

(27) Li, M.; Zhang, Q.; Zhu, S. *Polymer (Guildf).* **2016**, *99*, 521–528.

(28) Peterson, G. I.; Larsen, M. B.; Ganter, M. A.; Storti, D. W.; Boydston, A. J. *ACS Appl. Mater. Interfaces* **2015**, *7* (1), 577–583.

(29) Hiss, R.; Hobeika, S.; Lynn, C.; Strobl, G. *Macromolecules* **1999**, *32* (13), 4390–4403.

(30) Kim, J. W.; Jung, Y.; Coates, G. W.; Silberstein, M. N. *Macromolecules* **2015**, *48* (5), 1335–1342.

4.8 Supporting Information

Mold Dimensions

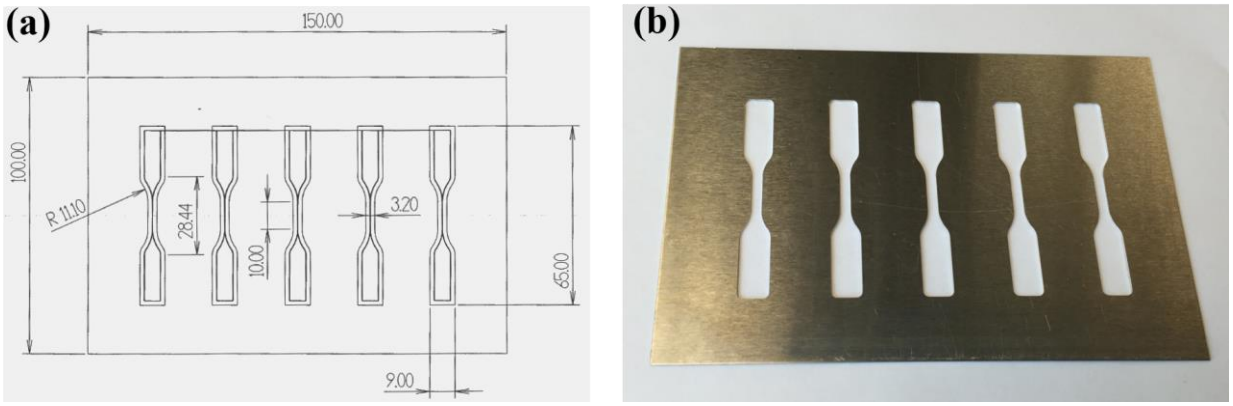

Figure S4-1 Dog bone shaped molds for preparing EVA samples. (a) Dimensions of the molds; (b) Molds for hot pressing polyolefin.

Onset Strain for SP Activation

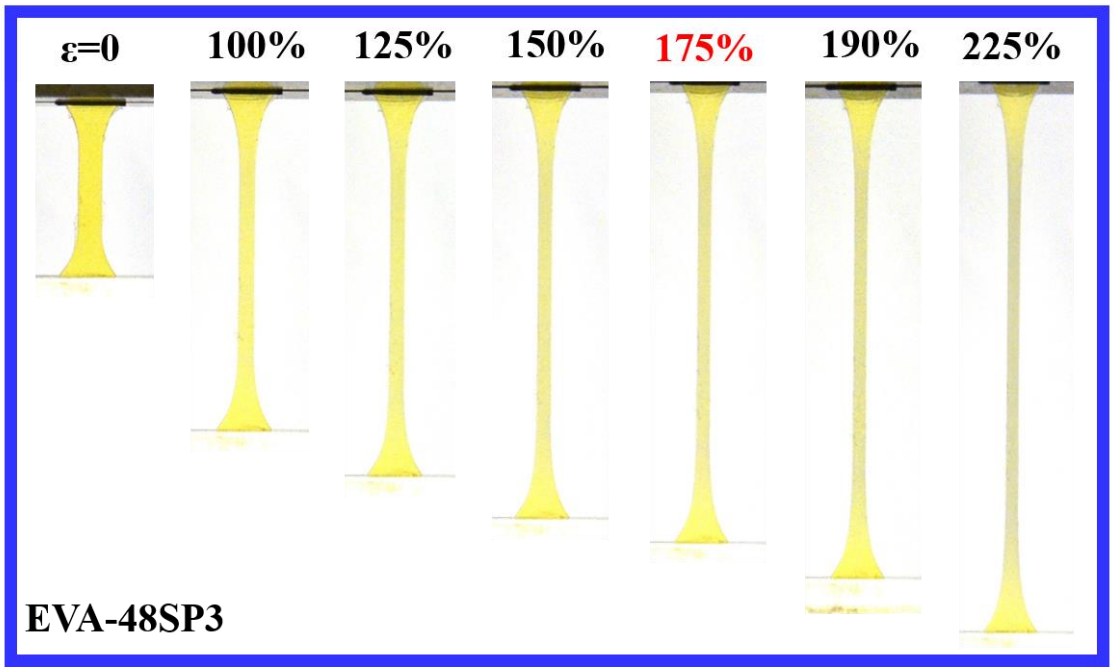

Figure S4-2 Optical images of the gauge of EVA-48SP3 during uniaxial tensile test at the strain rate of 30 mm/min. The onset strain for SP activation was ~175%.

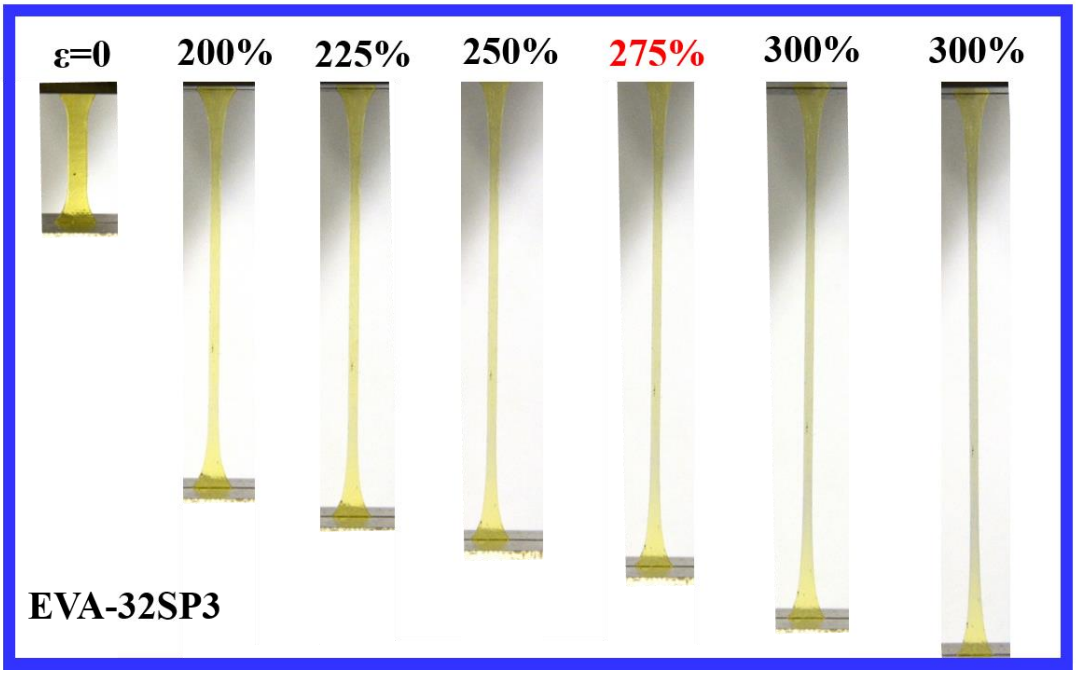

Figure S4-3 Optical images of the gauge of EVA-32SP3 during uniaxial tensile test at the strain rate of 30 mm/min. The onset strain for SP activation was ~275%.

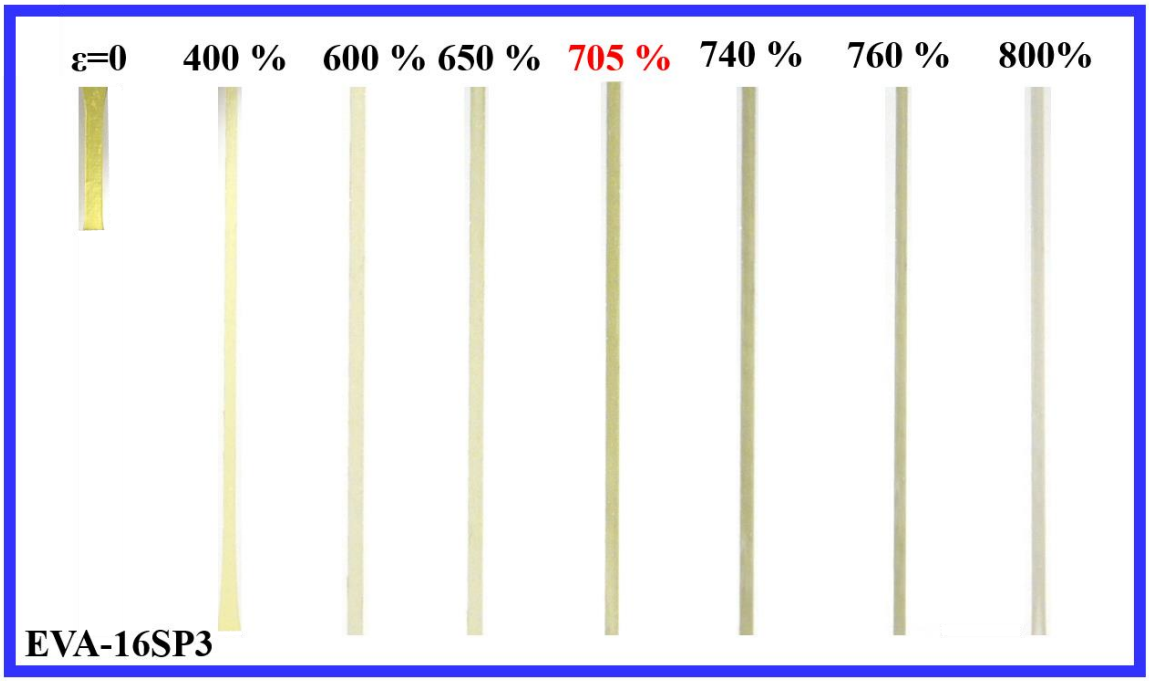

Figure S4-4 Optical images of the gauge of EVA-16SP3 during uniaxial tensile test at the strain rate of 30 mm/min. The onset strain for SP activation was ~705%.

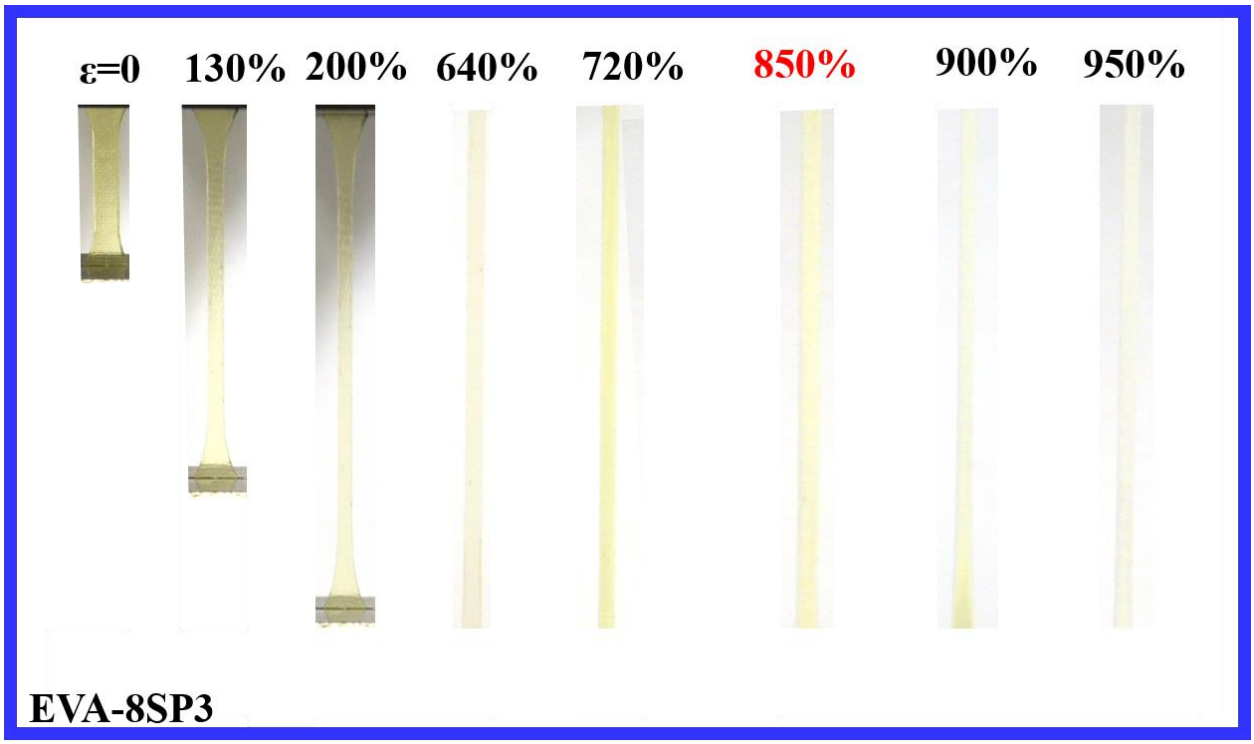

Figure S4-5 Optical images of the gauge of EVA-8SP3 during uniaxial tensile test at the strain rate of 30 mm/min. The onset strain for SP activation was ~850%.

Chapter 5 Mechanoactivation of Spiropyran in Acrylic Latex Coating

This chapter is based on the manuscript entitled "Mechanical Force Sensitive Acrylic Latex Coating", published on *ACS Applied Materials & Interfaces*, **2017**, 9 (17), p.15156-15163 (doi: 10.1021/acsami.7b04154). The permission of this reproduction is granted by American Chemical Society. This work represents the first example of mechanoresponsive acrylic latex coating through color changing and also potentially broadens the application of mechanophore into latex paint, adhesives and protective coating for damage sensing.

Author Contributions

The original idea of incorporating spiropyran into acrylic latex coating was generated jointly by Meng Li, Dr. Qi Zhang and Prof. Shiping Zhu. Meng Li performed all the experiments and prepared the manuscript draft, which was then revised by Dr. Weifeng Liu, Dr. Qi Zhang and Prof. Shiping Zhu.

5.1 Abstract

In this work, we prepared force sensitive acrylic latex coatings by covalently incorporating spiropyran mechanophore. The acrylic latexes were obtained through emulsion copolymerization of butylacrylate (BA), methyl methacrylate (MMA) with vinyltriethoxysilane (VTES) as inter-

particle cross-linker and (1'-(2-(methacryloyloxy)ethyl)-3',3'dimethylspiro(chromene-2,2'-indolin)-6-yl)methyl methacrylate) (SP) as intra-particle cross-linker. The latexes of P(BA-*co*-MMA-*co*-SP-*co*-VTES) were subsequently cast onto Teflon coated surface to form latex coatings. The condensation of hydrolyzed VTES provided inter-particle cross-linking and improved mechanical properties of the formed thin films. Intra-particle cross-linker SP endowed the coatings with mechanoreponsiveness. The mechanoactivation of SP-containing latex films was demonstrated. Increasing the content of intra-cross-linker SP resulted in higher stress sensitivity and lower critical stress required for mechanoactivation. Increasing the content of inter-particle cross-linker VTES resulted in higher critical stress for SP mechanoactivation but had little effect on the stress sensitivity. T_g and operation temperature also showed significant effect on mechanoactivation. Slower strain rate allowed for higher SP-to-MC conversion. This work represents the first example of mechanochromic acrylic latexes and provides insight into the design of force-sensitive and self-reporting polymer coatings.

5.2 Introduction

Over the past decades, there has been increasing interest in smart polymers that are responsive to external stimuli, such as temperature, pH, light, voltage and redox agents.[1] Mechanically responsive polymers elicit advantageous chemical reactivity in response to mechanical force, including changes in color, fluorescence, stiffness and conductivity.[2,3] The most prevalent method to design a mechanoactive polymer is to incorporate force-sensitive molecule (mechanophore) into polymer backbone. The mechanophore can be converted to another chemical species under

sufficient mechanical loading. A diverse range of mechanophores have been designed and investigated, facilitating various mechanoreactivity, such as mechanochromism,[4] mechanoluminescence,[5] mechanocatalysis,[6] damage healing,[7] remodeling of polymers,[7] release of small molecules.[8]

Spiropyran (SP) is an effective mechanophore, which undergoes reversible 6-π ring-opening reaction to generate merocyanine (MC) when mechanical force is applied across C_{spiro}-O bond (Scheme 5-1a).[9] The ring-closed SP form is colorless or yellow and non-fluorescent, whereas the ring-opened MC isomer is purple or blue or red and fluorescent. So far, three types of SP mechanophores have been reported in literature, shown in Scheme 5-1b. Containing different functional groups, SP mechanophores have been used as initiator in polycondensation, initiator in ATRP and cross-linker in free radical polymerization. Moore's group pioneered incorporating SP1 mechanophore into poly (methyl methacrylate), poly (methyl acrylate) and polyurethane.[4,1011] Weng et al. studied mechanoreactivity of SP2 in triblock copolymer polystyrene-*b*-poly(*n*-butylacrylate)-SP-poly(*n*-butylacrylate)-*b*-polystyrene and dual cross-linked elastomer.[12,13] Craig's group investigated the performance of SP2 in poly(dimethylsiloxane).[14] Boydston et al. reported the mechanoreactivity of SP3-containing poly(ε-caprolactone).[15] Compared to the other two types of SP mechanophores that are sensitive to both UV irradiation and mechanical force, SP3 is sensitive to mechanical force but not to UV irradiation due to the absence of nitro group. The unique signature of SP3 makes it a promising stress/strain probe for outdoor materials.

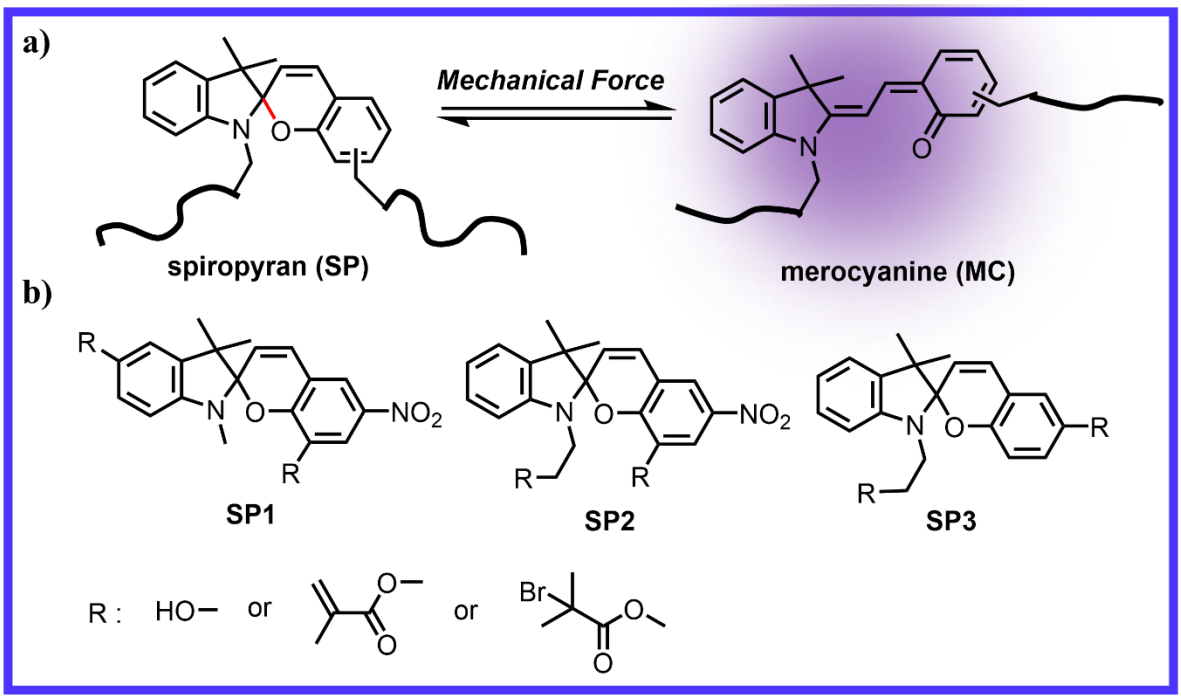

Scheme 5-1 (a) Ring-opening reaction of SP to MC in response to mechanical force. (b) Three types of SP mechanophores. The functional group R on SP mechanophores can be hydroxyl group, methylacryloyl ester group and α-bromoisobutyryl group.

Recently, our group has launched a research program of broadening the application of SP mechanophore into functional and structural polymeric materials. Inspired by the unique features of SP3, we designed and synthesized divinyl SP3 cross-linker mechanophore, suitable for free radical polymerization, which is the major mechanism for polymer production. We prepared SP3 cross-linked poly(methylacrylate) and investigated its mechanoactivation behavior.[16] We incorporated SP3 cross-linker into CO_2-breathing microgels and studied breathing-induced SP mechanoactivation.[17] We also embedded SP3 cross-linker into polyolefins, which account for

more than half of the total commercial polymers, and demonstrated its mechanoactivation.[18] The objective of the program is to expand potential applications of the stress/strain sensitive color changing polymers, making the most important commodity polymers, such as olefins and acrylics "smart" by imparting mechanoresponsiveness.

Rendering polymer coatings with color changing in response to mechanical force enables structural health monitoring (SHM) for various structural components in real time. Mechanochromic polymer coatings that can give off early visible warnings are of great importance to prevent catastrophic damage to the structural components from occurring. So far the designs of mechanochromic coatings have been achieved via the incorporation of mechanophore and mechanochromic crystals into polymer coatings.[19–21] Microencapsulation is another alternative to give off color indication of mechanical damage through the release of a payload upon mechanical rupture.[22,23] However, the existing mechanochromic polymer coatings are still limited to solvent-based formulations. Demanding environmental regulations call for polymer coatings with low volatile organic compounds (VOC). Water-borne acrylic latex coatings are important substitutes to meet the requirement of the environmental friendly policies. Therefore, it becomes highly desirable to design mechanochromic water-borne acrylic latex coatings, which can change color in response to mechanical force.

Aqueous acrylic latexes have been widely used in various areas, such as protective coatings, paints and adhesives. Imparting acrylic latex coatings with force sensitive feature provides lots of

potential applications. Herein, we propose to incorporate SP mechanophore into aqueous acrylic latexes to obtain color changing polymer coating in response to mechanical loadings. As is shown in Scheme 5-2, latexes of P(BA-*co*-MMA-*co*-SP-*co*-VTES) are prepared via emulsion copolymerization. The introduction of siloxane monomer VTES is to enable inter-particle cross-linking, which can give better "welding" between latex particles and improve the mechanical properties of latex films.[24–26] After film formation, the hydrolysis and condensation of siloxane results in cross-linking at room temperature.[24,25] The incorporation of divinyl monomer SP is to render the latex coating with force sensitivity. The focus of this work is to investigate the mechanoactivation of P(BA-*co*-MMA-*co*-SP-*co*-VTES) latex coatings under uniaxial stretching. The effects of intra-particle cross-linker SP content, inter-particle cross-linker VTES content and T_g on the mechanoactivation behavior of polymer latex coatings are studied in great detail. The effect of strain rate on the performance of mechanoactivation is also demonstrated. To the best of our knowledge, it is the first example of mechanochromic acrylic latex coatings, which would offer deep insight of stress distribution of latex coatings under deformation and broaden the application of stress/strain sensitive and self-reporting features into coatings.

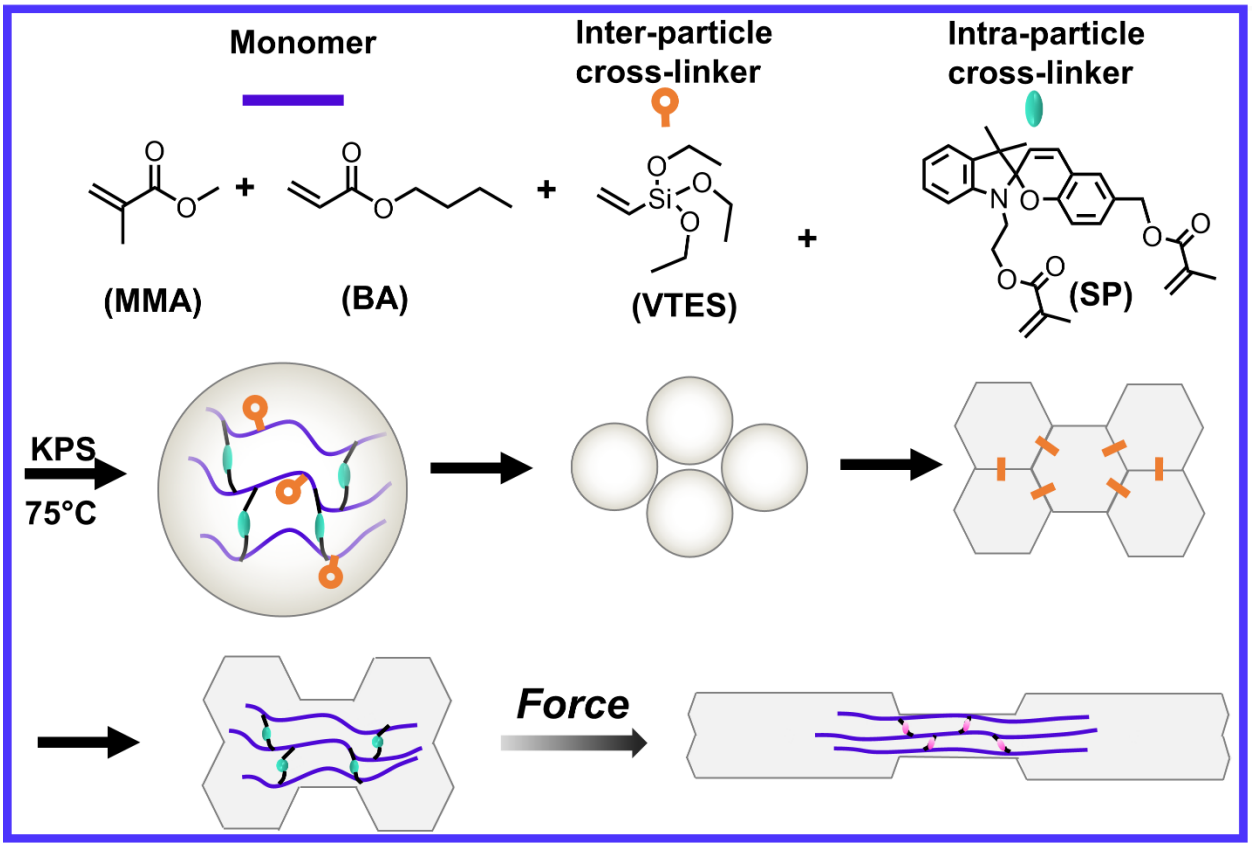

Scheme 5-2 Preparation of P(BA-*co*-MMA-*co*-SP-*co*-VTES) latexes through emulsion polymerization, latex film formation and mechanoactivation of the latex film under deformation

5.3 Experimental Methods

5.3.1 Materials

Methyl methacrylate (MMA, 99%, Aldrich) and butyl acrylate (BA, ≥ 99%, Aldrich) were passed through an inhibitor remover-packed column to remove monomethyl ether hydroquinone and stored at -10 °C before use. Vinyltriethoxysilane (VTES, 97%, Aldrich), potassium persulfate (KPS, ≥ 99%, Sigma-Aldrich), sodium dodecyl sulfate (SDS, ≥ 99%, Sigma-Aldrich), and sodium bicarbonate ($NaHCO_3$, ≥ 99.7%, Sigma-Aldrich) were used as received unless stated otherwise. (1'-(2-(Methacryloyloxy)ethyl)-3',3'dimethylspiro(chromene-2,2'-indolin)-6-yl)methyl methacrylate (SP) was synthesized *via* the methods outlined by Meng *et al*.[27] Mili-Q grade water was generated by Barnstead Nanopure Diamond System and used for all emulsion polymerizations.

5.3.2 Preparation of P(BA-co-MMA-co-SP-co-VTES) Latexes

The recipes for the emulsion polymerization to prepare P(BA-*co*-MMA-*co*-SP-*co*-VTES) (BMSV) latexes were summarized in Table 5-1. Take BMSV-4 as an example: 0.165 g SDS and 0.0395 g $NaHCO_3$ were charged into a 50 mL round-bottomed flask containing 6.5 mL Mili-Q grade water. The monomer mixture of 2.30 g BA, 1.93 g MMA, 0.15 g SP, and 0.37 g VTES was emulsified in the aqueous solution. The emulsion polymerization was carried out by a batch process. The pre-emulsified mixture was stirred with a magnetic bar at 300 rpm and flushed with N_2 for 30 min,

during which the reactor was brought up to 75 °C. 0.0455 g KPS in 1 mL water was then added to the reactor. The reaction mixture turned from white to light blue after ~1 min and gradually became white thereafter. The reaction was continued for 3.5 h at 300 rpm before cooled down to room temperature.

5.3.3 Characterization of Latex Emulsions

Solid Content The solid content of the filtered latex emulsion was determined by the gravimetric method. A weight of M' of latex emulsion was cast onto a Teflon coated surface and finally gave a constant weight of M'' of the latex film after thoroughly dried at room temperature for 48 h and then 60 °C in a vacuum oven for 24 h. The solid content was determined as the weight ratio of M''/M'.

DLS Dynamic light scattering (DLS) was used to measure hydrodynamic diameters of the latex particles. The measurements were conducted on a particle size analyzer (Brookhaven, 900 Plus) with a 35 mW red diode laser source at 634 nm with a detection angle of 90°. The latex emulsions were first equilibrated for 3 min and then measured 3 times with 3 min interval.

5.3.4 Preparation and Characterization of Latex Films

Latex emulsions were cast into Teflon coated molds (40 mm × 40 mm × 0.05 mm), placed under room temperature for 48 h, and then further dried at 60 °C in a vacuum oven for 24 h to remove volatiles. The latex films were easily removed from the molds for the following characterizations.

Gel Fraction Measurements A latex polymer film was dried to a constant weight M_0. The dried polymer was then immersed in tetrahydrofuran (THF) with gentle agitation for 48 h to remove sol contents. The remaining latex film was then dried in vacuum oven for 24 h to a constant weight M_1. The gel content was determined as M_1/M_0.

ATR-FTIR Since the latex films were elastic, it was difficult to obtain polymer powder for FTIR characterization. Instead, Attenuated Total Reflectance (ATR, Thermal NICOLET 6700) was used to characterize the latex films BMSV-1~6 (0.2 mm in thickness). The latex films were placed on the stage and scanned for 64 times at a resolution of 0.5 cm^{-1} by DTGS KBr Detector. After deduction of background, ATR spectra of the samples were obtained with a wavelength ranging from 4000 to 500 cm^{-1}.

Glass Transition Temperature The glass transition temperature (T_g) of the latex films was measured using TA Instruments Differential Scanning Calorimetry (DSC) 2910. In each experiment, around 10 mg of polymer was placed in a hermetic aluminum pan. For each polymer

sample, two cycles of a cooling-heating process were performed. In each cycle, the sample was equilibrated at -50 °C for 3 min, then heated up to 100 °C at the rate of 20 °C/min, held at 100 °C for 3 min and cooled down to -50 °C again. T_g of the polymer was determined by the cross-over point of two tangent lines before and after the transition area in the second heating cycle. T_g of latex particles was also measured for comparison. For characterization, the latex samples were prepared by freeze drying of latex emulsions.

5.3.5 Mechanical Property and Mechanoactivation Characterization

Tensile Tests Tensile tests were performed at a strain rate of 30 mm/min with an Instron 3366 tester (Instron, Corporation; Canton, MA) at room temperature. Each stress-strain curve was obtained based on three repeated measurements. All the stress mentioned in this paper is engineering stress unless stated otherwise. The following procedure was utilized to prepare the samples for tensile tests. The dried latex films were hot pressed into a mold (35 mm × 35 mm × 0.032 mm) between two polytetrafluoroethylene (PTFE) sheets under Carver Press 4389 at 120 °C for 5 min to remove air bubbles and other defects. The films were then easily removed from the molds and cut into smaller specimens (2 mm × 35 mm × 0.032 mm) for tensile tests.

RGB Color Analysis Mechanoactivation of the polymer latex films was characterized by RGB color analysis. A digital camera (NIKON, D5300) with a NIKOR 18-55 mm 1: 3.5-5.6 G ED lens was set to take optical images of the specimens every 2 s with a white board as background during

tensile tests. Images were analyzed in Adobe Photoshop CS6 Software to obtain the average intensity of red (R), green (G) and blue (B) at the region of interest for RGB ratio calculation. Using Grassmann's law[28], the RGB ratio of each optical image was calculated as rRC=R/(R+G+B), rGC=G/(R+G+B) and rBC=B/(R+G+B). Herein, rBC was used as the indication of blue color intensity, which was the characteristic color of the mechanoactivated SP.

5.4 Results and Discussion

5.4.1 Characterization of Acrylic Latex Emulsions and Coatings

Emulsion copolymerization of BA and MMA was carried out at 75 °C for 3.5 h using KPS as initiator, SDS as surfactant and $NaHCO_3$ as pH buffer to minimize the hydrolysis of silane during reaction. A small amount of SP and VTES were added as intra-particle cross-linker and inter-particle cross-linker, respectively. The latex emulsion was then cast on a Teflon coated surface to obtain latex coatings. The recipes of emulsion polymerization runs and the properties of latex emulsions as well as the corresponding latex films are summarized in Table 5-1. The SP content was regulated at 0 ~ 3 wt% in BMSV-1 ~ 4 to study the effect of SP content on mechanoactivation. The effect of T_g on mechanoactivation was also investigated by adjusting the ratio of BA/MMA, while the content of SP and VTES were kept constant in BMSV-5. The effect of inter-particle cross-linker VTES content on mechanoactivation was also studied by increasing VTES amount and keeping BA/MMA ratio and SP content constant in BMSV-6.

Table 5-1 Recipes of the Emulsion Polymerization Runs, Properties of the Latex Emulsions and the Latex Films

Sample[a]	Monomer (wt %)				Particle Size (nm)	PDI	Solid Content (wt %)	Gel Fraction (wt%)	T_g[b] (°C)	T_g[c] (°C)
	BA	MMA	SP	VTES						
BMSV-1	46	41.6	0	7.4	70.2 ± 1.3	0.11	36.1	86.2	13.7	-3.8
BMSV-2	46	40.6	1	7.4	64.8 ± 1.3	0.11	36.3	93.3	12.0	-4.2
BMSV-3	46	39.6	2	7.4	64.5 ± 2.3	0.12	34.4	93.0	5.7	-4.1
BMSV-4	46	38.6	3	7.4	64.0 ± 2.8	0.10	33.5	93.1	-4.1	-4.5
BMSV-5	33.9	50.7	3	7.4	65.5 ± 1.6	0.10	33.2	94.0	27.1	26.4
BMSV-6	44	36.9	3	11.1	93.0 ± 5.4	0.15	36.3	93.8	11.9	11.8

[a] BMSV-1 ~ 6 were prepared with 0.91 wt% of KPS, 3.3 wt% of SDS and 0.79 wt% of $NaHCO_3$ at 75 °C for 3.5 h.

[b] T_g of the latex films.

[c] T_g of latex particles, obtained from freeze drying of latex emulsions.

After polymerization, all the runs yielded stable latexes, with SP and silane monomer incorporated. The optical images of latex emulsions of BMSV-1 ~ 6 are shown in Figure S5-1. The nascent latex

emulsion BMSV-1 with no SP exhibited white, while the latex emulsions with SP incorporated appeared to be pale yellow from embedded spiropyran.[14] The yellow coloration deepened with the increased SP amount.

During film formation, hydrolysis and condensation of VTES provided inter-particle cross-linking. Even though the hydrolysis and condensation of silane would still occur during emulsion polymerization, the latex particles were stabilized by surfactant and separated from each other.[25,29] Due to hydrophobicity, the silane moiety resided inside the separated latex particles, largely reducing the possibility of inter-particle cross-linking during emulsion polymerization. Therefore, inter-particle cross-linking mainly occurred during film formation instead of emulsion polymerization.

The intensity average particle sizes of the latex emulsions were between 53.3 and 93.0 nm with PDI ranging between 0.10 and 0.15. The relatively small diameters resulted from the high surfactant concentration. For BMSV-1~4, the particle diameter decreased from 70.2 nm to 64.0 nm, probably due to the increased cross-linking density in the latex particles. Adding high VTES content resulted in an increase in diameter from 64.0 nm to 93.0 nm. When the high content of VTES was added, more hydrolysis and condensation would occur during emulsion polymerization, which caused latex particle coagulation easier. Due to the coagulation, the diameter of latex particles increased and the particle size distribution became broad with more VTES incorporated. This agreed with the reports in the literatures.[24,26] Compared with the theoretical 40% solid content,

the filtered latex emulsion had solid content ranged from 32.7% to 36.3% mainly due to the coagulant.

The gel fraction of the latex films was also estimated through sol extraction experiment to confirm effective cross-linking of the latex films. Compared with 86.2% gel fraction of BMSV-1, the gel fraction increased to 93.3% when 1 wt% of intra-particle cross-linker SP was added, but levelled off with further increase of SP content. The increased amount of inter-particle cross-linker from 7.4% to 11.1% had virtually little effect on the gel fraction. Therefore, the obtained latex films were all highly cross-linked.

The cross-linked structure of the latex films was also confirmed by ATR-FTIR. Figure S5-2a shows the ATR spectrum of the latex film BMSV-4. The absorbance bands at 1727, 1447, 1380 and 1158 cm^{-1} were the characteristic peaks of MMA and BA. The disappearance of absorbance band at ~1718 cm^{-1} corresponding to C=C stretching confirmed the high conversion of monomers and cross-linkers. The band at 1118 cm^{-1} (υ(Si-O-Si)) indicated the formation of inter-particle cross-linking. All the ATR spectra of latex films shown in Figure S5-2b are almost the same, suggesting all the latex films were well cross-linked through the condensation of hydrolyzed silane. However, the band at 1075 cm^{-1} (δ(Si-O-C)) indicated an incomplete hydrolysis of VTES and the absorption band between 3100 and 3600 cm^{-1} (υ(Si-O-H)) also suggested an incomplete condensation.

Through DSC analysis, the latex films T_g were obtained and listed in Table 5-1. Increasing the content of intra-particle cross-linker decreased T_g from 12.0 to -4.1 °C. The higher SP content resulted in more highly cross-linked microgels, which constrained the movement of polymer chains and limited their ability to meet and react with –OH groups from polymer chains in the other particles. Hence, T_g of the latex films decreased with the fewer inter-particle cross-links. When VTES content was increased from 7.4 % to 11.1%, T_g of latex films increased from -4.1 °C to 11.9 °C, due to more inter-particle cross-links and thus higher rigidity.[25] T_g of the latex particles was also measured for comparison. By freeze drying the latex emulsions, the dried latex particles were obtained for the analysis of latex particle T_g. BMSV-2~4 latex particles possessed almost the same T_g (~ -4.3 °C), due to the same total amount of MMA and SP in latex particles. Comparing T_g of latex films and latex particles, we found that containing lower intra-particle cross-linker content (0 ~ 2 wt%), the latex films exhibited much higher T_g than latex particles, attributed to the formation of inter-particle cross-links in latex films. When the latex contained high intra-particle cross-linker content (3 wt%), the latex film had almost the same T_g as that of the latex particles, probably due to impeded inter-particle diffusion and poor inter-particle cross-linking.

5.4.2 Tensile Tests and Mechanoactivation of Latex Thin Films

The mechanoresponsive properties of the SP-containing acrylic latex thin films were investigated. BMSV-4 was taken as an example to demonstrate the SP mechanoactivation. The rectangular latex films were subjected to a uniaxial tensile loading till failure at a controlled strain rate of 30 mm/min at room temperature. The mechanical force induced coloration was monitored by digital camera

and the optical images were taken every 2 s. The blue channel intensity (rBC) of the gauge section was calculated via RGB method, described in Experimental Methods.

The representative optical images of the mechanoactivation behavior of BMSV-4 during the tensile test are shown in Figure 5-1a. Upon stretching, the latex film turned from the original yellow to white. The white coloration at strain between 100% and 294% was probably attributed to crazing, probably due to relatively low inter-particle cross-linking degree. Although the amount of VTES added was as high as 7.4 wt%, the reactivity ratio of VTES was two orders magnitude lower than BA,[29] resulting in rather low amount of silane monomer incorporated into acrylic copolymer and thus low degree of inter-particle cross-linking. After ~294% strain, the blue coloration started to emerge, indicating the ring-opening reaction of colorless SP form to blue MC form. The blue coloration deepened with the increasing deformation until failure. The stress-strain curve of BMSV-4 is shown in Figure 5-1b. During elongation, the latex film yielded at 168% strain, associated with crazing, and finally failed at 686% strain.

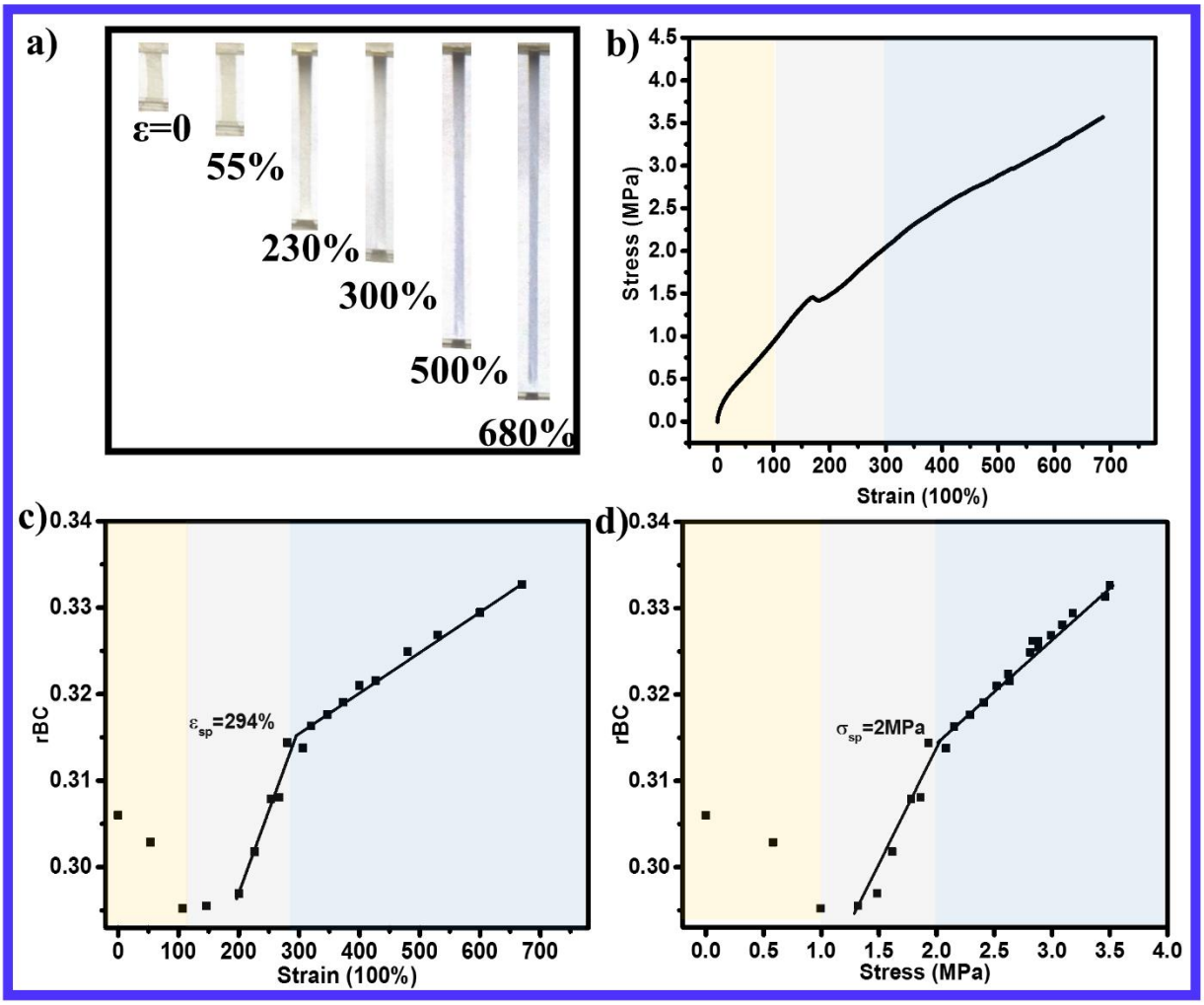

Figure 5-1 (a) Optical images of BMSV-4 at different strains during tensile test. (b) Stress-strain curve of BMSV-4. (c) rBC as a function of strain for BMSV-4. (d) rBC as a function of stress for BMSV-4. In b-d, the yellow, white and blue region indicate the coloration of latex film during tensile test.

Figure 5-1c and 5-1d present rBC as a function of strain and stress, respectively. The initial decrease of rBC at 0 ~ 100% strain and the subsequent increase of rBC at 100% ~294% of strain

could be explained by the whitening effect. The onset strain of mechanoactivation of SP (ε_{sp}) was estimated to be 294%, determined by the crossover point of two tangent lines in Figure 5-1c. The onset stress of SP mechanoactivation (σ_{sp}) was around 2 MPa. After 294% of strain (2 MPa in stress), the blue coloration emerged and deepened with the further elongation. Increasing strain induced higher stress applied on the mechanophore, leading to higher SP-to-MC conversion. The increase of rBC with strain and stress appeared linear between 294% and 686% of strain. Even though it would be helpful to quantify the conversion of SP-to-MC, the mechanophore used in this work was SP3 type, which is not UV sensitive and thus the conversion could not be quantitatively determined.

5.4.3 Effect of Intra-particle Cross-linker SP Content on Mechanoactivation

The effect of intra-particle cross-linker SP content on mechanoactivation of the latex films was then studied. The mechanical properties and mechanoactivation of three latex films containing different SP content (BMSV-4, BMSV-3 and BMSV-2) were evaluated in comparison with the nascent latex film without SP (BMSV-1). In uniaxial tensile tests, all latex films were stretched at the strain rate of 30 mm/min, during which optical images were taken for RGB analysis.

The stress-strain curves of the three SP-containing latex films and SP-absent latex films are shown in Figure 5-2a. The Young's modulus decreased significantly as the SP content reached 3 wt%. It is probably because adding more SP led to the formation of microgels with high cross-linking

density, and the highly cross-linked polymer chains impeded the effective inter-diffusion and inter-particle mixing. Therefore, the poor mechanical properties of latex films containing high SP content were the result of poor inter-particle welding. However, adding a small amount of intra-particle cross-linker SP (1~2 wt%) improved the strength of latex films, compared to the nascent latex film (BMSV-1). Nevertheless, the incorporation of intra-particle cross-linker resulted in the failure of the latex films at an earlier strain during stretching.

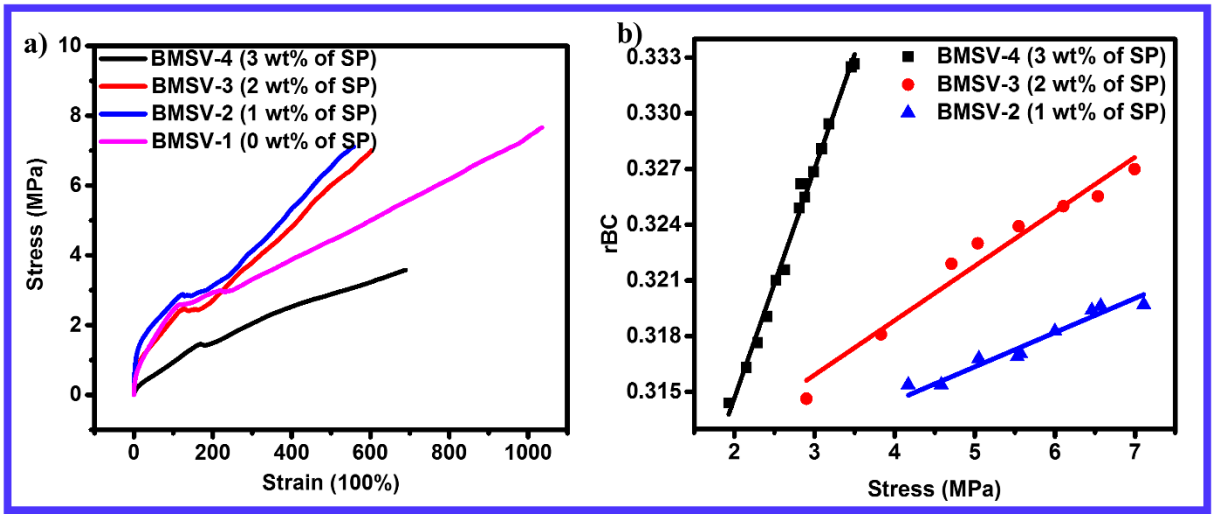

Figure 5-2 (a) The stress-strain curves of three latex films containing different SP content and nascent latex coating with no SP. (b) The rBC as a function of stress for the three latex films containing different SP content.

The rBC of latex films containing various SP content is plotted against stress in Figure 5-2b. All of the SP-containing latex films underwent "whitening" effect, followed by the emergence of blue

coloration. The profile of rBC vs. stress of the three latex films exhibited linear relationship but with different slopes. The slope increased with the increasing SP content. Assuming same SP-to-MC conversion under the same stress, a higher initial content of SP would afford higher content of the blue MC form, resulting in higher blue intensity. Therefore, the latex films with higher SP content appeared to be more sensitive to stress. Moreover, it was also observed that increasing SP content led to lower critical stress for activation, which agreed with our previous work.[16,18] The onset stresses of mechanoactivation of SP to MC for BMSV-4, BMSV-3 and BMSV-2 were estimated to be 2, 2.7 and 4.2 MPa, respectively.

5.4.4 Effect of Inter-particle Cross-linker VTES Content on Mechanoactivation

The effect of inter-particle cross-linker VTES content on the mechanoactivation of SP was also investigated. BMSV-6 containing 11.1 wt% VTES was used to compare with BMSV-4, containing 7.4 wt% VTES. The mechanical properties and mechanoactivation of the two polymer films were compared and studied.

Figure 5-3a shows the stress-strain curves of BMSV-4 and BMSV-6. The Young's modulus of latex films increased with the increasing content of VTES. Unlike BMSV-4, BMSV-6 showed a steep stress peak, followed by a slower stress increase up to the failure at ~ 7 MPa. There were two possible reasons for the enhanced Young's modulus in BMSV-6. On the one hand, when more VTES was introduced into the polymer, more cross-linking would be obtained, limiting the

movement of polymer segments and thus increasing Young's modulus. On the other hand, higher content of inter-particle cross-linker gave better welding between the microgel particles during film formation, which improved the mechanical strength of latex films. Compared with the elastomer BMSV-4, BMSV-6 exhibited elastoplastic feature. After ~2 MPa, higher stress was required for further elongation, because the stronger cross-linking could hinder plastic flow of the polymer.

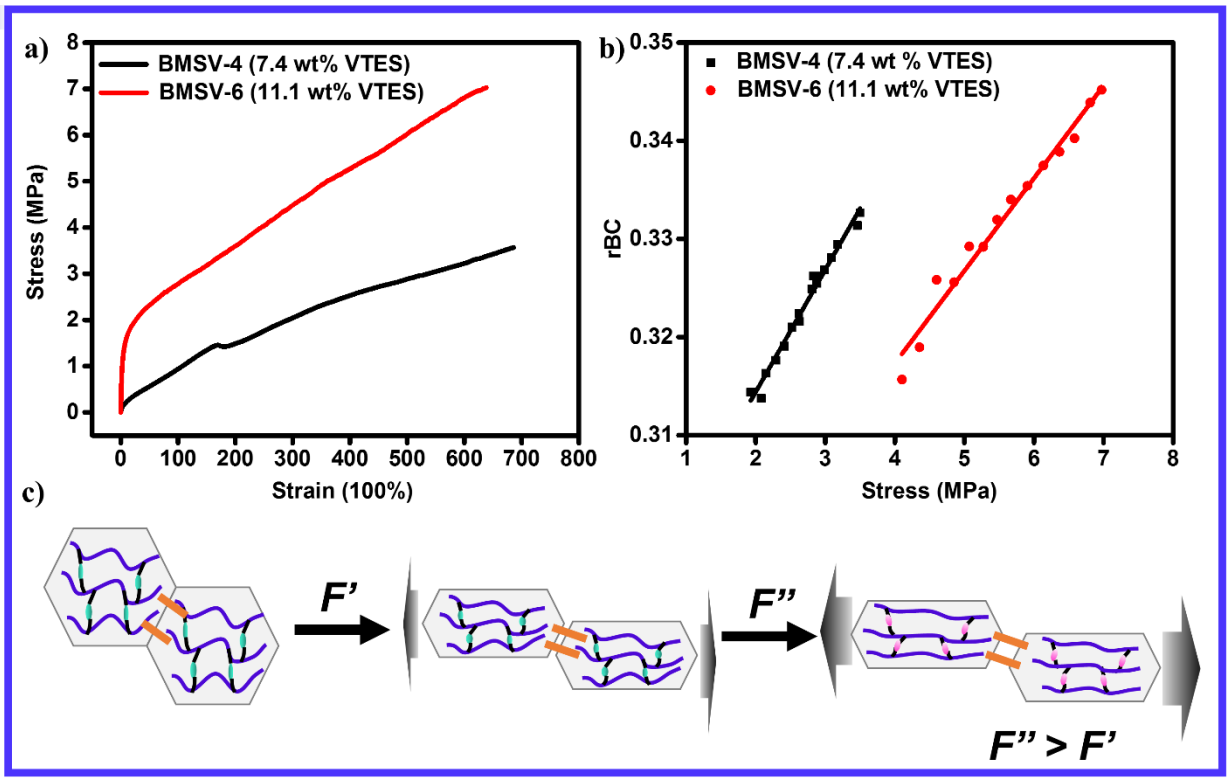

Figure 5-3 (a) The stress-strain curves of two latex films containing different amount of VTES. (b) The rBC of two latex films containing different amount of VTES as a function of stress. (c) Schematic illustration of stress distribution and mechanoactivation of SP during deformation

The rBC of BMSV-4 and BMSV-6 is plotted against stress in Figure 5-3b. The slopes of rBC vs. stress of the two latex films were almost the same, indicating the same sensitivity to stress. The inter-particle cross-linker content had little influence on the sensitivity of mechanophore to mechanical force. However, the content of VTES made a significant difference in the critical stress for mechanoactivation of SP to MC. The threshold stress of SP mechanoactivation for BMSV-4 and BMSV-6 were 2 and 3.6 MPa, respectively. The higher threshold stress of mechanoactivation for BMSV-6 should be related to the high inter-particle cross-linking. The possible mechanism for this phenomenon was illustrated in Figure 5-3c. Upon stretching, the force was loaded onto the inter-particle cross-linker. In BMSV-6, there were more inter-particle cross-links, which could bear higher stress before the relative motion of the particles. After the stress was increased above the value that the inter-particle cross-link could bear, the adjacent latex particles started to be aligned along the elongation direction. The stress was then transferred to the inside of latex particles, and finally to the intra-cross-linker and induced the activation of SP-to-MC.

Therefore, the incorporation of SP mechanophore within latex particles enables stress mapping on the molecular level and provides deeper insight of the effect of inter- and intra-particle cross-linker on the mechanical properties of latex films. It is suggested that applying mechanophore as inter-particle cross-linker could be another alternative for stress mapping during latex film deformation and possibly enable visual detection of small changes of strain/stress.

5.4.5 Effect of T_g and Operation Temperature on Mechanoactivation

By adjusting the ratio of MMA/BA, we were able to obtain latex films with different T_g. Containing the same amount of SP and VTES, BMSV-5 with higher MMA/BA ratio was prepared to compare with BMSV-4 for the purpose of discussing the effect of T_g on the mechanoactivation of latex films. Figure 5-4 shows the stress-strain curves of BMSV-4 (T_g= -4.1 °C) and BMSV-5 (27.1 °C) at room temperature (~ 23 °C). The uniaxial mechanical response of BMSV-5 showed plastic feature, exhibiting a distinct yield peak and ductility with a strain up to 313%. Even though the failure stress of BMSV-5 was much higher than that of BMSV-4, no mechanically induced blue coloration was observed for BMSV-5 prior to failure. During the stretching of BMSV-5, the plastic deformation was not sufficient to allow for the alignment of polymer chains and mechanophore SP and thus the force was not transferred across mechanophore yet to activate SP before failure. To improve the polymer chain mobility, we carried out the tensile test of BMSV-5 at elevated temperature (just above T_g). Vibrant blue coloration was observed when BMSV-5 was heated up during elongation. Therefore, T_g of the latex coating and corresponding operation temperature are two important factors to be considered in the design of mechanochromic acrylic latex coatings for different environments.

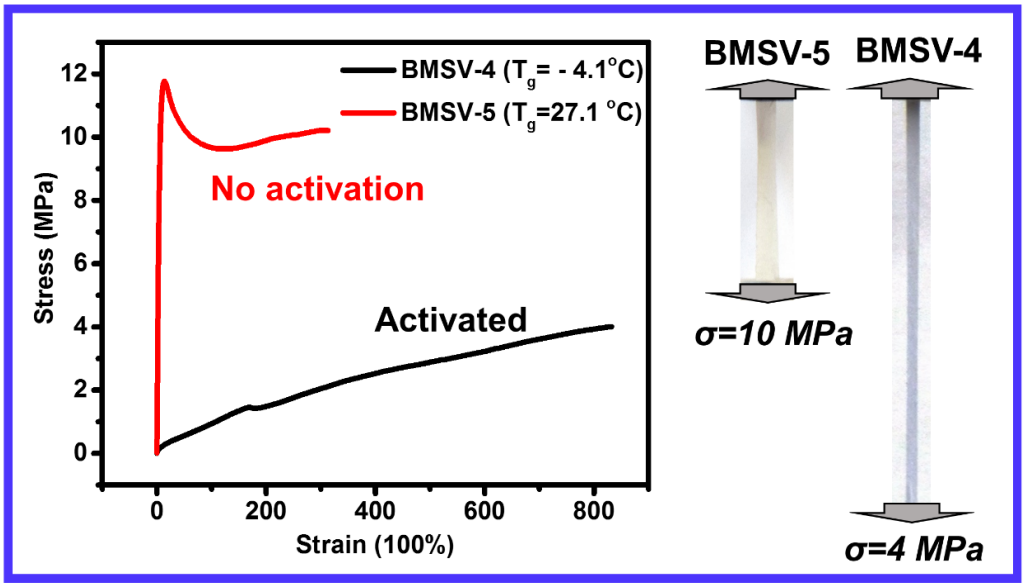

Figure 5-4 Stress-strain curves of BMSV-4 and BMSV-5 and optical images of the two latex films during elongation just before failure

5.4.6 Effect of Strain Rate on Mechanoactivation

To investigate the effect of strain rate on mechanoactivation of SP, tensile tests of BMSV-4 were performed at three different strain rates, which were 30, 120 and 180 mm/min. As shown in Figure 5-5a, with the increasing strain rate, the Young's modulus increased, but the failure strain decreased. The rBC vs. stress at different strain rates is plotted in Figure 5-5b. The rBC value at certain stress appeared to be higher at slower strain rates, which agreed with the previous observations in literature.[18,30] It was attributed to the time-dependent feature of the ring-opening

reaction of SP. When force was applied on the mechanophore at a slower strain, more time was given to allow for the higher conversion of SP-to-MC.

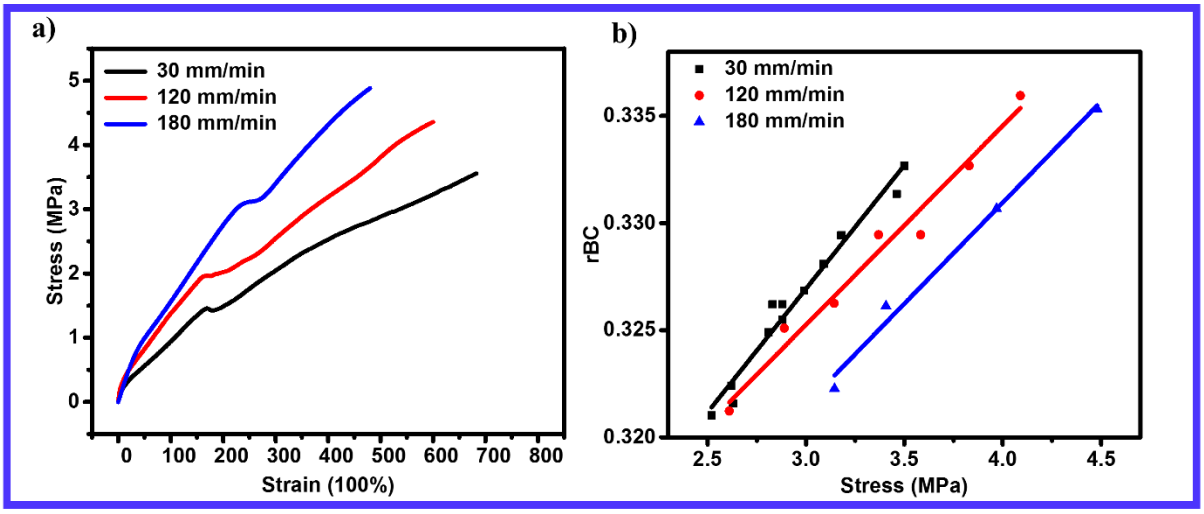

Figure 5-5 (a) The stress-strain curves of BMSV-4 under different strain rates (30, 120, 180 mm/min). (b) The rBC as a function of stress at different strain rates.

5.5 Conclusion

In conclusion, we have prepared P(MMA-*co*-BA-*co*-VTES-*co*-SP) latexes via emulsion polymerization and the corresponding latex coatings. Mechanical force-induced activation of SP in the latex films was demonstrated. Increasing the content of intra-particle cross-linker SP led to higher stress sensitivity and lower critical stress for activation. However, increasing the content of inter-particle cross-linker resulted in higher critical stress for mechanoactivation of SP and no

change in stress sensitivity. Moreover, the mechanoactivation was not observed in the latex films with high T_g (27.1 °C) stretched at room temperature, due to the insufficient plastic flow to enable SP mechanophore activation. Elevated operation temperature enabled mechanoactivation of SP in the high T_g latex film prior to failure. In the end, we also demonstrated slower strain rate enabled higher conversion of SP-to-MC due to the time-dependent feature of the reaction. As far as we are concerned, this work represents the first example of force sensitive acrylic latex coatings, which not only enriches the fundamental knowledge of mechanical properties of latex coatings, but also opens up potential application of mechanophore in various potential areas, such as force-sensitive paints, adhesives and protective coatings with little VOC.

5.6 Acknowledgement

The authors sincerely acknowledge the Natural Science and Engineering Research Council (NSERC) (RGPIN-2015-05841) of Canada for supporting this fundamental research through Discovery Grant program. We also thank the Canada Foundation for Innovation (CFI) (200154) for the equipment and facilities. S. Z. thanks the Canada Research Chair (CRC) (950-229035) program for supporting his research.

5.7 References

(1) Wei, M.; Gao, Y.; Li, X.; Serpe, M. J. *Polym. Chem.* **2017**, *8* (1), 127–143.

(2) Beyer, M. K.; Clausen-Schaumann, H. *Chem. Rev.* **2005**, *105* (8), 2921–2948.

(3) Caruso, M. M.; Davis, D. A.; Shen, Q.; Odom, S. A.; Sottos, N. R.; White, S. R.; Moore, J. S. *Chem. Rev.* **2009**, *109* (11), 5755–5798.

(4) Davis, D. A.; Hamilton, A.; Yang, J.; Cremar, L. D.; Van Gough, D.; Potisek, S. L.; Ong, M. T.; Braun, P. V; Martínez, T. J.; White, S. R.; Moore, J. S.; Sottos, N. R. *Nature* **2009**, *459* (7243), 68–72.

(5) Chen, Y.; Spiering, a J. H.; Karthikeyan, S.; Peters, G. W. M.; Meijer, E. W.; Sijbesma, R. P. *Nat. Chem.* **2012**, *4*(7), 559–562.

(6) Jakobs, R. T. M.; Ma, S.; Sijbesma, R. P. *ACS Macro Lett.* **2013**, *2* (7), 613–616.

(7) Lenhardt, J. M.; Black, A. L.; Craig, S. L. *J. Am. Chem. Soc.* **2009**, *131* (31), 10818–10819.

(8) Diesendruck, C. E.; Steinberg, B. D.; Sugai, N.; Silberstein, M. N.; Sottos, N. R.; White, S. R.; Braun, P. V; Moore, J. S. *J. Am. Chem. Soc.* **2012**, *134* (30), 12446–12449.

(9) Klajn, R. *Chem. Soc. Rev.* **2014**, *43* (1), 148–184.

(10) Beiermann, B. A.; Davis, D. A.; Kramer, S. L. B.; Moore, J. S.; Sottos, N. R.; White, S. R. *J. Mater. Chem.* **2011**, *21* (23), 8443.

(11) Lee, C. K.; Davis, D. a; White, S. R.; Moore, J. S.; Sottos, N. R.; Braun, P. V. *J. Am. Chem. Soc.* 2010, pp 16107–16111.

(12) Jiang, S.; Zhang, L.; Xie, T.; Lin, Y.; Zhang, H.; Xu, Y.; Weng, W.; Dai, L. *ACS Macro Lett.* **2013**, *2* (8), 705–709.

(13) Chen, Y.; Zhang, H.; Fang, X.; Lin, Y.; Xu, Y.; Weng, W. *ACS Macro Lett.* **2014**, *3* (2), 141–145.

(14) Gossweiler, G. R.; Hewage, G. B.; Soriano, G.; Wang, Q.; Welshofer, G. W.; Zhao, X.; Craig, S. L. *ACS Macro Lett.* **2014**, *3*, 216–219.

(15) Peterson, G. I.; Larsen, M. B.; Ganter, M. A.; Storti, D. W.; Boydston, A. J. *ACS Appl. Mater. Interfaces* **2015**, *7* (1), 577–583.

(16) Li, M.; Zhang, Q.; Zhu, S. *Polymer.* **2016**, *99*, 521–528.

(17) Li, M.; Lei, L.; Zhang, Q.; Zhu, S. *Macromol. Rapid Commun.* **2016**, *37* (12), 957–962.

(18) Li, M.; Liu, W.; Zhu, S. *Polymer.* **2017**, *112*, 219–227.

(19) Charles R. Hickenbot, Gregory J. McCollum, E. F. *US Pat.* **2012**, *13* (549), 818.

(20) Anu Chopra, Jun Deng, Charles R. Hickenboth, R. M. P. *US Pat.* **2012**, *13* (447), 604.

(21) Grady, M. E.; Beiermann, B. A.; Moore, J. S.; Sottos, N. R. *ACS Appl. Mater. Interfaces* **2014**, *6* (8), 5350–5355.

(22) White, S. R.; Sottos, N. R.; Geubelle, P. H.; Moore, J. S.; Kessler, M. R.; Sriram, S. R.; Brown, E. N.; Viswanathan, S. *Nature* **2001**, *409* (6822), 794–797.

(23) Blaiszik, B. J.; Kramer, S. L. B.; Olugebefola, S. C.; Moore, J. S.; Sottos, N. R.; White, S. R. *Annu. Rev. Mater. Res.* **2010**, *40* (1), 179–211.

(24) Ramos-Fernández, J. M.; Beleña, I.; Romero-Sánchez, M. D.; Fuensanta, M.; Guillem, C.; López-Buendía, Á. M. *Prog. Org. Coatings* **2012**, *75* (1), 86–91.

(25) Guo, T. Y.; Xi, C.; Hao, G. J.; Song, M. D.; Zhang, B. H. *Adv. Polym. Technol.* **2005**, *24* (4), 288–295.

(26) Guo, T.; Chen, X.; Song, M.; Zhang, B. *J. Appl. Polym. Sci.* **2006**, *100* (3), 1824–1830.

(27) Li, M.; Zhang, Q.; Zhu, S. *Polymer.* **2016**, *99*, 521–528.

(28) *Colorimetry*; Schanda, J., Ed.; John Wiley & Sons, Inc.: Hoboken, NJ, USA, 2007.

(29) Marcu, I.; Daniels, E. S.; Dimonie, V. L.; Hagiopol, C.; Roberts, J.; El-Aasser, M. *Macromolecules* **2003**, *36* (2), 328–332.

(30) Kim, J. W.; Jung, Y.; Coates, G. W.; Silberstein, M. N. *Macromolecules* **2015**, *48* (5), 1335–1342.

5.8 Supporting Information

Figure S5-1 Optical images of latex dispersions of BMSV-1~7.

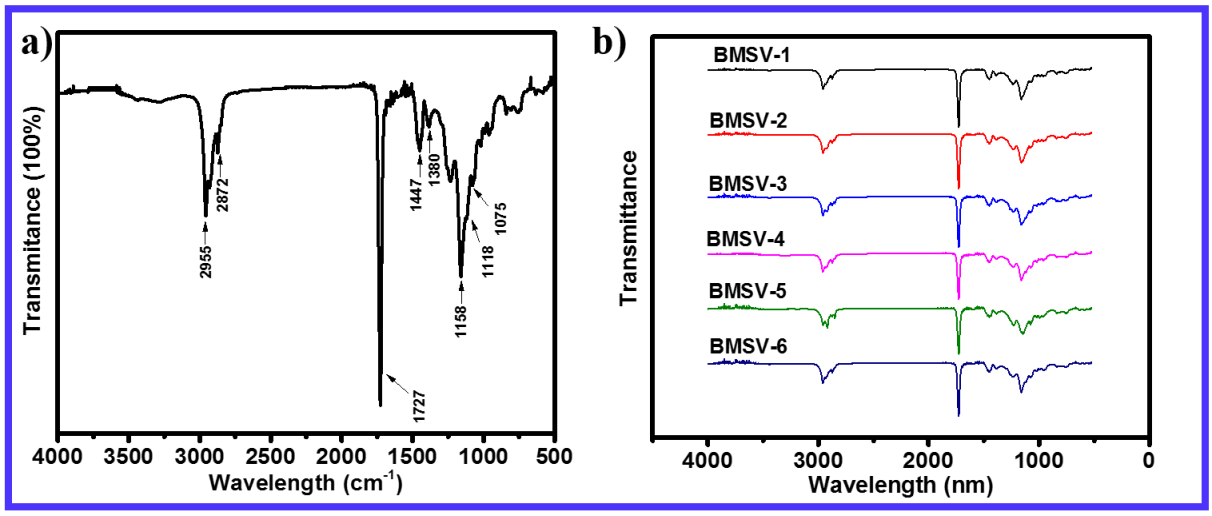

Figure S5-2 (a) ATR of BMSV-4 (b) ATR of BMSV-1~6

Chapter 6 Mechanoactivation of Spiropyran in CO_2-Breathing Microgels

This chapter is based on the manuscript entitled "CO_2-Breathing Induced Reversible Activation of Mechanophore within Microgels", published on *Macromolecular Rapid Communication*, **2016**, *37* (12), p.957–962. (doi: 10.1002/marc.201600119). The permission of this reproduction is granted by John Wiley and Sons. This work represents the first example of CO_2-breathing activation of mechanophore within microgels in aqueous system.

Author Contributions

The original idea of using CO_2 breathing to induce mechanoactivation of spiropyran was generated jointly by Meng Li, Dr. Qi Zhang and Prof. Shiping Zhu. Meng carried out all the experiments and prepared the manuscript draft, which was then revised by Dr. Qi Zhang and Prof. Shiping Zhu.

6.1 Abstract

In this work, CO_2-breathing induced reversible activation of mechanophore within microgels is reported. The microgels were prepared through soap free emulsion polymerization (SFEP) of CO_2-switchable monomer 2-(diethylamino)ethyl-methacrylate (**DEA**), using spiropyran (SP) based mechanophore **MA-SP-MA** as cross-linker. The microgels could be swollen by CO_2 aeration. The swelling of microgels activated the SP mechanophore into merocyanine (MC), causing

distinguished color and fluorescence change. Moreover, these transitions were highly reversible, and the initial states of microgels could be easily recovered by "washing off" CO_2 with N_2. The present contribution represents the first example of CO_2-breathing activation of mechanophore within microgels.

6.2 Introduction

Over the past decades, stimuli-responsive polymers have received growing attention from researchers due to their applications in many areas.[1] Stimuli come into various types, for example, pH,[2] temperature,[3] light,[4] ultrasound,[5] redox agents,[6] and voltage.[7] However, each type of these triggers has its drawbacks, limiting their applicability. For instance, base or acid addition results in salt accumulation and buffer contamination.[8] Due to the limited heat transfer rate, the change of temperature for a large volume system is time consuming and energy intensive. Short penetration depth and potential damage to biological tissues largely limit the applications of ultraviolet (UV) light.

Recent advances of gas trigger/stimuli have opened up new horizons in stimuli-responsive polymers. Compared with base or acid addition, CO_2 treatment has superior features, like benign, inexpensive, nontoxic, highly abundant, no accumulative effect because it is easy to remove by N_2 or Ar purging. It can reversibly react with amidine, amine or carboxyl groups to tune their hydrophilicity within a large window.[9] Yuan et al. prepared CO_2-breathing vesicles self-assembled

from poly (ethylene oxide)-*b*-poly (*N*-amidino) dodecyl acrylamide.[10] Zhao et al. developed a triblock copolymer poly(ethylene oxide)-*b*-poly((*N*-amidine)dodecylacrylamide)-*b*-polystyrene that displayed CO_2-driven self-assembly and shape transformation.[11] They also developed polymer assemblies of triblock copolymers poly(ethylene oxide)-*b*-polystyrene-*b*-poly((2-diethylamino)ethyl methacrylate), which displayed CO_2-driven deformation.[12] Feng et al. synthesized a block random copolymer poly(ethylene oxide)-*b*-poly(2-(diethylamino) ethyl methacrylate-*co*-styrene) and demonstrated CO_2-induced vesicle-to-micelle transformation of its polymer assemblies.[13] Zhu's group reported O_2 and CO_2 dual responsive nanoaggregates of fluoro- and amino-containing polymers.[14] They also developed O_2 and CO_2 dual gas-responsive and switchable microgels.[15] CO_2 has offered great opportunities and possibilities due to its "green" feature.

On the other side, polymer mechanochemistry has recently attracted increasing attention of researchers because the macroscopic mechanical force can be expressed in the form of specific and useful chemical reactions.[16] In the bulk, mechano-responsive polymers have inspired promising applications, such as stress/strain sensing,[17] mechano-catalysis,[18] self-reinforcing,[19] scaffolds for the release of small molecules. [20] The most prevalent method to impart the mechano-responsive feature is to incorporate a labile chemical entity (mechanophore) that is responsive to exogenous mechanical forces. Recent advances in developing new mechanophore have been reported in literatures. Of all types of mechanophores, the most identifiable response is luminescence and color change induced by stress/strain. Meijer, Sijbesma and their coworkers reported bis(adamantly)-1,2-dioxetane that emitted blue luminescence on mechanical

stimulation.[21] In terms of mechanically induced color change, the isomerization of colorless spiropyran (SP) to vibrant purple merocyanine (MC) can be accomplished when mechanical forces are applied across the C_{spiro}-O bond. Moore et al. pioneered employing spiropyran (SP) as mechanophore in poly(methyl acrylate), poly(methyl methacrylate) and polyurethane.[22–24] Craig et al. used SP in elastic poly(dimethylsiloxane), based on which they designed novel devices such as electro-mechano-chemically responsive elastomers and active soft robots.[25–27] Weng et al. incorporated SP into thermoplastic elastomers with supramolecular interactions.[28]

Recently, Zhu et al. reported a novel SP mechanophore cross-linker that had good selectivity towards mechanical force and fast recovery rate from the excited MC state.[29] Herein, we incorporated this SP mechanophore as cross-linker in a CO_2-responsive PDEA microgel system, which was inspired by the work of solvent swelling activation of SP mechanophore in cross-linked PMMA.[24] As is shown in Scheme 6-1, the deformation of microgels could be regulated by CO_2 aeration, which subsequently induced reversible activation of the SP mechanophore previously embedded in the microgels. We demonstrated CO_2 induced breathing behavior and SP activation within microgels. The fluorescence intensity of CO_2-treated microgel dispersions was systematically investigated as a function of cross-linker content. We further studied the relationship among cross-linker content, swelling ratio and fluorescence intensity. To our best knowledge, it is the first time that mechanophores were embedded into smart microgel system to visualize swelling force within microgels. The novelty of our work lies in the combination of color changing mechanophore with CO_2-responsive microgels. Moreover, the behavior of dual responses of the smart microgels (shape deformation and concomitant color change/fluorescence

switch) as a reply to a single external stimulus (CO_2) is compared to biomimetic processes, in which the deformation of cells or living creatures are usually accompanied by concomitant functional transformation (e.g. colorimetric and fluorescent response) upon environmental stimuli. For example, cephalopods (e.g. octopuses, squids and cuttlefish) exhibit vibrant colors, which are controlled by contracting and releasing muscles.[30]

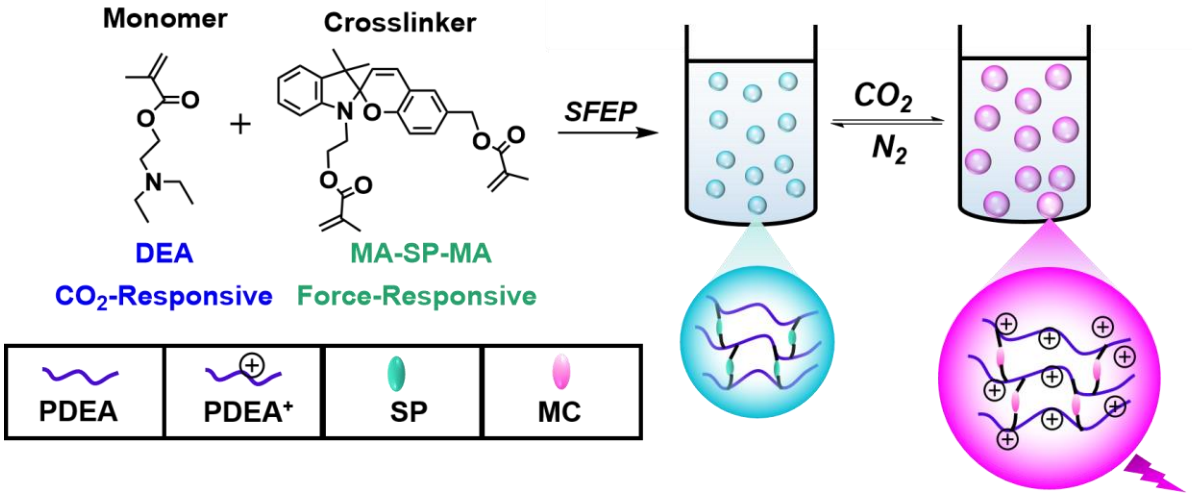

Scheme 6-1 Preparation of P (DEA-*co*-SP) microgel dispersion and CO_2-breathing induced mechanophore activation within microgels

6.3 Experimental Methods

6.3.1 Materials

2-(Diethylamino) ethyl methacrylate (DEA, 99%, Aldrich) was passed through a column filled with inhibitor remover to remove monomethyl ether hydroquinone prior to use. The initiator potassium persulfate (KPS, 99.99%, Aldrich) was used as received. Other chemicals were used directly without further purification unless stated otherwise. Mili-Q grade water for preparation of all microgel aqueous dispersions was generated from Barnstead Nanopure Diamond System. The SP mechanophore cross-linker (1'-(2-(methacryloyloxy)ethyl)-3',3'-dimethylspiro(chromene-2,2'-indolin)-6-yl)methyl methacrylate (**MA-SP-MA**) was synthesized as our previous work.

6.3.2 Preparation of PDEA Microgels

Poly (2-(diethylamino) ethyl methacrylate) (PDEA) microgels with different cross-linker contents were prepared via surfactant-free emulsion polymerization. All the microgels contained 4 wt% initiator KPS (with respect to DEA) and 0.5 ~ 4 wt% of cross-linker **MA-SP-MA** (with respect to DEA), with a fixed solid content of 4 wt%. For PDEA microgels with 1 wt% cross-linker: 0.5 g of monomer DEA and 5 mg of cross-linker **MA-SP-MA** were mixed thoroughly and were charged into a 50 mL round bottom flask containing 10 mL of Mili-Q water. The flask was sealed and flushed with N_2 for 30 min under stirring at 300 rpm. In the meanwhile, the flask was gradually

heated to 70 °C. The degassed solution of 0.02 g of initiator KPS in 2 mL of water were then injected. The reaction mixture turned from light white to blue after 1 ~ 2 min, then to milky white after 10 min. The reaction was allowed to proceed for 24 h before cooled down to room temperature.

6.3.3 CO_2-breathing Induced Reversible Activation of Mechanophore within Microgels

Microgel aqueous dispersions were treated with constant CO_2 flow at 10 mL/ min for 1 h, which was later reversibly expelled by purging N_2 at 10 mL/ min for 1 h. To demonstrate repeatability, another two cycles of the gas aeration were carried out. To illustrate color and turbidity change of microgels stimulated by gaseous aeration, digital pictures were taken after each gaseous aeration. The particle sizes of microgels before and after purging gases were estimated from dynamic light scattering (DLS) measurements. Transmission electron microscope (TEM) images were taken to visualize the morphology and volume change of microgels. The mechanophore activation was further confirmed by UV-vis absorption spectra and fluorescence emission spectra.

6.3.4 Characterization

The hydrodynamic diameters (D_h) of microgels were measured by DLS on particle size analyzer (Brookhaven 900 Plus). Microgel aqueous dispersions of 10 mL (1 mg/ mL) were purged with gases aeration for three cycles. All the gases were purged constantly at 10 mL/ min for 1 h. After

each gas treatment, the microgel dispersions were equilibrated for 180 s before measurement and conducted for 5 times by DLS over a scattering angular range of 90° with interval time of 30 s.

TEM images of microgels were obtained on a JEOL JEM 1200 EX TEMSCAN transmission electron microscope operated at an accelerating voltage of 80 KV. The images were acquired with an AMT 4 megapixel digital camera (Advanced Microscopy Techniques). To obtain the stained samples, one drop of 0.2 wt% of phosphotungstic acid (PTA) aqueous solution was added to 1.5 mL microgel dispersions (1 mg/ mL) before and after gaseous treatment. The specimen was prepared by drop-casting the stained dispersion onto a copper grid, immediately frozen by liquid nitrogen and was subsequently freeze-dried for TEM tests. Fluorescent microscope images of the microgels were taken by confocal laser scanning microscope (LSM510) with excitation wavelength at 543 nm and emission band pass filter at 516 ~ 615 nm. The samples were prepared by drop-casting microgel dispersions (40 mg/ mL) before and after CO_2 treatment onto the microscope slides and then were covered by coverslips. The UV-vis absorption spectra of the CO_2-treated microgel dispersion were obtained on UV-vis spectrometer (Beckman Coulter DU 800) by scanning wavelength from 300 nm to 800 nm. Fluorescence emission spectra of the CO_2-treated microgel dispersion were recorded on fluorescence spectrometer (SPEX Fluorolog 3-22) by scanning wavelength from 560 nm to 800 nm with excitation wavelength at 550 nm and slit at 5 nm. All the spectra were obtained based on 40 mg/ mL of microgel dispersions.

6.4 Results and Discussion

6.4.1 Microgel Preparation

MA-SP-MA was used as cross-linker for PDEA microgel preparation via SFEP. The cross-linker content was regulated at 0.5 ~ 4 wt% with respect to monomer mass. KPS (4 wt% with respect to DEA monomer) was used to initiate the polymerization at 70 °C. After reaction for 24 h, all the runs yielded stable dispersions with little coagulum. The intensity average diameters of microgels were 179 ~ 193 nm with a narrow size distribution (polydispersity index ≤ 0.1), as measured by DLS. The diameter of the initial microgel particles did not show a systematic change with varying cross-linker content.

6.4.2 CO_2-breathing Induced Reversible Activation of Mechanophore within Microgels

The PDEA microgel system with 2 wt% of cross-linker (Run 3 in Table 6-1) was taken as an example to thoroughly investigate CO_2-breathing behavior and mechanophore activation. Figure 6-1a shows that the microgel dispersion underwent turbid-to-transparent transition and concomitant vibrant color change after CO_2 treatment. The increase in transparency was attributed to the decrease of refractive index,[31] induced by increasing the average microgel diameter from ~193 nm to ~375 nm, as shown in Figure 6-1b. The white-to-pink color change indicated SP-to-MC transition within the microgels. After bubbling N_2 to remove CO_2, the dispersion turned back

to turbid white. The turbidity increase was due to shrinkage of the microgels to their initial diameter ~193 nm. The disappearance of pink color was attributed to MC-to-SP isomerization. The reversible CO_2-breathing induced activation of the microgels exhibited good repeatability for at least three cycles with little discoloration due to the potential photo oxidation, as reported in literature.[25] The phenomenon, which was the decoloration after each cycle, was also observed when the cross-linker was incorporated in polymer films. Moreover, this SP bearing no electron withdrawing nitro group is not photochromic. Therefore, the reproducibility of photo activation and its comparison with mechanical activation could not be performed.

Table 6-1 Performance of the microgels as a function of the cross-linker content

Run	SP / wt %	D_0 / nm	D_{CO2} / nm	Swelling ratio a	Emission intensity at 622nm
1	0.5	179	423	13	0.51
2	1	183	400	10	0.64
3	2	193	375	7.3	1.00
4	4	180	310	5.1	0.81

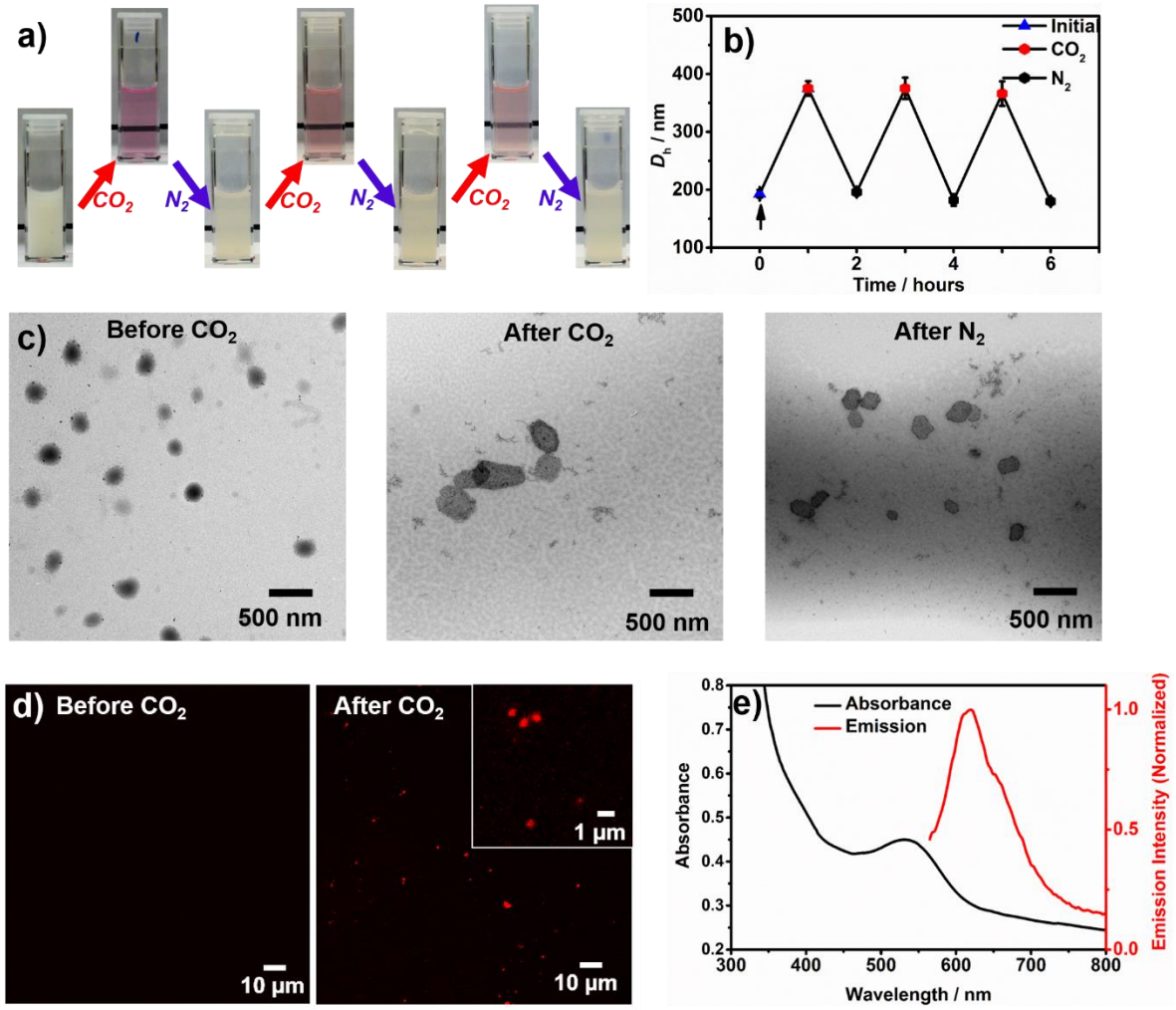

Figure 6-1 Shape deformation and mechanophore activation characterization of P(DEA-*co*-SP) microgel dispersion (2 wt% cross-linker) after gaseous treatment. a) Digital photos of microgel dispersion; b) DLS data of microgels; c) TEM images of microgels; d) Confocal laser fluorescence microscope images of microgel dispersion; e) UV/vis absorption spectrum and fluorescence emission spectrum of microgel dispersion.

TEM was employed to visualize the morphology and shape deformation of the microgels. Stained by PTA, the spherical polymer microgels could be clearly observed, as shown in Figure 6-1c. The

average diameter of the initial microgels was 209 ± 25 nm, statistically calculated from TEM images. The average diameter of microgels increased to 376 ± 60 nm after purging CO_2 and dropped back to 201 ± 26 nm after purging N_2. Almost no aggregation was observed during the microgel expansion and contraction. The diameters estimated from the TEM images were slightly bigger than the DLS results. The microgels after gaseous treatment appeared to be rectangular in TEM images. These might be attributed to the rupture and deformation of the microgels during freeze-drying process.

Confocal fluorescence microscope was employed to investigate the fluorescence properties of microgels before and after CO_2 treatment. Almost no fluorescent microgels (only black background in Figure 6-d, left) could be seen before CO_2 treatment, whereas a large amount of fluorescent microgels (red dots in Figure 6-1d, right) appeared after CO_2 treatment, indicating the SP-to-MC transition. The low pixel resolution made it difficult to observe the distinct boundaries of microgels and thus the size of fluorescent microgels (400 nm ~ 600 nm) appeared to be bigger than the DLS measurements (~363 nm).

To further elucidate this, the UV-vis absorption spectrum of CO_2-treated microgel dispersion (40 mg/mL) was recorded, depicted as the black line in Figure 6-1e. The absorbance band at 550 nm appeared, corresponding to the open MC form. Fluorescence emission spectrum of CO_2-treated microgel dispersion (40 mg/mL) was also characterized, as shown as red line in Figure 6-1e. The emission band at 622 nm was the characteristic peak for the MC form. However, the spectrum of initial microgel dispersion at the same concentration could not be recorded because light could not

penetrate the turbid microgel dispersion. As an alternative, the diluted sample (2 mg/mL) showed no absorption at 550 nm in UV-vis absorption spectrum and no emission at 622 nm in fluorescence emission spectrum, which indicated only negligible amount of MC state in the initial microgel dispersion. Therefore, we can come to a conclusion that a significant amount of SP mechanophore within microgels was activated to the open MC form after CO_2 stimulation. However, fluorescence or UV spectroscopy could not be used for monitoring microgel expansion process to get onset swelling ratio for SP-to-MC isomerization. It is because that the spectrum of the initial microgel solution could only be recorded when it was diluted 20 times (2 mg/mL). However, the fluorescence signal of CO_2-treated microgel dispersion (2 mg/mL) was too weak to be captured. Therefore, it was the light reflection of microgels that limited the possibility of using UV or fluorescence spectroscopy to monitor CO_2 amount and microgel swelling ratio.

A mechanism is proposed here to explain how CO_2 regulated microgel shape deformation and mechanophore activation. It has been well reported that CO_2 could effectively regulate the PDEA microgel volume.[32] In the presence of CO_2, the tertiary amine groups on P(DEA-*co*-SP) became increasingly protonated, which caused increasing osmotic pressure. It drove water molecules to swell into microgels and thus caused the microgel swelling. The amine groups could be reversibly deprotonated after bubbling N_2 to expel CO_2, which led to microgel deswelling.

Herein, swelling ratios were defined as $a = V_{CO2}/V_0 = (D_{CO2}/D_0)^3$, where "$D_0$"and "$D_{CO2}$" were hydrodynamic diameters of the microgels before and after CO_2 treatment, respectively. Therefore, the swelling ratio of CO_2-treated microgels was estimated to be 7.3. It has been reported that

mechanophore SP could be activated at a swelling degree ($\Delta m/m_0$) of only 0.4 in solvent-induced swelling of SP cross-linked PMMA.[24] Therefore, the CO_2-induced swelling force of network was more than sufficient to activate the electro cyclic ring-opening of SP cross-linker. The open MC form showed vibrant pink color. It is known that the thermal SP-to-MC conversion could occur in aqueous media, attributed to hydrogen bond interaction between MC and water molecules. However, the timescale of the thermal SP-to-MC conversion is much longer than the experiments in our work.[33] This effect, therefore, could be neglected. The potential low pH induced SP-to-MC isomerization was also negligible because C_{spiro}-O bond could only be cleaved at pH<4 and pH of CO_2 saturated microgel dispersion could only reach 6.48 in our experiments. Therefore, it was CO_2-induced swelling that facilitated the activation of SP mechanophore.

6.4.3 The Effect of Cross-linker Content on Mechanophore Activation

Microgel dispersions with 0.5 ~ 4 wt% of cross-linker **MA-SP-MA** were prepared and employed to investigate the effect of SP content on the swelling ratio and fluorescence intensity. As is shown in Table 6-1, the swelling ratio was 13 for the least cross-linked microgels (0.5 wt%), while it was only 5.1 for the highest cross-linked microgels (4 wt%). The swelling ratio decreased with increasing the cross-linker content, which agreed with the previous reports.[34] Figure 6-2a shows the fluorescence spectra of CO_2-treated microgel dispersions with varying SP content. All spectra of microgel dispersions displayed the characteristic emission peak at 622 nm. However, the fluorescence intensity varied between different microgel dispersions, as shown in Table 6-1. It is interesting to note that fluorescence intensity increased when the cross-linker content increased

from 0.5 wt% to 2 wt%. However, further increasing the cross-linker content from 2 wt% to 4 wt% resulted in a decrease in the fluorescence intensity. Figure 6-2b shows the relationship among the fluorescence emission intensity, cross-linker content and swelling ratio.

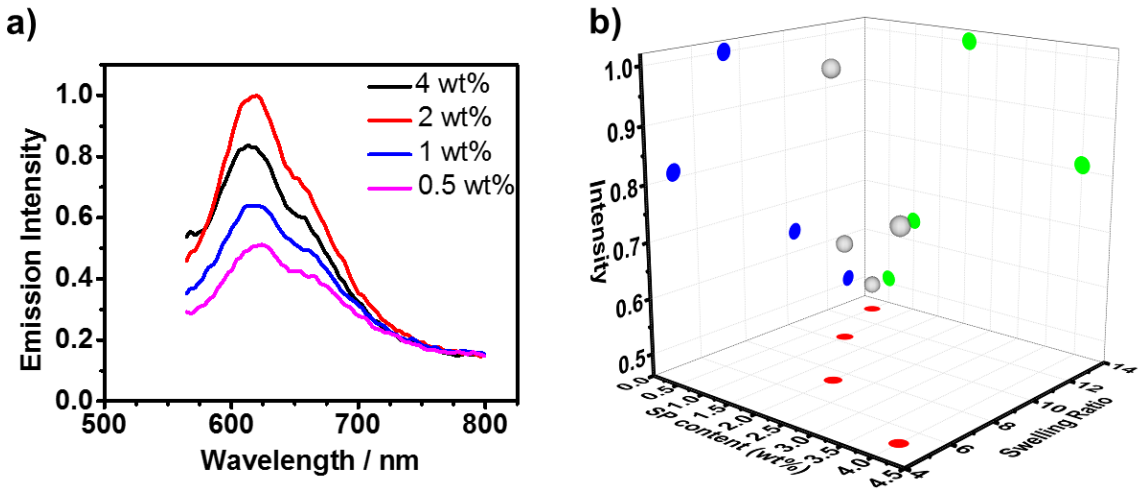

Figure 6-2 a) Fluorescence spectra of microgel dispersions after CO_2 aeration; b) The relationship among fluorescence emission intensity, cross-linker content and swelling ratio. The grey sphere is extracted data, whose x, y and z are SP content, swelling ratio and intensity. The blue, green and red dots are the projection in each plane.

The notable observation can be explained as follows. When the cross-linker content was in the lower range (0.5 ~ 2 wt%), the swelling ratio was higher to induce effective SP activation. Therefore, the higher SP content in the microgels, the more MC amount generated after CO_2 treatment. However, when the cross-linker content was increased to 4 wt%, the swelling ratio was reduced to only 5.1. The swelling force was inadequate in enabling an effective SP-to-MC

activation and thus less MC amount generated. Therefore, microgels with 2 wt% of cross-linker showed an optimal SP activation and the highest fluorescence emission intensity of all the samples.

6.5 Conclusions

We have successfully developed a novel CO_2-switchable color-changeable PDEA microgel system. The microgels were prepared through SFEP of CO_2-responsive monomer DEA, using SP based mechanophore MA-SP-MA as cross-linker. The swelling force induced by CO_2-breathing activated SP-to-MC isomerization, causing distinguished color and fluorescence changes. Moreover, these transitions were highly reversible. The present contribution represents the first example of CO_2-breathing activation of mechanophore within microgels and it provides an effective approach to study the forces inside swollen microgels. It also demonstrates the biomimetic processes with shape deformation and concomitant color/fluorescence change.

6.6 Acknowledgements

The authors sincerely acknowledge the Natural Science and Engineering Research Council (NSERC) of Canada for supporting this fundamental research through Discovery Grant program. We also thank the Canada Foundation of Innovation (CFI) for the equipment and facilities. SZ thanks the Canada Research Chair (CRC) program for supporting his research.

6.7 References

(1) Yoshida, M.; Lahann, J. *ACS Nano* **2008**, *2* (6), 1101–1107.

(2) Dai, S.; Ravi, P.; Tam, K. C. *Soft Matter* **2008**, *4* (3), 435.

(3) Lutz, J.-F.; Akdemir, O.; Hoth, A. *J. Am. Chem. Soc.* **2006**, *128* (40), 13046–13047.

(4) Zhao, Y. *Macromolecules* **2012**, *45* (9), 3647–3657.

(5) Chen, W.; Du, J. *Sci. Rep.* **2013**, *3*, 2162.

(6) Napoli, A.; Valentini, M.; Tirelli, N.; Müller, M.; Hubbell, J. A. *Nat. Mater.* **2004**, *3* (3), 183–189.

(7) Yan, Q.; Yuan, J.; Cai, Z.; Xin, Y.; Kang, Y.; Yin, Y. *J. Am. Chem. Soc.* **2010**, *132* (27), 9268–9270.

(8) Fielding, L. A.; Edmondson, S.; Armes, S. P. *J. Mater. Chem.* **2011**, *21* (32), 11773.

(9) Han, D.; Tong, X.; Boissière, O.; Zhao, Y. *ACS Macro Lett.* **2012**, *1* (1), 57–61.

(10) Yan, Q.; Zhou, R.; Fu, C.; Zhang, H.; Yin, Y.; Yuan, J. *Angew. Chem. Int. Ed. Engl.* **2011**, *50* (21), 4923–4927.

(11) Yan, Q.; Zhao, Y. *Angew. Chemie* **2013**, *125* (38), 10132–10135.

(12) Yan, Q.; Zhao, Y. *J. Am. Chem. Soc.* **2013**, *135* (44), 16300–16303.

(13) Liu, H.; Guo, Z.; He, S.; Yin, H.; Fei, C.; Feng, Y. *Polym. Chem.* **2014**, *5* (16), 4756.

(14) Zhang, Q.; Zhu, S. *ACS Macro Lett.* **2014**, *3* (8), 743–746.

(15) Lei, L.; Zhang, Q.; Shi, S.; Zhu, S. *Langmuir* **2015**, *31* (7), 2196–2201.

(16) Caruso, M. M.; Davis, D. A.; Shen, Q.; Odom, S. A.; Sottos, N. R.; White, S. R.; Moore, J. S. *Chem. Rev.* **2009**, *109* (11), 5755–5798.

(17) Davis, D. A.; Hamilton, A.; Yang, J.; Cremar, L. D.; Van Gough, D.; Potisek, S. L.; Ong, M. T.; Braun, P. V; Martínez, T. J.; White, S. R.; Moore, J. S.; Sottos, N. R. *Nature* **2009**, *459* (7243), 68–72.

(18) Jakobs, R. T. M.; Ma, S.; Sijbesma, R. P. *ACS Macro Lett.* **2013**, *2* (7), 613–616.

(19) Ramirez, A. L. B.; Kean, Z. S.; Orlicki, J. A.; Champhekar, M.; Elsakr, S. M.; Krause, W. E.; Craig, S. L. *Nat. Chem.* **2013**, *5* (9), 757–761.

(20) Diesendruck, C. E.; Steinberg, B. D.; Sugai, N.; Silberstein, M. N.; Sottos, N. R.; White, S. R.; Braun, P. V; Moore, J. S. *J. Am. Chem. Soc.* **2012**, *134* (30), 12446–12449.

(21) Chen, Y.; Spiering, a J. H.; Karthikeyan, S.; Peters, G. W. M.; Meijer, E. W.; Sijbesma, R. P. *Nat. Chem.* **2012**, 4(7), 559–562.

(22) Davis, D. a; Hamilton, A.; Yang, J.; Cremar, L. D.; Van Gough, D.; Potisek, S. L.; Ong, M. T.; Braun, P. V; Martínez, T. J.; White, S. R.; Moore, J. S.; Sottos, N. R. *Nature*. **2009**, 68–72.

(23) Lee, C. K.; Davis, D. A.; White, S. R.; Moore, J. S.; Sottos, N. R.; Braun, P. V. *J. Am. Chem. Soc.* **2010**, *132* (45), 16107–16111.

(24) Lee, C. K.; Diesendruck, C. E.; Lu, E.; Pickett, A. N.; May, P. A.; Moore, J. S.; Braun, P. V. *Macromolecules* **2014**, *47* (8), 2690–2694.

(25) Gossweiler, G. R.; Hewage, G. B.; Soriano, G.; Wang, Q.; Welshofer, G. W.; Zhao, X.; Craig, S. L. *ACS Macro Lett.* **2014**, *3*, 216–219.

(26) Wang, Q.; Gossweiler, G. R.; Craig, S. L.; Zhao, X. *Nat. Commun.* **2014**, *5*, 4899.

(27) Gossweiler, G. R.; Brown, C. L.; Hewage, G. B.; Sapiro-Gheiler, E.; Trautman, W. J.; Welshofer, G. W.; Craig, S. L. *ACS Appl. Mater. Interfaces* **2015**, *7* (40), 22431–22435.

(28) Zhang, H.; Chen, Y.; Lin, Y.; Fang, X.; Xu, Y.; Ruan, Y.; Weng, W. *Macromolecules* **2014**, *47* (19), 6783–6790.

(29) Li, M, Zhang, Q., Zhu, S. *Polymer*, **2016**, 99, 521-528.

(30) Hanlon, R. *Curr. Biol.* **2007**, *17* (11), R400-4.

(31) D. A. W. Alberto Fernandez-Nieves, Hans M. Wyss, Johan Mattsson, *Wiley-VCH* **2011**.

(32) Yan, Q.; Zhao, Y. *Chem. Commun.* **2014**, *50* (79), 11631–11641.

(33) Shiraishi, Y.; Itoh, M.; Hirai, T. *Phys. Chem. Chem. Phys.* **2010**, *12* (41), 13737–13745.

(34) Varga, I.; Gilányi, T.; Mészáros, R.; Filipcsei, G.; Zrínyi, M. *J. Phys. Chem. B* **2001**, *105* (38), 9071–9076.

Chapter 7 Major Contributions and Recommendations for Future Work

In this chapter, major contributions of this project are summarized, followed by some recommendations and perspectives of possible future research directions based on the current advances of spiropyran mechanochemistry and existing challenges that need to be tackled to broaden the application of spiropyran mechanophore into polymers.

7.1 Major Contributions

The major contributions made in applying spiropyran mechanochemistry into various polymeric systems can be summarized as follows:

- Divinyl SP3 mechanophore cross-linker was firstly synthesized, which is suitable for chain growth polymerization, accounting for more than 80% of total polymer products. It was utilized as an effective cross-linker in the free radical polymerization of MA. The characterization of mechanoactivation of SP3-containing PMA revealed that SP3 has two unique features: (1) SP3 is only sensitive to mechanical force but not to UV, suitable for outdoor materials; (2) The reversion of MC-to-SP is faster in SP3 than other types of SP mechanophores, good for real-time stress-sensing.

- SP3 cross-linker was covalently embedded into two polyolefins, EVA and EOC to enable polyolefins to feel mechanical force by color changing. SP3 exhibited its superiority in high-temperature processing, because SP could not be thermally driven to MC during cross-linking. Increasing SP content led to mechanoactivation at lower strains. Slower strain rates allowed for higher SP-to-MC conversion. When held at constant strain, MC gradually reverted to SP.

- SP3 cross-linker was introduced into acrylic latexes to endow the coatings with force sensitivity. The mechanoactivation of the latex thin film of P(BA-*co*-MMA-*co*-SP-*co*-VTEST) revealed that increasing SP content resulted in higher stress sensitivity and lower critical stress for activation and that increasing VTES content resulted in higher critical stress for SP mechanoactivation.

- SP3 cross-linker was introduced into CO_2-breathing microgels, and its breathing-induced mechanoactivation was demonstrated. When microgels were treated with CO_2, the protonation of tertiary amine groups of PDEA led to microgel swelling, which further mechanically activated SP to MC, causing the emergence of vibrant purple and fluorescence. The transition was highly reversible by treatment with N_2 to wash off CO_2.

- The developments and studies of spiropyran mechanophores were summarized into a comprehensive review from an engineering perspective. SP mechanochemistry, applications in various polymer systems and impacting factors of mechanoactivation behavior were

discussed in great detail in the review, aiming to offer deep insight and perspective into polymer mechanochemistry and provide studying approaches to explore other mechanophores to be applied into polymers.

7.2 Publications

The following is a list of the publications that I have achieved during PhD study. Four research papers are published, and the review paper is under revision.

- Let Spiropyran Help Polymers Feel Force! **M. Li**, S. Zhu, Submitted to *Progress in Polymer Science*, 2017
- Mechanical Force Sensitive Acrylic Latex Coating, **M. Li**, W. Liu, Q. Zhang, S. Zhu, *ACS Appl. Mater. Interface*, 2017, 9(17), 15156-15163.
- Smart Polyolefins Feeling the Force: Color Changeable Poly(Ethylene-Vinyl Acetate) and Poly(Ethylene-Octene) in Response to Mechanical Force, **M. Li**, W. Liu, S. Zhu, *Polymer*, 2017, 112, 219-227.
- Photo-inactive Divinyl Spiropyran Mechanophore Cross-linker for Real-time Stress Sensing, **M. Li**, Q. Zhang, S. Zhu, *Polymer*, 2016, 99, 521-528.
- CO_2-Breathing Induced Reversible Activation of Mechanophore within Microgels, **M. Li**, L. Lei, Q. Zhang, S. Zhu, *Macromol. Rapid. Commun.* 2016, 12 957-962.

7.3 Recommendations for Future Work

In this study, we have covalently introduced SP mechanophore into polyacrylate, polyolefins, latex coating and CO_2-breathing microgels. The significance of this study is not only to enrich the fundamental knowledge of mechanochemistry, but also to open up a door to the application of mechanophores into various polymers, which can be used in our industry and daily life. However, there still some challenges to be tackled regarding the potential applications.

First, the conversion of SP-to-MC under mechanical loading is very limited and reported to be only 20 ~ 30% relative to those that are UV-activated.[1] Strength limitation of the polymer itself and insufficient chain orientation might contribute to the low degree of activation. More studies on developing polymers with superior mechanical properties (i.e. strong, tough and elastic) and pre-straining to align polymer chains and mechanophores are called for to improve SP mechanoactivation yield.

Second, effective SP mechanoactivation usually occurs at large deformation. This largely impedes its application in constructional components, which requires instant color-changing at very low strains. Improving chain mobility and pre-straining to align mechanophores can be employed to achieve activation at low strains. More related studies are needed to enable acute mechanoactivation at very low strains. This might be achieved by adjusting the linking architecture of mechanophore in the polymer system, such as the center of linear polymer and cross-linker in

cross-linked polymer. Increasing the strain rate can be another approach to achieve mechanoactivation at low strains.[2]

Third, mechanoactivation of SP is still limited to homogeneous environments so far. It is desired to investigate mechanoactivation behavior of SP at interfaces of organic/inorganic and organic/organic. To be anchored at the interface, SP molecule should contain two different functional groups. There have been some studies on mechanoactivation of other mechanophores at interfaces.[3,4] Employing SP mechanophore at interfaces can be used to monitor force distribution of composite materials via visual color changing, which is a more direct and easier method for stress detection.

Moreover, SP mechanoactivation in polymer network shows a discrepancy in the results obtained from simulation and experiments, which indicates the inhomogeneity of the polymer network in the experiment.[5,6] It is worthwhile to study how homogeneity influences SP mechanoactivation, which can not only assists in the understanding of stress distribution in polymer networks, but also provides another approach to study the homogeneity of polymer networks.

Last but not least, the development of SP-based mechanoresponsive is still limited to the lab scale. At this stage of the research, we should start to broaden the application of SP mechanochemistry in various areas. There are three potential areas of application for SP-based mechanoresponsive polymers. (1) Employing mechanoresponsive polymer in constructive component for stress-

sensing and damage reporting is highly desired. To achieve this, developing mechanoresponsive polymers with acute responsiveness and long-lasting visual warnings is the key. (2) The color-changing force-sensitive polymers can be used in daily applications, such as soft robot,[7] writing panel,[8] color-changing balloons[7] and toys. (3) The SP mechanophore provides efficient and direct approaches to study force distribution within polymer systems, largely enriching fundamental studies of polymers.

7.4 References

(1) Lee, C. K.; Davis, D. A.; White, S. R.; Moore, J. S.; Sottos, N. R.; Braun, P. V. *J. Am. Chem. Soc.* **2010**, *132* (45), 16107–16111.

(2) Grady, M. E.; Beiermann, B. A.; Moore, J. S.; Sottos, N. R. *ACS Appl. Mater. Interfaces* **2014**, *6* (8), 5350–5355.

(3) Li, J.; Shiraki, T.; Hu, B.; Wright, R. A. E.; Zhao, B.; Moore, J. S. *J. Am. Chem. Soc.* **2014**, *136* (45), 15925–15928.

(4) Woodcock, J. W.; Beams, R.; Davis, C. S.; Chen, N.; Stranick, S. J.; Shah, D. U.; Vollrath, F.; Gilman, J. W. *Adv. Mater. Interfaces* **2017**, *4* (10), 1601018.

(5) Silberstein, M. N.; Cremar, L. D.; Beiermann, B. A.; Kramer, S. B.; Martinez, T. J.; White, S. R.; Sottos, N. R. *J. Mech. Phys. Solids* **2014**, *63*, 141–153.

(6) Silberstein, M. N.; Min, K.; Cremar, L. D.; Degen, C. M.; Martinez, T. J.; Aluru, N. R.; White, S. R.; Sottos, N. R. *J. Appl. Phys.* **2013**, *114* (2), 23504.

(7) Gossweiler, G. R.; Brown, C. L.; Hewage, G. B.; Sapiro-Gheiler, E.; Trautman, W. J.; Welshofer, G. W.; Craig, S. L. *ACS Appl. Mater. Interfaces* **2015**, *7* (40), 22431–22435.

(8) Gossweiler, G. R.; Hewage, G. B.; Soriano, G.; Wang, Q.; Welshofer, G. W.; Zhao, X.; Craig, S. L. *ACS Macro Lett.* **2014**, *3*, 216–219.

Appendix A Exploiting Spiropyran Mechanophore to Indicate Homogeneity of Cross-linked Polymer System

The objective of this project is to utilize the mechanochromism of spiropyran to indicate the homogeneity difference of cross-linked polymer system. Polymethylacrylate (PMA) with spiropyran mechanophore as cross-linker were prepared via free radical polymerization (FRP) and controlled/living radical polymerization (CLRP), respectively. Due to the homogeneity difference in the two cross-linked polymer systems, the first derivative of the plot for color intensity vs. stress of the PMA prepared by FRP is expected to be broader than that prepared via CLRP. Repeated experiments were carried out and the evidence did not show the obvious difference in first derivative of the curves of the two PMA. Instead, we found the PMA prepared via FRP gave lower onset strain for mechanoactivation compared with CLRP.

A.1 Introduction

Studying free radical polymerization (FRP) of multifunctional vinyl monomer is of great importance due to the various applications, such as dental fillings, optical fiber coatings, and ophthalmic lenses.[1–7] However, the network microstructure cannot be well controlled using conventional FRP. As is shown in the top of Figure A-1, it takes seconds for hundreds of monomer to be propagated into an individual polymer chain.[8,9] The fast propagation leaves little time for chain relaxation, leading to the rapid reaction between the radicals and the pendant double bonds

in the vicinity, giving rise to cycles and microgels. With the increasing number of microgels, intermolecular cross-linking began to occur, contributing to microgel aggregation and network formation. The gel radical propagation with monomers and incorporation of microgel lead to the heterogeneous microstructure of the polymer network.

The development of homogeneous cross-linked polymer systems with controlled microstructure have attracted increasing attention. The homogeneity of cross-linked polymer systems plays a crucial rule in high-performance applications, such as drug delivery, catalyst support, molecular sieves, information storage materials, fuel cell membranes.[1,10] Controlled/living radical polymerization (CLRP) offers the possibility to prepare polymers with controlled microstructure, chain topology and functionality.[11–14] As one of the most versatile and robust CLRP, reversible addition-fragmentation chain transfer (RAFT) polymerization method has been utilized to obtain homogeneous polymer network. In RAFT, the chain growth is frequently and temporarily interrupted by the fast exchange between propagating radicals and dormant chains, resulting in few monomers added to the growing chain during each cycle of activation/deactivation, shown in bottom of Figure A-1.[1] The slow chain growth provided sufficient time for chain relaxation, allowing for uniform distribution of reaction species, which suppresses intramolecular cross-linking such as cyclization and facilitates intermolecular cross-linking to generate a homogeneous polymer network.

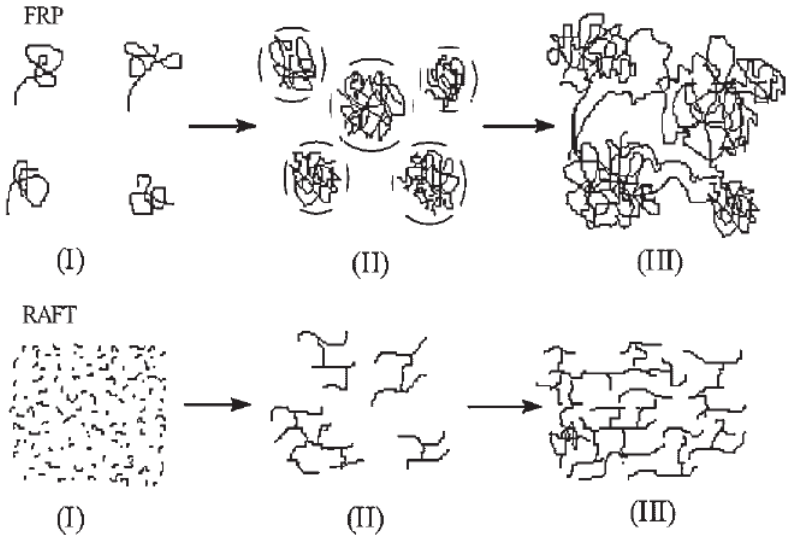

Figure A-1 The network formation process for FRP (top) and RAFT (bottom) polymerization.[1] Copyright 2008, reproduced with the permission from John Wiley and Sons.

Herein, we propose to use SP mechanophore for the indication of the homogeneity of polymer network. Divinyl SP mechanophore has been used as cross-linker in polymers for stress/strain sensing on molecular level through color-changing.[15–17] We believe that the homogeneity difference of polymer network will lead to a difference in the mechanoactivation behavior of the polymer upon stretching. Usually, the performance of SP mechanoactivation in a polymer is characterized by plotting fluorescence intensity or blue color intensity against stress or strain. As a demonstration, a comparison of the blue color intensity vs. strain and stress of the SP-cross-linked PMA, synthesized via FRP and RAFT, is carried out. We assume the first derivative of the curve of PMA prepared by FRP would be broader than that prepared by RAFT due to heterogeneity.

A.2 Experimental Methods

A.2.1 Materials

Prior to use, methyl acrylate (MA, 99%, Aldrich) and ethylene glycol dimethacrylate (EGDMA, 98%, Aldrich) were passed through inhibitor remover to remove monomethyl ether hydroquinone. Benzoyl peroxide (BPO, ≥ 98%, Sigma-Aldrich), *N*, *N*-dimethylaniline (DMA, ≥ 99.5%, Aldrich) and 2-(dodecylthiocarbonothioylthio)-2-methylpropionic acid (DMP, 98%, Aldrich) were used as received. (1'-(2-(methacryloyloxy)ethyl)-3',3'-dimethylspiro(chromene-2,2'-indolin)-6-yl)methyl methacrylate (MA-SP-MA) was synthesized via the procedures reported by Meng et al.[15]

A.2.2 Synthesizing PMA via FRP and RAFT Polymerization Method

For a typical FRP of PMA under room temperature, the polymerization procedure is as follows. A mixture of MA (0.012 mol, 1.2 mL), SP3 (0.06 mmol, 30 mg), EGDMA (0.06 mmol, 11.6 mg), and BPO (0.03 mmol, 7.3 mg) was charged into a sealed reaction vial and flushed with N_2 for 30 min. The reaction mixture was subsequently transferred to PTFE mold capped with rubber stop. Then DMA (3.84 μl, 0.03 mmol) was injected into the mold to start the reaction, shortly after which the viscosity of the mixture increased because of gel effect. To remove the bubbles trapped

in the viscous reaction mixture, the mold was gently tapped. The polymerization was allowed to proceed for 24 h at room temperature (~23 °C). The polymer film PMA1 was easily removed from the mold and used for the later tensile test.

For a typical RAFT of PMA under room temperature, the polymerization procedure was similar to FRP. A mixture of MA (0.012 mol, 1.2 mL), SP3 (0.06 mmol, 30 mg), EGDMA (0.06 mmol, 11.6 mg), BPO (0.03 mmol, 7.3 mg), and DMP (0.03 mmol, 10.8 mg) was treated with N_2 for 30 min in a sealed vial before transferred to the mold. Then the polymerization was started by adding DMA (3.84 μl, 0.03 mmol). After reaction at room temperature for 24 h, the polymerization yielded smooth polymer film PMA2, which was ready for the tensile test.

A.2.3 Tensile Test & RGB Analysis

The tensile test and the RGB analysis of the specimens were carried out in the same way as our previous work.[15]

A.3 Results and Discussion

Figure A-2 shows the stretching-induced mechanoactivation of SP in the specimen PMA1 and PMA2, synthesized via FRP and RAFT, respectively. The original coloration of PMA1 appeared

to be more yellow than PMA2, due to the addition of DMP, the RAFT agent. The addition of DMP might also account for the difference in coloration of the specimens after being stretched. The PMA1 gave off vibrant blue coloration during elongation, whereas PMA2 appeared to be purple during stretching. The emergence of blue and purple coloration indicated the mechanical activation of SP-to-MC. It was also found that PMA2 showed many minor cracks during stretching, which was probably attributed to low Mw of the polymer, prepared via RAFT polymerization.

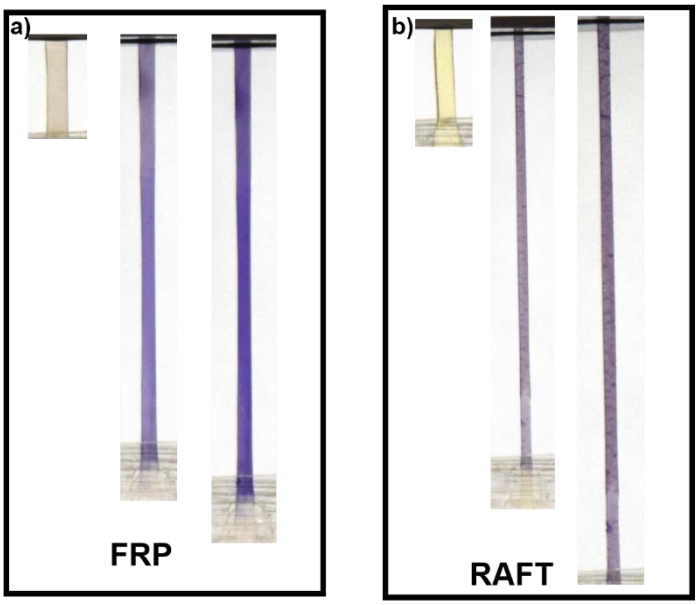

Figure A-2 Optical images of the elongated specimens PMA1 and PMA2, which were prepared via FRP and RAFT, respectively.

During tensile tests, optical images were taken every 2 seconds and analyzed in Photoshop to obtain the red (r), green (g) and blue (b) channel intensity of the gauge section. Intensity change and stress are plotted against strain for PMA1 and PMA2 in Figure A-3a and Figure A-3b. For PMA1, the failure stress is ~12 MPa, whereas for PMA2 the failure stress is only ~ 6MPa. The weak mechanical properties of PM2 was attributed to the low Mw, which was in agreement with the observation in Figure A-2.

Since blue and purple is the characteristic coloration of mechanoactivated SP, drBC was replotted against strain and stress for PMA1 and PMA2 in Figure A-3c and Figure A-3d. It was found that the onset strain for mechanoactivation of SP in PMA1 was lower than PMA2. This is in agreement with the simulation results reported by Sottos et al.[18] They revealed that force inhomogeneity results in mechanoactivation at lower strains because the force at some locations is higher than the macroscopic stress for heterogeneous polymer network. The onset stress of SP mechanoactivation of PMA1 did not significantly differ from that of PMA2. Moreover, the first derivative of drBC vs. strain and drBC vs. stress of the two specimens also did not exhibit an obvious difference. The low failure stress of PMA2 also made the comparison hard to achieve.

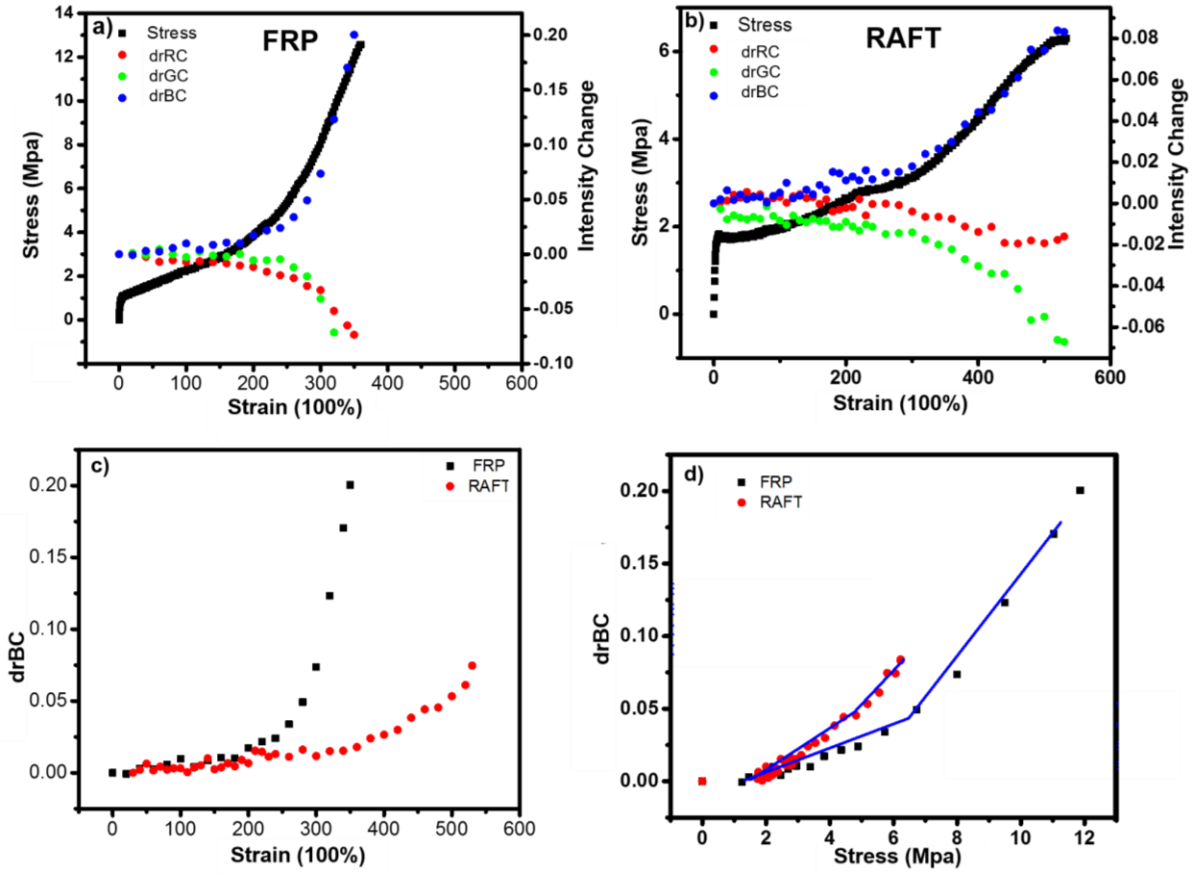

Figure A-3 (a) Stress and intensity change as a function of strain for PMA1 prepared via FRP; (b) Stress and intensity change as a function of strain for PMA2 prepared via RAFT; (c) drBC vs. strain for PMA1 and PMA2; (d) drBC vs. stress PMA1 and PMA2.

A.4 Challenges

Therefore, there is a big challenge to tackle to compare the mechanoactivation behavior of the two polymeric systems, which is Mw of the two polymers should be roughly the same. Though GPC

cannot be used to characterize Mw for the cross-linked polymer, mechanical properties (failure strain and stress) is the direct reflection of Mw. However, the polymers synthesized via RAFT polymerization method always failed at much lower stress, indicating Mw was lower than that prepared via FRP. How to design the recipe and adjust polymerization procedure to ensure the same Mw and similar mechanical properties becomes the key to compare the mechanoactivation behavior of two polymers prepared via FRP and CLRP.

A.5 References

(1) Yu, Q.; Zhu, Y.; Ding, Y.; Zhu, S. *Macromol. Chem. Phys.* **2008**, *209* (5), 551–556.

(2) Allen, P. E. M.; Simon, G. P.; Williams, D. R. G.; Williams, E. H. *Macromolecules* **1989**, *22* (2), 809–816.

(3) Rey, L.; Duchet, J.; Galy, J.; Sautereau, H.; Vouagner, D.; Carrion, L. *Polymer (Guildf).* **2002**, *43* (16), 4375–4384.

(4) Bowman, C. N.; Carver, A. L.; Kennett, S. N.; Williams, M. M.; Peppas, N. A. *Polymer (Guildf).* **1990**, *31* (1), 135–139.

(5) Dušek, K. *Angew. Makromol. Chemie* **1996**, *240* (1), 1–15.

(6) Kannurpatti, A. R.; Anderson, K. J.; Anseth, J. W.; Bowman, C. N. *J. Polym. Sci. Part B Polym. Phys.* **1997**, *35* (14), 2297–2307.

(7) Kloosterboer, J. G. *Adv. Polym. Sci.* **1988**, *84*, 1–61.

(8) Zhu, S.; Hamielec, A. E. *Macromolecules* **1992**, *25* (20), 5457–5464.

(9) Tobita, H.; Hamielec, A. E. *Macromolecules* **1989**, *22* (7), 3098–3105.

(10) Norisuye, T.; Morinaga, T.; Tran-Cong-Miyata, Q.; Goto, A.; Fukuda, T.; Shibayama, M. *Polymer (Guildf).* **2005**, *46* (6), 1982–1994.

(11) Wang, J.-S.; Matyjaszewski, K. *J. Am. Chem. Soc.* **1995**, *117* (20), 5614–5615.

(12) Battjes, K. P.; Kuo, C.-M.; Miller, R. L.; Saam, J. C. *Macromolecules* **1995**, *28* (3), 790–792.

(13) Otsu, T.; Yoshida, M. *Die Makromol. Chemie, Rapid Commun.* **1982**, *3* (2), 127–132.

(14) John Chiefari; Y. K. Chong; Frances Ercole; Julia Krstina; Justine Jeffery; Tam P. T. Le; Roshan T. A. Mayadunne; Gordon F. Meijs; Catherine L. Moad; Moad, G.; Rizzardo, E.; Thang, S. H. *Macromolecules* **1998**, *31* (16), 5559–5562.

(15) Li, M.; Zhang, Q.; Zhu, S. *Polymer (Guildf).* **2016**, *99*, 521–528.

(16) Davis, D. A.; Hamilton, A.; Yang, J.; Cremar, L. D.; Van Gough, D.; Potisek, S. L.; Ong, M. T.; Braun, P. V; Martínez, T. J.; White, S. R.; Moore, J. S.; Sottos, N. R. *Nature* **2009**, *459* (7243), 68–72.

(17) Beiermann, B. A.; Davis, D. A.; Kramer, S. L. B.; Moore, J. S.; Sottos, N. R.; White, S. R. *J. Mater. Chem.* **2011**, *21* (23), 8443.

(18) Silberstein, M. N.; Cremar, L. D.; Beiermann, B. A.; Kramer, S. B.; Martinez, T. J.; White, S. R.; Sottos, N. R. *J. Mech. Phys. Solids* **2014**, *63*, 141–153.

Appendix B Mechanical Force Sensitive Compatibilizer

The objective of this project is to design and prepare spiropyran-based compatibilizer, which can not only stitch two immiscible polymers together but also provide stress/strain indications via color changing. This study will also enrich the fundamental knowledge of spiropyran mechanoactivation behavior at interfaces in polymer composites. In this study, a series of X-SP-Y were successfully synthesized to obtain SP with two different polymer at two ends. However, the biggest challenge of this project lies in that HO-SP-Br could not initiate the atom-transfer radical-polymerization (ATRP) of butyl acrylate (BA) and styrene (St). Deeper investigation must be performed to explain the unsuccessful ATRP polymerization of BA and St with HO-SP-Br as initiator.

B.1 Introduction

The mechanoactivation of spiropyran mechanophore has been intensively studied in various polymer systems, such as polyacrylates,[1,2] polyesters,[3] polyolefins,[4] polyurethanes,[5] poly(dimethylsiloxane)[6,7] and polyamide.[8] However, all the studies on SP-based polymers are limited to homogeneous systems. So far, there have been only few literatures about mechanoactivation of other mechanophores at interfaces.[9] Therefore, it is desirable to study the mechanoactivation behavior of SP at interfaces. It would also enrich the fundamental knowledge of the stress distribution of polymer composites.

Inspired by the idea of using SP for mechanical force sensing at interfaces, we propose to design SP-based compatibilizer for two immiscible polymers for stress sensing. Containing two different functional groups, X-SP-Y can be used for obtaining SP with different polymers at two ends. Figure B-1 lists three symmetric SP mechanophore, including HO-SP-OH, MA-SP-MA and Br-SP-Br, and six asymmetric SP mechanophore, including HO-SP-MA, MA-SP-OH, HO-SP-Br, Br-SP-OH, MA-SP-Br and Br-SP-MA. Vinyl-containing SP, such as HO-SP-MA and MA-SP-OH, can be used to obtain brush copolymer. HO-SP-Br / Br-SP-OH can be used to obtain block copolymer.

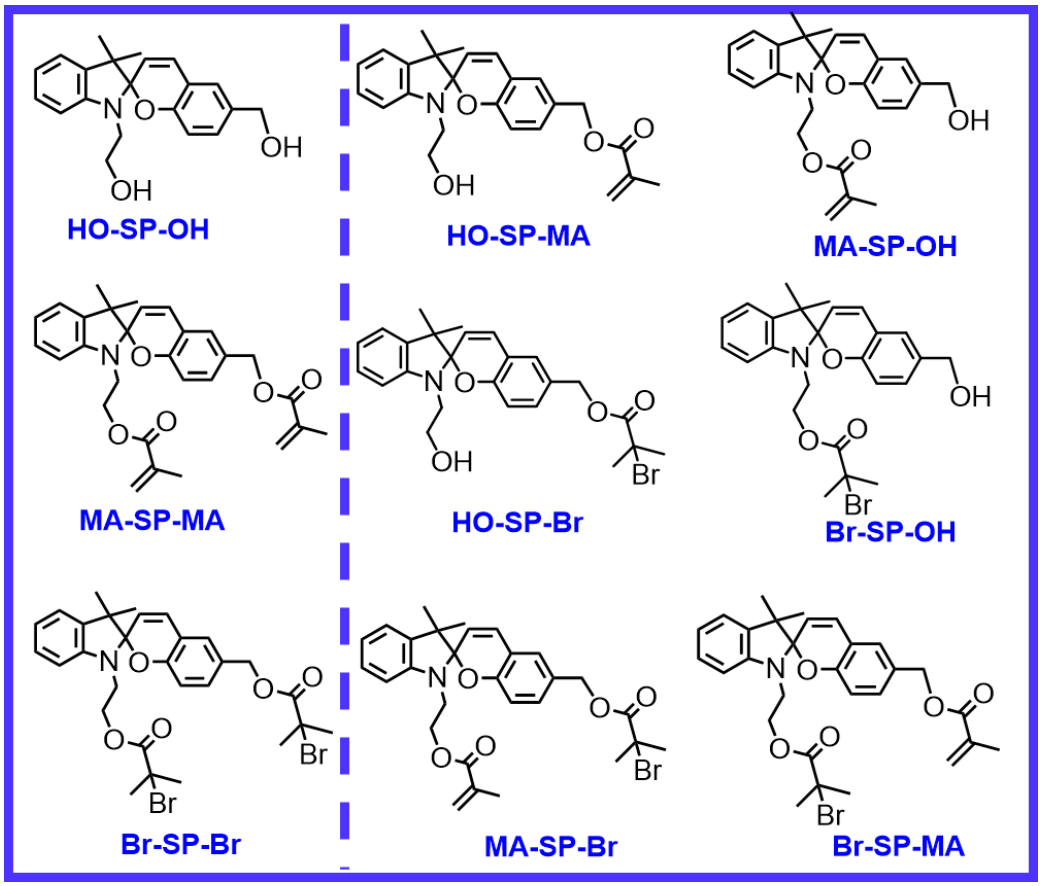

Figure B-1 Symmetric spiropyrans X-SP-X (left) and asymmetric spiropyrans X-SP-Y (right).

In this work, we have successfully synthesized (1'-(2-hydroxyethyl)-3',3'-dimethylspiro[chromene-2,2'-indolin]-6-yl)methyl methacrylate (HO-SP-MA), 2-(6-(hydroxymethyl)-3',3'-dimethylspiro[chromene-2,2'-indolin]-1'-yl)ethyl methacrylate (MA-SP-OH), 2-(6-(hydroxymethyl)-3',3'-dimethylspiro[chromene-2,2'-indolin]-1'-yl)ethyl 2-bromo-2-methylpropanoate (Br-SP-OH), and (1'-(2-hydroxyethyl)-3',3'-dimethylspiro[chromene-2,2'-indolin]-6-yl)methyl 2-bromo-2-methylpropanoate (HO-SP-Br). To better control polymer structure and obtain better performance of compatibilizing, HO-SP-Br were used to prepare block copolymer via ring opening polymerization (ROP) of ε-caprolactone (CL) at one end and atom transfer radical polymerization (ATRP) of butyl acrylate (BA) and styrene (St) at the other end, shown in Figure B-2b. Two immiscible polymers, P(BA-*co*-St) and PCL, can be "stitched" together when P(BA-*co*-St)-SP-PCL is added as a compatibilizer. As is shown in Figure B-2a, when PCL is being peeled off P(BA-*co*-St), the polymer stitch P(BA-*co*-St)-SP-PCL undergoes mechanoactivation due to the applied mechanical forces.

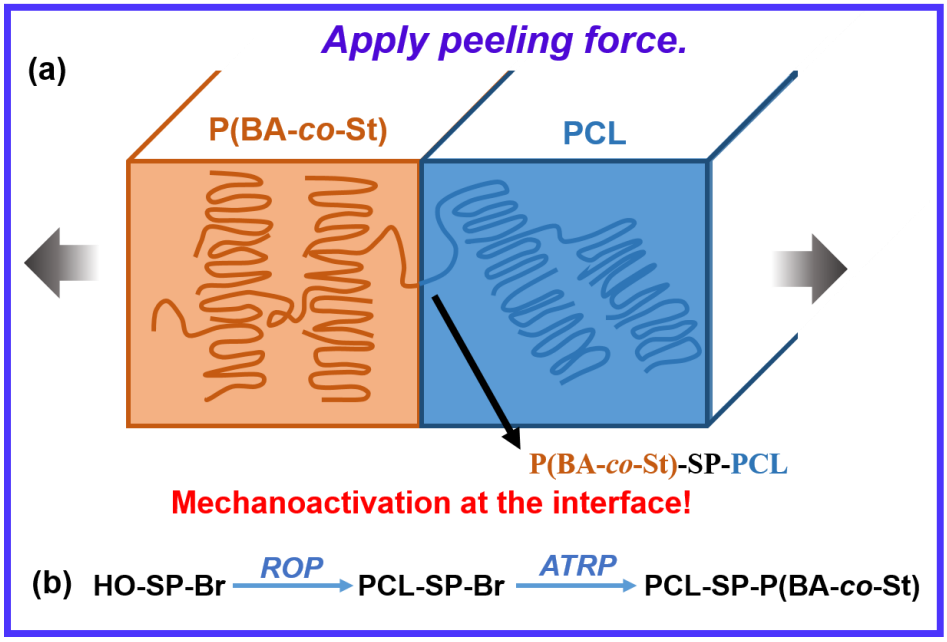

Figure B-2 (a) Mechanoactivation of polymer stitch P(BA-*co*-St)-SP-PCL at the interface of P(BA-*co*-St) and PCL under peeling force; (b) Schematic illustration of the synthetic process to obtain polymer stitch P(BA-*co*-St)-SP-PCL.

B.2 Experimental Methods

B.2.1 Materials

HO-SP-OH was synthesized via the methods outlined by G. Peterson et al.[10] 4-(Dimethylamino) pyridine (≥ 99%, Aldrich), triethylamine (TEA, ≥ 99.5%, Sigma), methacryloyl chloride (97%, Aldrich), and α-bromoisobutyl bromide (BiBB, 98%, Aldrich) were used directly as received.

Butyl acrylate (BA, ≥ 99%, Aldrich) and styrene (St, ≥ 99.5%, Aldrich) were passed through inhibitor remover columns to remove monomethyl ether hydroquinone and 4-tert-butylcatechol, respectively. ε-Caprolactone (CL, ≥ 97%, Aldrich), diphenyl phosphate (DPP, ≥ 99%, Aldrich), copper (I) bromide (CuBr, ≥ 99.99%, Aldrich), and *N*,*N*,*N'*,*N''*,*N''*-pentamethyldiethylenetriamine (PMDETA, 99.%, Aldrich) were used as received.

B.2.2 Synthesis of X-SP-Y

HO-SP-MA and MA-SP-OH were prepared from an esterification of HO-SP-OH, similarly to MA-SP-MA.[10,11] The main difference lies in the ratio of methacryloyl chloride over HO-SP-OH. The ratio of methacryloyl chloride over HO-SP-OH was more than 3 to prepare MA-SP-MA, whereas the ratio was 1.2 to prepare MA-SP-OH and HO-SP-MA. Thin layer chromatography (TLC) was used to monitor the reaction. Figure B-3 shows the TLC results of pure HO-SP-OH, the crude product (a mixture of HO-SP-OH, HO-SP-MA, MA-SP-OH and MA-SP-MA) and pure MA-SP-MA. The polarity of MA-SP-OH and HO-SP-MA is between HO-SP-OH and MA-SP-MA. The pure MA-SP-OH and HO-SP-MA were collected by chromatography eluting with ethyl acetate/hexane (1:6). Similarly, HO-SP-Br and Br-SP-OH were also synthesized by esterification of HO-SP-OH with BiBB.

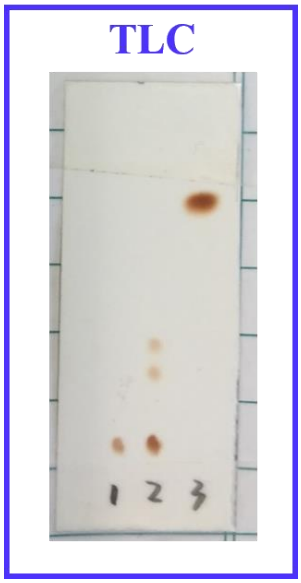

Figure B-3 The TLC result of (1) pure HO-SP-OH; (2) crude produce (mixture of HO-SP-OH, HO-SP-MA, MA-SP-OH and MA-SP-MA); (3) pure MA-SP-MA.

B.2.3 Synthesis of Br-SP-PCL via ROP

CL (2.82 g, 24.7 mmol), DPP (0.078 g, 0.31 mmol) and Br-SP-OH (0.15 g, 0.31 mmol) were dissolved in 3 mL toluene. After three cycles of free-pump-thaw, the reaction mixture was allowed to react at room temperature for 5 h. At the end of the reaction, TEA was added to terminate the reaction. The polymer product was washed with cold hexane for three times, dried completely and weighed. In the end, we obtained Br-SP-PCL (2.6 g, 74%).

B.2.4 Synthesis of P(BA-*co*-St)-SP-PCL via ATRP

A mixture of BA (0.8 g, 6.24 mmol), St (0.22 g, 2.08 mmol), CuBr (0.015 g, 0.104 mmol), PMDETA (0.036 g, 0.208 mmol), Br-SP-PCL (1 g, 0.104 mmol) and toluene (3 mL) were charged into a 10 mL reaction vial. After three cycles of free-pump-thaw, the reaction mixture was heated up to 90 °C. The reaction was allowed to proceed for 48 h before termination. The polymer product was washed in cold hexane for three times and dried completely in the oven.

B.3 Results and Discussion

The successful synthesis of HO-SP-MA, MA-SP-OH, HO-SP-Br and Br-SP-OH was confirmed by ^{1}H NMR NMR, shown in Figure B-4. In this work, Br-SP-OH was used for the synthesis of block copolymer P(BA-*co*-St)-SP-PCL as the compatibilizer for P(BA-*co*-St) and PCL. Compared with polymer brush that can be prepared from HO-SP-MA / MA-SP-OH, block copolymer from Br-SP-OH / HO-SP-Br is expected to give better miscibility of P(BA-*co*-St) and PCL.

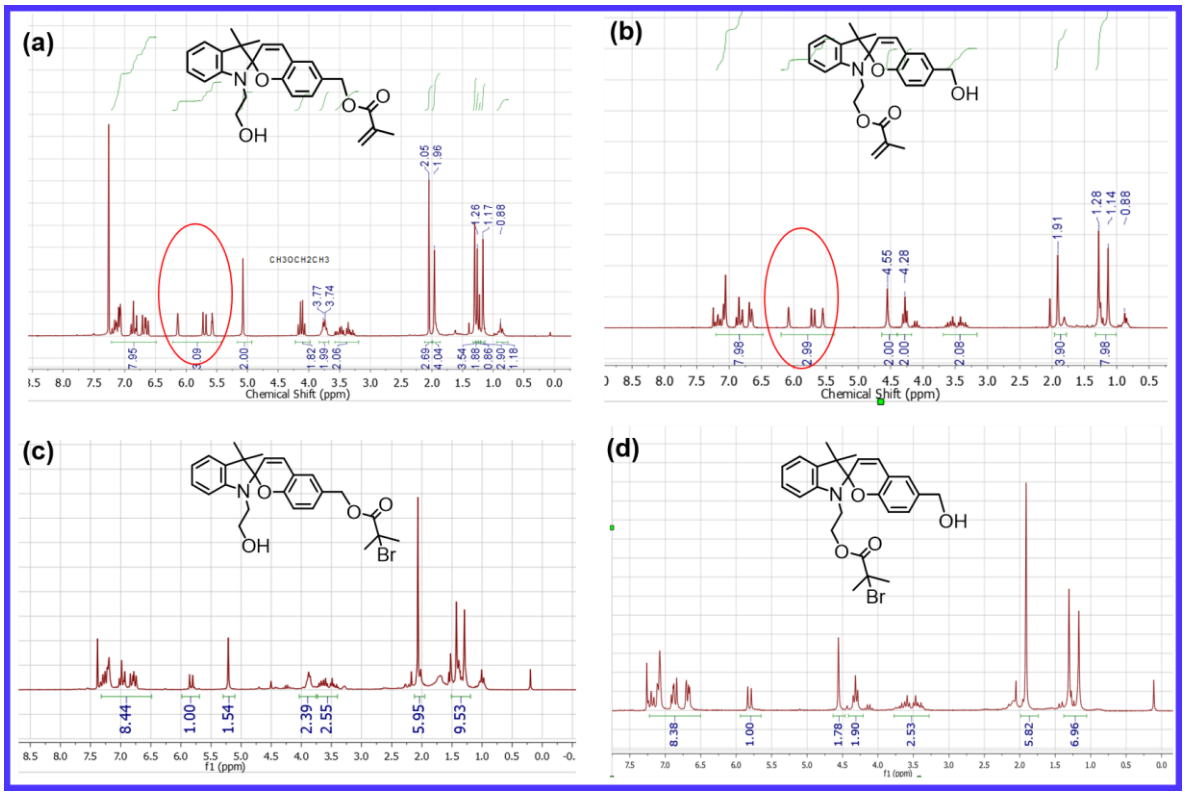

Figure B-4 ^{1}H NMR of (a) HO-SP-MA, (b) MA-SP-OH, (c) OH-SP-Br and (d) Br-SP-OH.

DPP-catalyzed ROP of CL under room temperature yielded Br-SP-PCL, which was further confirmed by ^{1}H NMR results, shown in Figure B-5a. The characteristic peaks of SP are not noticeable, probably attributed to too low traces of SP compared to PCL. The obtained Br-SP-PCL was further used as the initiator for the ATRP polymerization of BA and St. The ^{1}H NMR result of the final polymer product is shown in Figure B-5b. Only small amount of St was polymerized, whereas BA was not polymerized at all. We speculate the small amount of PSt was attributed to thermally induced polymerization but not ATRP. Therefore, ATRP polymerization of BA and St

using Br-SP-PCL as initiator turned out to be a failure. The experiment was repeated for another three times, none of which gave expected results.

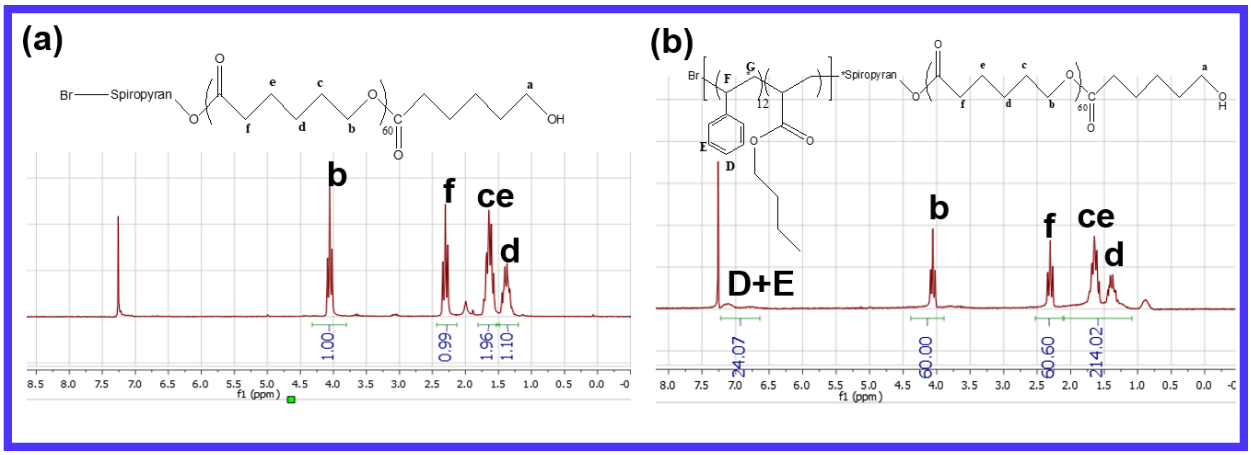

Figure B-5 ^{1}H NMR of (a) Br-SP-PCL (SP is short for spiropyran) and (b) the polymer product after ATRP.

B.4 Challenges

(1) Though ^{1}H NMR result in Figure B-5a shows the successful ROP of CL, PCL might not be covalently linked to SP. No direct evidence proves it is the hydroxyl group of SP that initiates the ROP of CL. The resulting polymer could be simply PCL, initiated by water. Since no drying of CL monomer was carried out before ROP, only small traces of water would initiate the polymerization. Therefore, using molecular sieves or high-temperature furnace to dry CL monomer is very important to obtain Br-SP-PCL.

(2) Figure B-5b shows the failed attempt of ATRP polymerization of BA and St using Br-SP-PCL as the initiator. We speculate if PCL affected the initiation activity of isobutyl bromide. To verify this, we simply carried out ATRP polymerization of BA and St using Br-SP-OH as initiation. No polymer was obtained after 48 h of reaction. The initiation activity of isobutyl bromide of SP might be the main issue. This must be further explored in future studies.

B.5 References

(1) Davis, D. A.; Hamilton, A.; Yang, J.; Cremar, L. D.; Van Gough, D.; Potisek, S. L.; Ong, M. T.; Braun, P. V; Martínez, T. J.; White, S. R.; Moore, J. S.; Sottos, N. R. *Nature* **2009**, *459* (7243), 68–72.

(2) Degen, C. M.; May, P. A.; Moore, J. S.; White, S. R.; Sottos, N. R. *Macromolecules* **2013**, *46* (22), 8917–8921.

(3) O'Bryan, G.; Wong, B. M.; McElhanon, J. R. *ACS Appl. Mater. Interfaces* **2010**, *2* (6), 1594–1600.

(4) Li, M.; Liu, W.; Zhu, S. *Polymer (Guildf).* **2017**, *112*, 219–227.

(5) Lee, C. K.; Davis, D. A.; White, S. R.; Moore, J. S.; Sottos, N. R.; Braun, P. V. *J. Am. Chem. Soc.* **2010**, *132* (45), 16107–16111.

(6) Gossweiler, G. R.; Hewage, G. B.; Soriano, G.; Wang, Q.; Welshofer, G. W.; Zhao, X.; Craig, S. L. *ACS Macro Lett.* **2014**, *3*, 216–219.

(7) Wang, Q.; Gossweiler, G. R.; Craig, S. L.; Zhao, X.; Bao, Z. *Nat. Commun.* **2014**, *5*, 4899.

(8) Chen, H.; Yang, F.; Chen, Q.; Zheng, J. *Adv. Mater.* **2017**, 1606900.

(9) Li, J.; Shiraki, T.; Hu, B.; Wright, R. A. E.; Zhao, B.; Moore, J. S. *J. Am. Chem. Soc.* **2014**, *136* (45), 15925–15928.

(10) Peterson, G. I.; Larsen, M. B.; Ganter, M. A.; Storti, D. W.; Boydston, A. J. *ACS Appl. Mater. Interfaces* **2015**, *7* (1), 577–583.

(11) Li, M.; Zhang, Q.; Zhu, S. *Polymer (Guildf).* **2016**, *99*, 521–528.

Appendix C Thermally Induced Mechanoactivation within PNIPAM Hydrogel

The objective of this project is to design and prepare poly(*N*-isopropylacrylamide) (PNIPAM) hydrogel with spiropyran mechanophore as cross-linker. Below the lower critical solution temperature (LCST, ~32 °C), the swelling of PNIPAM hydrogel would further mechanoactivate SP to MC. The activation could be recovered by increasing temperature above LCST. Repeated experiments proved our original assumption. Additionally, we found the protonated MC, MCH, was more favorable after equilibrium under the thermally induced mechanoactivation. The reasons to account for MCH must be explored in future studies.

C.1 Introduction

Recently, there have been several studies on using spiropyran (SP) mechanophore for stress/strain sensing within gels. Moore's group initially demonstrated solvent swelling-induced mechanoactivation of SP within PMMA gel.[1] Later, our group has developed CO_2-breathing induced reversible mechanoactivation of SP within microgels.[2] Lately, Zheng's group incorporated SP moiety into mechanically strong hydrogels for stress sensing.[3] Exploiting SP mechanophore within hydrogels provides approaches to map stress within hydrogels and thus is desired to be further explored.

Thermal responsive hydrogels have been intensively studied during the past decades. Particularly, poly(*N*-isopropylacrylamide) (PNIPAM) hydrogel has received great attention due to its great potential application in drug delivery and biotechnology.[4–6] PNIPAM undergoes a dramatic volume change at lower critical solution temperature (LCST, ~32 °C), which is close to physiological temperature. Below the LCST, the PNIPAM hydrogel exhibits hydrophilicity due to the binding between amide functionality and the water molecules through hydrogel bonding. Above the LCST, polymer expels water molecules and undergoes coil-to-globule transition due to the breaking of hydrogen bonding.[7]

Herein, we propose to incorporate SP mechanophore into PNIPAM hydrogel as cross-linker. It is expected that temperature-induced swelling would further mechanically activate SP mechanophore within the PNIPAM hydrogel. As is shown in Figure C-1, the swelling of hydrogel would mechanoactivate SP-to-MC when the temperature is below LCST, which can be recovered by increasing the temperature above LCST.

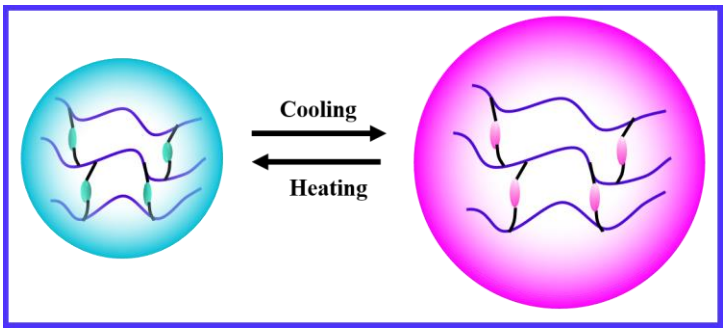

Figure C-1 Thermally induced mechanoactivation of SP within the PNIPAM hydrogel

C.2 Experimental Methods

C.2.1 Materials

Ethylene glycol dimethacrylate (EGDMA, 98%, Aldrich) was passed through inhibitor remover to remove monomethyl ether hydroquinone. *N*-isopropylacrylamide, (NIPAM, 97%, Aldrich), benzoyl peroxide (BPO, ≥ 98%, Sigma-Aldrich) and *N*, *N*-dimethylaniline (DMA, ≥ 99.5%, Aldrich) were used as received. (1'-(2-(methacryloyloxy)ethyl)-3',3'-dimethylspiro(chromene-2,2'-indolin)-6-yl)methyl methacrylate (MA-SP-MA) was synthesized via the procedures reported by Meng et al.[8]

C.2.2 Synthesis of P(NIPAM-*co*-SP) Hydrogel

NIPAM (0.57 g, 5 mmol), BPO (28 mg, 0.12 mmol), EGDMA (20 μL, 0.005 mmol) and MA-SP-MA (5.9 mg, 0.0125 mmol) were well dissolved in 1 mL DMF, which was flushed with N_2 for 30 min. The reaction mixture was transferred into a PTFE mold, which was degassed previously. DMA was quickly added to the mold to start the reaction. The reaction was allowed to proceed for 24 h at room temperature (~23 °C). After the reaction, the polymer film was easily removed from the mold and placed in 20 °C water for dialysis to remove DMF for 24 h.

C.3 Results and Discussion

C.3.1 Mechanoresponsiveness

After reaction for 24 h, the polymer gel was removed from the mold. As is shown in Figure C-2, the polymer gel exhibited slight yellow, probably attributed to the covalent incorporation of SP moiety. After shearing, the P(NIPAM-*co*-SP) gel turned blue, indicating SP was mechanically activated to MC. The emergence of blue coloration after shearing confirmed the mechanoresponsiveness of the P(NIPAM-*co*-SP) gel.

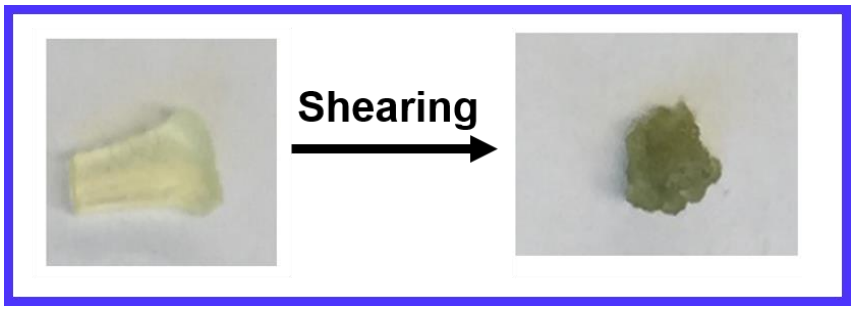

Figure C-2 Shearing induced mechanoactivation of P(NIPAM-*co*-SP) gel

C.3.2 Thermal Responsiveness

To characterize the thermal responsiveness of the P(NIPAM-*co*-SP), the gel was further dialyzed in 20 °C water for 24 h to remove DMF. During dialysis, the gel volume slowly increased, and the color gradually changed from yellow to purple, attributed to the slow mechanoactivation of SP-to-MC. The resulting hydrogel exhibited transparent purple in the water of 20 °C, whereas turbid white in the water of 40 °C, shown in Figure C-3a top. UV-vis absorbance spectrum in Figure C-3b showed two characteristic peaks at 550 nm and 450 nm when hydrogel was placed in the water of 20 °C. The two peaks were attributed to the mechanoactivated MC state and the protonated MCH state, respectively. The possible explanation for the phenomenon is as follows. When the hydrogel was placed in the water of 20 °C, the amide functionality bond with water due to hydrogen bonding and PNIPAM became more hydrophilic. More water molecules swole into the polymer network and thus the volume of the hydrogel increased. The swelling of hydrogel further mechanically activated the yellow SP state to the purple MC state. However, the reason to account for the protonated MC state, MCH, is not understood and thus needs to be further explored. The thermally induced mechanoactivation process is also reversible by increasing temperature above LCST. When the hydrogel is placed in water of 40 °C, PNIPAM expelled water and underwent coil-to-globule transition. The force applied on SP mechanophore cross-linker was then released. The hydrogel turned back to turbid white.

After being placed in the water of 20 °C for 1 h, the hydrogel slowly turned orange from purple, shown in Figure C-3a bottom. UV-vis absorbance spectrum in Figure C-3c showed significantly

increased absorbance at 450 nm (MCH) and slightly increased absorbance at 550 nm (MC). The evidence showed the MCH was more favorable state than MC for the swollen P(NIPAM-*co*-SP) hydrogel. Since no additional H^+ was added, the reason to account for MCH is not understood yet.

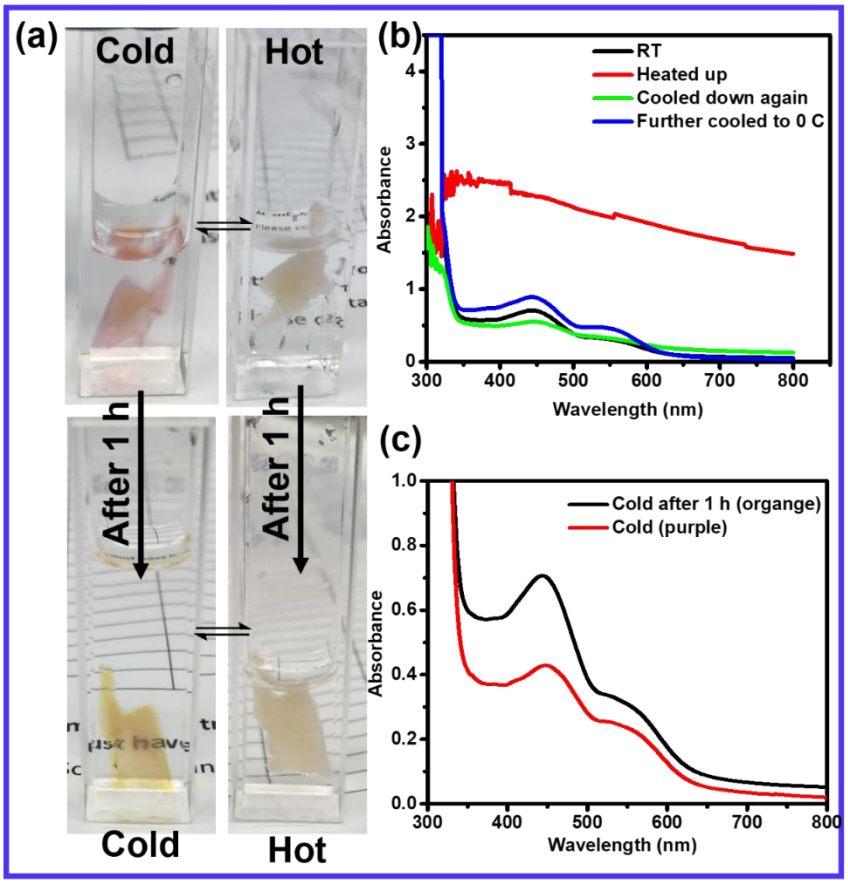

Figure C-3 (a) The P(NIPAM-*co*-SP) hydrogel in cold (20 °C) and hot (30 °C) water (top) and in cold (20 °C) and hot (40 °C) after 1 h (bottom); (b) The UV/vis absorbance spectrum of the hydrogel, which underwent 20 °C (black line), 40 °C (red line), 20 °C (green line), and finally 0 °C (blue line); (c) The UV/vis absorbance spectrum of the hydrogel, which was just placed in 20 °C water (red) and placed in 20 °C water for 1 h (black).

C.4 Challenges

(1) The coloration of mechanoactivated P(NIPAM-*co*-SP) hydrogel is not stable. With the increasing time in the water of 20 °C, the hydrogel turned from purple to orange. The UV/vis absorbance spectrum also showed significant increment in the absorbance peak of MCH. The reason to account for MCH must be further investigated in future studies.

(2) During dialysis, the P(NIPAM-*co*-SP) gel was placed in the water of 20 °C. Therefore, the initial state of the hydrogel is already mechanoactivated. Water of 40 °C was also tried for dialysis to ensure the initial state of hydrogel state is not activated. However, the effect of dialysis was not good and DMF could not be removed. Therefore, thermal responsive polymers with upper critical solution temperature (UCST) should be considered.

C.5 References

(1) Lee, C. K.; Diesendruck, C. E.; Lu, E.; Pickett, A. N.; May, P. A.; Moore, J. S.; Braun, P. V. *Macromolecules* **2014**, *47* (8), 2690–2694.

(2) Li, M.; Lei, L.; Zhang, Q.; Zhu, S. *Macromol. Rapid Commun.* **2016**, *37* (12), 957–962.

(3) Chen, H.; Yang, F.; Chen, Q.; Zheng, J. *Adv. Mater.* **2017**, 1606900.

(4) Jeong, B.; Kim, S. W.; Bae, Y. H. *Adv. Drug Deliv. Rev.* **2012**, *64*, 154–162.

(5) Okano, T.; Yamada, N.; Okuhara, M.; Sakai, H.; Sakurai, Y. *Biomaterials* **1995**, *16* (4), 297–303.

(6) Dehai Liang; Shuiqin Zhou; Liguo Song; Zaitsev, V. S.; Chu, B. *Macromolecules* **1999**, *32* (19), 6326–6332.

(7) JagadeeshBabu, P. E.; Suresh Kumar, R.; Maheswari, B. *Colloids Surfaces A Physicochem. Eng. Asp.* **2011**, *384* (1–3), 466–472.

(8) Li, M.; Zhang, Q.; Zhu, S. *Polymer (Guildf).* **2016**, *99*, 521–528.